Towards an understanding of nonlinear electrokinetics at large applied voltages in concentrated solutions

Martin Z. Bazant[*,a,b,d], Mustafa Sabri Kilic[b], Brian D. Storey[c], Armand Ajdari[d]

[a] *Department of Chemical Engineering, Massachusetts Institute of Technology, Cambridge, MA 02139*
[b] *Department of Mathematics, Massachusetts Institute of Technology, Cambridge, MA 02139*
[c] *Franklin W. Olin College of Engineering, Needham, MA 02492*
[d] *CNRS UMR Gulliver 7083, ESPCI, 10 rue Vauquelin, 75005 Paris, France*

Abstract

The venerable theory of electrokinetic phenomena rests on the hypothesis of a dilute solution of point-like ions in quasi-equilibrium with a weakly charged surface, whose potential relative to the bulk is of order the thermal voltage ($kT/e \approx 25$ mV at room temperature). In nonlinear electrokinetic phenomena, such as AC or induced-charge electro-osmosis (ACEO, ICEO) and induced-charge electrophoresis (ICEP), several Volts $\approx 100\,kT/e$ are applied to polarizable surfaces in microscopic geometries, and the resulting electric fields and induced surface charges are large enough to violate the assumptions of the classical theory. In this article, we review the experimental and theoretical literatures, highlight discrepancies between theory and experiment, introduce possible modifications of the theory, and analyze their consequences. We argue that, in response to a large applied voltage, the "compact layer" and "shear plane" effectively advance into the liquid, due to the crowding of solvated counter-ions. Using simple continuum models, we predict two general trends at large voltages: (i) ionic crowding against a blocking surface expands the diffuse double layer and thus decreases its differential capacitance, and (ii) a concomitant viscosity increase near the surface reduces the electro-osmotic mobility. The former effect can predict high-frequency flow reversal in ACEO pumps, while the latter may explain the universal decay of ICEO flow with increasing salt concentration. Through several colloidal examples, such as ICEP of an uncharged metal sphere in an asymmetric electrolyte, we predict that nonlinear electrokinetic phenomena are generally ion-specific. Similar theoretical issues arise in nanofluidics (due to molecular confinement) and ionic liquids (due to the lack of solvent), so the paper concludes with a general framework of modified electrokinetic equations for finite-sized ions.

Key words: Nonlinear electrokinetics, microfluidics, induced-charge electro-osmosis, electrophoresis, AC electro-osmosis, concentrated solution, modified Poisson-Boltzmann theory, steric effects, hard-sphere liquid, lattice-gas, viscoelectric effect, solvation, ionic liquids, non-equilibrium thermodynamics

[*] Corresponding author
Email address: bazant@mit.edu (Martin Z. Bazant)

1. Introduction

1.1. Nonlinear "induced-charge" electrokinetic phenomena

Due to favorable scaling with miniaturization, electrokinetic phenomena are finding many new applications in microfluidics [1, 2], but often in new situations that raise fundamental theoretical questions. The classical theory of electrokinetics, dating back to Helmholtz and Smoluchowski a century ago [3], was developed for the effective *linear* hydrodynamic slip driven by an electric field past a surface in chemical *equilibrium* with the solution, whose double-layer voltage is of order the thermal voltage, $kT/e = 25$ mV, and approximately constant [4, 5, 6, 7, 8, 9]. The discovery of AC electro-osmositic flow (ACEO) over micro-electrodes has shifted attention to a new *nonlinear* regime, where the *induced* double-layer voltage is typically several Volts $\approx 100\,kT/e$, oscillating at frequencies up to 100 kHz, and nonuniform at the micron scale [10, 11, 12]. Related phenomena of induced-charge electro-osmosis (ICEO) [13, 14] also occur around polarizable particles [15, 16] and microstructures [17] (in AC or DC fields), as well as driven biological membranes [18]. Due to broken symmetries in ICEO flow, asymmetric colloidal particles undergo nonlinear, induced-charge electrophoresis (ICEP) [13, 19, 20]. Some of these fundamental nonlinear electrokinetic phenomena are illustrated in Fig. 1.

A "Standard Model" (outlined below) has emerged to describe a variety of induced-charge electrokinetic phenomena, but some crucial aspects remain unexplained. In their pioneering work 25 years ago in the USSR, which went unnoticed in the West until recently [13, 14], V. A. Murtsovkin, A. S. Dukhin and collaborators first predicted quadrupolar flow (which we call "ICEO") around a polarizable sphere in a uniform electric field [24] and observed the phenomenon using mercury drops [25] and metal particles [26], although the flow was sometimes in the opposite direction to the theory, as discussed below. (See Ref. [15] for a review.) More recently, in microfluidics, Ramos et al. observed and modeled ACEO flows over a pair of micro-electrodes, and the theory over-predicted the observed velocity by an order of magnitude [10, 27, 28, 29]. Around the same time, Ajdari used a similar model to predict ACEO pumping by asymmetric electrode arrays [11], which was demonstrated using planar electrodes of unequal widths and gaps [30, 31, 32, 33, 34, 35], but the model cannot predict experimentally observed flow reversal at high frequency and loss of flow at high salt concentration [34, 36, 37], even if extended to large voltages [38, 39]. The low-voltage model has also been used to predict faster three-dimensional ACEO pump geometries [40], prior to experimental verification [36, 41, 42, 43], but again the data departs from the theory at large voltages. Discrepancies between theory and experiments, including flow reversal, also arise in traveling-wave electro-osmosis (TWEO) for electrode arrays applying a wave-like four-phase voltage pulse [44, 45, 46, 47]. Recent observations of ICEO flow around metal microstructures [17, 48], ICEP rotation of metal rods [49], ICEP translation of metallo-dielectric particles [21] have likewise confirmed qualitative theoretical predictions [13, 14, 19, 50, 51], while exhibiting the same poorly understood decay of the velocity at high salt concentration. We conclude that there are fundamental gaps in our understanding of nonlinear electrokinetics.

In this article, we review a number of diverse literatures relating to nonlinear electrokinetics and analyze several possible modifications of the theory. Some of these ideas are new, while others were proposed long ago by O. Stern, J. J. Bikerman, J. Lyklema, and others, and effectively forgotten. We build the case that at least some failures of the Standard Model can be attributed to the breakdown of the dilute-solution approximation at large induced voltages. Using simple models, we predict two general effects associated with counterion crowding – decay of the double-layer capacitance and reduction of the electro-osmotic mobility – which begin to

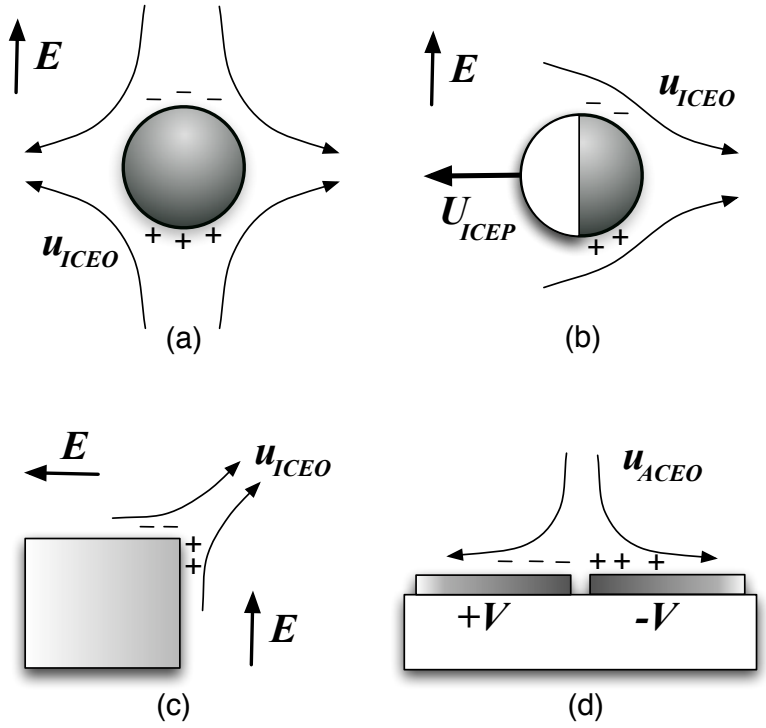

Figure 1: Examples of nonlinear electrokinetic phenomena, driven by induced charge (+, −)in the diffuse part of the electrochemical double layer at polarizable, blocking surfaces, subject to an applied electric field E or voltage V. (a) Induced-charge electro-osmosis (ICEO) around a metal post [13, 14, 17, 15], (b) induced-charge electrophoresis (ICEP) of a metal/insulator Janus particle [19, 21], (c) a nonlinear electrokinetic jet of ICEO flow at a sharp corner in a dielectric microchannel [22, 23], and (d) AC electro-osmosis (ACEO) over a pair of microelectrodes [10, 11].

explain the experimental data. Our models, although incomplete, also imply generic new ion-specific nonlinear electrokinetic phenomena at large voltages related to atomic-level details of polarizable solid/electrolyte interfaces.

1.2. Scope and context of the article

We first presented these ideas in a paper at the ELKIN International Electrokinetics Symposium in Nancy, France in June 2006 [52] and in a letter, which was archived online in March 2007 [53] and will soon be published [54]. The present article is a review article with original material, built around the letter, where its basic arguments are further developed as follows:

1. We begin with a critical review of recent studies of induce-charge electrokinetic phenomena in section 2. By compiling results from the literature and performing our own simulations of other experiments, we systematically compare theory and experiment across a wide range of nonlinear electrokinetic phenomena. To motivate modified electrokinetic models, we also review various concentrated-solution theories from electrochemistry and electrokinetics in sections 3 and 4.
2. In our original letter, the theoretical predictions of steric effects of finite ion sizes in electrokinetics were based on what we call the "Bikerman's model" below [55, 56], a simple lattice-gas approach that allows analytical results. Here, we develop a general, mean-field theory of volume constraints and illustrate it with hard-sphere liquid models [57, 58]. In addition to the charge-induced thickening effect from the original letter, we also consider the field-induced viscoelectric effect in the solvent proposed by Lyklema and Overbeek [59, 60], in conjunction with our models for steric effects.
3. We provide additional examples of new electrokinetic phenomena predicted by our models at large voltages. In the letter [53], we predicted high-frequency flow reversal in ACEO (Fig. 8 below) and decay of ICEO flow at high concentration (Fig. 15). Here, we also predict two mechanisms for ion-specific, field-dependent mobility of polarizable colloids at large voltages. The first has to do with crowding effects on the redistribution of double-layer charge due to nonlinear capacitance, as noted by A. S. Dukhin [61, 62] (Fig. 10). The second results from a novel ion-specific viscosity increase at high charge density (Fig. 18).
4. We present a general theoretical framework of modified electrokinetic equations for concentrated solutions and/or large voltages in section 5, which may also be useful in modeling nano-confinement or solvent-free ionic liquids.

In spite of these major changes, the goal of the paper remains the same: to provide an overview of various physical aspects of electrokinetic phenomena, not captured by classical theories, which become important at large induced voltages. Here, we focus on general concepts, mathematical models, and simple analytical predictions. Detailed studies of some particular phenomena will appear elsewhere, e.g. Ref. [63] on high-frequency flow reversal in AC electro-osmosis.

There have been a few other attempts to go beyond dilute solution theory in electrokinetics, but in the rather different context of linear "fixed-charge" flows in nanochannels at low surface potentials. The first electrokinetic theories of this type may be those of Cervera et al. [64, 65], who used Bikerman's modified Poisson-Boltzmann (MPB) theory to account for the crowding of finite-sized ions during transport by conduction and electro-osmosis through a membrane nanopore. Recently, Liu et al. [66] numerically implemented a more complicated MPB theory [67, 68, 69] to predict effects of finite ion sizes, electrostatic correlations, and dielectric image forces on electro-osmotic flow and streaming potential in a nanochannel. In these studies

of linear electrokinetic phenomena, effects beyond the dilute solution approximation can arise due to nano-confinement, but, as we first noted in Ref. [56], much stronger and possibly different crowding effects also arise due to large induced voltages, regardless of confinement or bulk salt concentration. Our goal here is to make a crude first attempt to understand the implications of ion crowding for nonlinear electrokinetic phenomena, using simple mean-field approximations that permit analytical solutions in the thin double-layer limit.

Similar models for double-layer charging dynamics are also starting to be developed for ionic liquids and molten salts [70, 71, 72, 73], since describing ion crowding is paramount in the absence of a solvent. Kornyshev recently suggested using what we call the "Bikerman-Freise" (BF) mean-field theory below to describe the differential capacitance of the double layer, with the bulk volume fraction of ions appearing as a fitting parameter to allow for a slightly different density of ions [70]. (An equivalent lattice-gas model was also developed long ago for the double layer in an ionic crystal by Grimley and Mott [74, 75, 76], and a complete history of related models is given below in Section 3.1.2.) The BF capacitance formula, extended to allow for a thin dielectric Stern layer, has managed to fit recent experiments and simulations of simple ionic liquids rather well, especially at large voltages [71, 72]. However, we are not aware of any work addressing electrokinetic phenomena in ionic liquids, so perhaps the mean-field electro-hydrodynamic models developed here for concentrated electrolytes at large voltages might provide a useful starting point, in the limit of nearly close packing of ions.

As a by-product of this work, our attempts to model nanoscale phenomena in nonlinear electrokinetics may also have broader applicability in nanofluidics [77, 78]. Dilute-solution theory remains the state-of-the-art in mathematical modeling, and the main focus of the field so far has been on effects of geometrical confinement, especially with overlapping double layers. Although the classical Poisson-Nernst-Planck and Navier-Stokes equations provide a useful first approximation to understand effects such as the charge selectivity [79, 80, 81, 82] and mechanical-to-electrical power conversion efficiency [83, 84, 85, 86, 87, 88] of nanochannels, in many cases it may be essential to introduce new physics into the governing equations and boundary conditions to account for crowding effects and strong surface interactions. Molecular dynamics simulations of nanochannel electrokinetics provide crucial insights and can be used to test and guide the development of modified continuum models [89, 90, 91, 92, 93, 94] .

The article is organized as follows. In section 2, we review the standard low-voltage model for nonlinear electrokinetic phenomena and its failure to explain certain key experimental trends. We then review various attempts to go beyond dilute solution theory in electrochemistry and electrokinetics and analyze the effects of two types of new physics in nonlinear electrokinetic phenomena at large voltages: In section 3, we build on our recent work on diffuse-charge dynamics at large applied voltages [95, 56, 96] to argue that the crowding of counterions plays a major role in induced-charge electrokinetic phenomena by reducing the double-layer capacitance in ways that are ion-specific and concentration-dependent; In section 4, we postulate that the local viscosity of the solution grows with increasing charge density, which in turn decreases the electro-osmotic mobility at high voltage and/or concentration and introduces another source of ion specificity. Finally, in section 5, we present a theoretical framework of modified electrokinetic equations, which underlies the results in sections 3-4 and can be applied to general situations.

2. Background: Theory versus Experiment

2.1. The Standard Model

We begin by summarizing the "Standard Model" of nonlinear electrokinetics, used in most theoretical studies, and then noting some crucial experimental trends it fails to capture. The general starting point for the Standard Model is the coupling of the Poisson-Nernst-Planck (PNP) equations of ion transport to the Navier Stokes equations of viscous fluid flow. ICEO flows are rather complex, so many simplifications from this starting point have been made to arrive at an operational model [15, 10, 11, 14, 19]. For thin double layers compared to the geometrical length scales, the Standard Model is based on the assumption of "linear" or "weakly nonlinear" charging dynamics [95], which further requires that the applied voltage is small enough not to significantly perturb the bulk salt concentration, whether by double-layer salt adsorption or Faradaic reaction currents. In this regime, the problem is greatly simplified, and the electrokinetic problem decouples into one of electrochemical relaxation and another of viscous flow:

1. *Electrochemical relaxation.* – The first step is to solve Laplace's equation for the electrostatic potential across the bulk resistance,

$$\boldsymbol{\nabla} \cdot \mathbf{J} = \boldsymbol{\nabla} \cdot (\sigma \mathbf{E}) = -\sigma \nabla^2 \phi = 0 \tag{1}$$

   assuming Ohm's Law with a constant conductivity σ. A capacitance-like boundary condition for charging of the double layer at a blocking surface (which cannot pass normal current) then closes the "RC circuit" [95],

$$C_D \frac{d\Psi_D}{dt} = \sigma E_n, \tag{2}$$

   where the local diffuse-layer voltage drop $\Psi_D(\phi)$ (surface minus bulk) responds to the normal electric field $E_n = -\hat{n} \cdot \nabla \phi$. In the Standard Model, the bulk conductivity σ and diffuse-layer capacitance C_D are usually taken to be constants, although these assumptions can be relaxed [38, 39, 97]. The diffuse layer capacitance is calculated from the PNP equations by applying the justifiable assumption that the thin double layers are in thermal equilibrium; see section 3.1. A compact Stern layer or dielectric surface coating of constant capacitance C_S is often included [11, 95, 38], so that only part of the total double-layer voltage $\Delta\phi$ is dropped across the diffuse layer "capacitor",

$$\Psi_D = \frac{\Delta\phi}{1+\delta} = \frac{C_S \Delta\phi}{C_S + C_D}, \tag{3}$$

   where $\delta = C_D/C_S$ is the diffuse-layer to compact-layer capacitance ratio.
2. *Viscous flow.* – The second step is to solve for a (possibly unsteady) Stokes flow,

$$\rho_m \frac{\partial \mathbf{u}}{\partial t} = -\boldsymbol{\nabla} p + \eta_b \nabla^2 \mathbf{u}, \quad \boldsymbol{\nabla} \cdot \mathbf{u} = 0, \tag{4}$$

   with the Helmholtz-Smoluchowski (HS) boundary condition for effective fluid slip outside the double layer,

$$\mathbf{u}_s = -b\, \mathbf{E}_t = -\frac{\varepsilon_b \Psi_D}{\eta_b} \mathbf{E}_t \tag{5}$$

where $\mathbf{E}_t$ is the tangential field, $b = \varepsilon_b \zeta/\eta_b$ is the electro-osmotic mobility, ζ is the zeta potential at the shear plane (= Ψ_D in the simplest models), and ε_b, η_b, and ρ_m are the permittivity, viscosity, and mass density of the *bulk* solvent. Osmotic pressure gradients, which would modify the slip formula [98, 99], are neglected since the bulk salt concentration is assumed to be uniform.

Although this model can be rigorously justified only for very small voltages, $\Psi_D \ll kT/e$, in a dilute solution [28, 14, 95], it manages to describe many features of ICEO flows at much larger voltages.

There has been extensive theoretical work using the Standard Model, and it provides the basis for most of our understanding of induced-charge electrokinetics. In recent years, it has been widely used to model nonlinear electrokinetic phenomena in microfluidic devices, such as ACEO flows around electrode pairs [10, 27, 28, 29, 100] and arrays [11, 30, 40, 41, 42, 43, 101, 102], traveling-wave electro-osmotic flows (TWEO) [44, 45, 47], ICEO interactions between dielectric particles and electrodes [103, 104, 105, 106], ICEO flow around metal structures [13, 14, 17, 107, 108, 109, 48] and dielectric corners [22, 23] and particles [14, 110, 111], fixed-potential ICEO around electrodes with a DC bias [14, 112], ICEP motion of polarizable asymmetric particles [13, 14, 20, 19], collections of interacting particles [49, 50, 113, 114], particles near walls [115, 51], and particles in field gradients [19].

The Standard Model has had many successes in describing all of the these phenomena, but it also has some fundamental shortcomings, when compared to experimental data. Some theoretical studies have gone beyond the thin double layer approximation to solve the linearized equations of ion transport and fluid flow in a dilute solution in the regime of low voltages, for cases of ACEO [28] or TWEO [116] at electrode arrays or ICEP in uniform [117] or non-uniform [118] fields, but the results are mostly similar to the thin double layer limit of the Standard Model. In particular, the systematic discrepancies between theory and experiment discussed below do not seem tied to the double-layer thickness in the classical electrokinetic equations of low-voltage, dilute-solution theory. In this paper we build the case that some discrepancies are due to the fact that the classic PNP equations are not the proper starting point for many applications in nonlinear electrokinetics.

2.2. Open questions

2.2.1. The "correction factor"

Low-voltage, dilute-solution theories in nonlinear electrokinetics tend to over-predict fluid velocities, compared to experiments. A crude way to quantify this effect in the Standard Model is to multiply the HS slip velocity (5) on all surfaces by a fitting parameter Λ, the "correction factor" introduced by Green et al. [27, 29]. This approach works best at low voltages and in very dilute solutions, but even in such a regime, we should stress that it is generally impossible to choose Λ to fit complete flow profiles or multiple experimental trends, e.g. velocity vs. voltage and frequency, at the same time. Nevertheless, one can often make a meaningful fit of Λ to reproduce a key quantity, such as the maximum flow rate or particle velocity. Such a quantitative test of the model has been attempted for a number of data sets [27, 29, 17, 100, 112, 63, 21, 51], but there has been no attempt to synthesize results from different types of experiments to seek general trends in the correction factor.

As a background for our study, we provide a critical evaluation of the Standard Model based on Λ values for a wide range of experimental situations. In Table 1, we have complied all avail-

Reference	Type of Flow	Solution	c_0	$V_{max}^{induced}$	Λ	ζ_{max}	$e\zeta_{max}/kT$
Green et al. 2000 [27]	ACEO electrode pair	KCl	0.16mM	1.0 V	0.13	0.13 V	5.2
			0.67mM	1.0 V	0.055	0.055 V	2.2
			6.6mM	2.5 V	0.015	0.038 V	1.52
Green et al. 2002 [29]	ACEO electrode pair	KCl	0.16mM	0.5 V	$0.25^{\ddagger}$	0.125 V	5
			0.67mM	0.5 V	$0.24^{\ddagger}$	0.12 V	4.8
Studer et al. 2004 [34]	planar ACEO array	KCl	0.1mM	1.41 V	0.18	0.25 V	10
Ramos et al. 2005 [45]	TWEO electrode array	KCl	0.16mM	0.5 V	0.05	0.025V	1
				1.4V	0.026	0.036 V	1.44
Bown et al. 2006 [100]	Disk electrode ACEO	KCl	0.43mM	2.0 V	0.0025	0.005 V	0.2
Urbanski et al. 2007 [41]	3D ACEO array	KCl	3μM	1.5 V	0.2^{*}	0.3 V	12
Bazant et al. 2007 [37]	planar ACEO array	KCl	0.001mM	0.75 V	1^{*}	0.75 V	30
			0.003mM		0.88^{*}	0.66 V	26.4
			0.01mM		0.65^{*}	0.49 V	19.6
			0.03mM		0.47^{*}	0.35 V	14
			0.1mM		0.41^{*}	0.31 V	12.4
			0.3mM		0.24^{*}	0.18 V	6.4
			1mM		0.10^{*}	0.075 V	3
Storey et al. 2008 [63]	planar ACEO array	KCl	0.03mM	0.75 V	0.667	0.5 V	20
Levitan et al. 2005 [17]	metal cylinder ICEO	KCl	1mM	0.25 V	$0.4^{\ddagger}$	0.1 V	4
Soni et al. 2007 [112]	fixed-potential ICEO	KCl	1mM	9.0 V	0.005	0.045	1.8
Brown et al. 2000 [30]	ACEO array	$NaNO_3$	0.1mM	1.7V	0.068^{*}	0.115V	4.6
				1.41V	0.062^{*}	0.087 V	3.5
				1.13V	0.071^{*}	0.08 V	3.2
				0.85V	0.079^{*}	0.067 V	2.7
				0.57V	0.076^{*}	0.043 V	1.7
				0.28V	0.081^{*}	0.023 V	0.92
Urbanski et al. 2006 [36]	ACEO array	water	$\approx \mu$M	1.5 V	0.25^{*}	0.375 V	15
				1.0 V	0.5^{*}	0.5 V	20
Gangwal et al. 2008 [21]	Janus particle ICEP	water	$\approx \mu$M	0.085 V	$0.14^{\dagger}$	0.012 V	0.48
Kilic & Bazant 2008 [51]		NaCl	0.1mM		$0.14^{\dagger}$	0.012 V	0.48
			0.5mM		$0.105^{\dagger}$	0.009 V	0.36
			1mM		$0.08^{\dagger}$	0.007 V	0.27
			3mM		$0.048^{\dagger}$	0.004 V	0.16

Table 1: Comparison of the standard low-voltage model of induced-charge electrokinetic phenomena with experimental data (column 1) for a wide range of situations (column 2), although limited to a small set of aqueous electrolytes (column 3) at low bulk salt concentrations c_0 (column 4). In each case, the nominal maximum induced double-layer voltage V_{max} is estimated (column 5). A crude comparison with the Standard Model is made by multiplying the predicted slip velocity (5) everywhere by a constant factor Λ (column 6) for a given c_0 and V_{max}. In addition to Λ values from the cited papers, we have added entries to the table, indicated by *, by fitting our own standard-model simulations to published experimental data. Estimates indicated by ‡ assume a frequency-dependent constant-phase-angle impedance for the double layer, and those labeled by † are affected by particle-wall interactions, which are not fully understood. In each case, we also estimate the maximum induced zeta potential $\zeta_{max} = V_{max}\Lambda$ (column 7) in Volts and in units of thermal voltage kT/e (column 8).

able results from the literature. We have also added many entries by fitting our own Standard-Model simulations to published data, for which no comparison has previously been done.

It is striking that Λ is never larger than unity and can be orders of magnitude smaller. We managed to find only one published measurement where the Standard Model correctly predicts the maximum of the observed flow ($\Lambda = 1$), from a recent experiment on ACEO pumping of micromolar KCl by a planar, gold electrode array at relatively low voltage [37], but even in that data set the model fails to predict weak flow reversal at high frequency and salt concentration dependence (see below). Remarkably, there has not yet been a single ICEO experiment where the model has been able to predict, or even to fit, how the velocity depends on the basic operating conditions – voltage, AC frequency, and salt concentration – let alone the dependence on surface and bulk chemistries. The greatest discrepancies come from ACEO pumping by a disk-annulus electrode pair [100] ($\Lambda = 0.0025$) and fixed-potential ICEO around a metal stripe [112] ($\Lambda = 0.005$), both in millimolar KCl and at high induced voltages V_{max}.

In Table 1, we have also used Λ to convert the maximum nominal voltage V_{max} induced across the double layer in each experiment to a maximum zeta potential $\zeta_{max} = \Lambda V_{max}$. The range of ζ_{max} is much smaller for Λ, but still quite significant. It is clear that ζ_{max} rarely exceeds $10kT/e$, regardless of the applied voltage. For very dilute solutions, the largest value in the Table, $\zeta_{max} = 0.75\text{V} = 30kT/e$, comes from ACEO pumping of micromolar KCl [37], while the smallest values, $\zeta_{max} < 0.5kT/e$, come from ICEP of gold-latex Janus particles in millimolar NaCl.

The values of Λ and ζ_{max} from all the different experimental situations in Table 1 are plotted versus c_0 andV_{max} in Fig. 2, and some general trends become evident. In Fig. 2(b), we see that ζ_{max} decays strongly with increasing salt concentration and becomes negligible in most experiments above 10 mM. In Fig. 2(c), we see that ζ_{max} exhibits sub-linear growth with V_{max} and appears to saturate below ten times times the thermal voltage ($10kT/e = 0.25$ V at room temperature), or much lower values at high salt concentration. Even with applied voltages up to 10 Volts in dilute solutions, the effective maximum zeta potential tends to stay well below 1 Volt. From the perspective of classical electrokinetic theory, this implies that most of the voltage applied to the double layer is dropped across the immobile, inner "compact layer", rather than the mobile outer "diffuse layer", where electro-osmotic flow is generated.

This effect can be qualitatively, but not quantitatively, understood using the Standard Model. Many authors have assumed a uniform, uncharged Stern layer (or dielectric thin film) of permittivity ε_S and thickness $h_S = \varepsilon_S/C_S$, acting as a capacitor in series with the diffuse layer. Via Eq. (3), this model implies

$$\Lambda = \frac{1}{1+\delta}, \quad \text{with} \quad \delta = \frac{C_D}{C_S} = \frac{\varepsilon_b}{\varepsilon_S}\frac{h_S}{\lambda_D} = \frac{\lambda_S}{\lambda_D}, \tag{6}$$

where λ_D is the Debye-Hückel screening length (diffuse-layer thickness) and λ_S is an effective width for the Stern layer, if it were a capacitor with the same dielectric constant as the bulk. Inclusion of the Stern layer only transfers the large, unexplained variation in the correction factor Λ to the parameter λ_S (or $C_S = \varepsilon_b/\lambda_S$) without any theoretical prediction of why it should vary so much with voltage, concentration, and geometry. Using these kinds of equivalent circuit models applied to differential capacitance measurements [119], electrochemists sometimes infer a tenfold reduction in permittivity in the Stern layer versus bulk water, $\varepsilon_b/\varepsilon_S \approx 10$, but, even if this were always true, it would still be hard to explain the data. For many experimental situations in Table 1, the screening length λ_D is tens of nanometers, or hundreds of molecular widths, and the effective Stern-layer width λ_S would need to be much larger – up to several microns – to

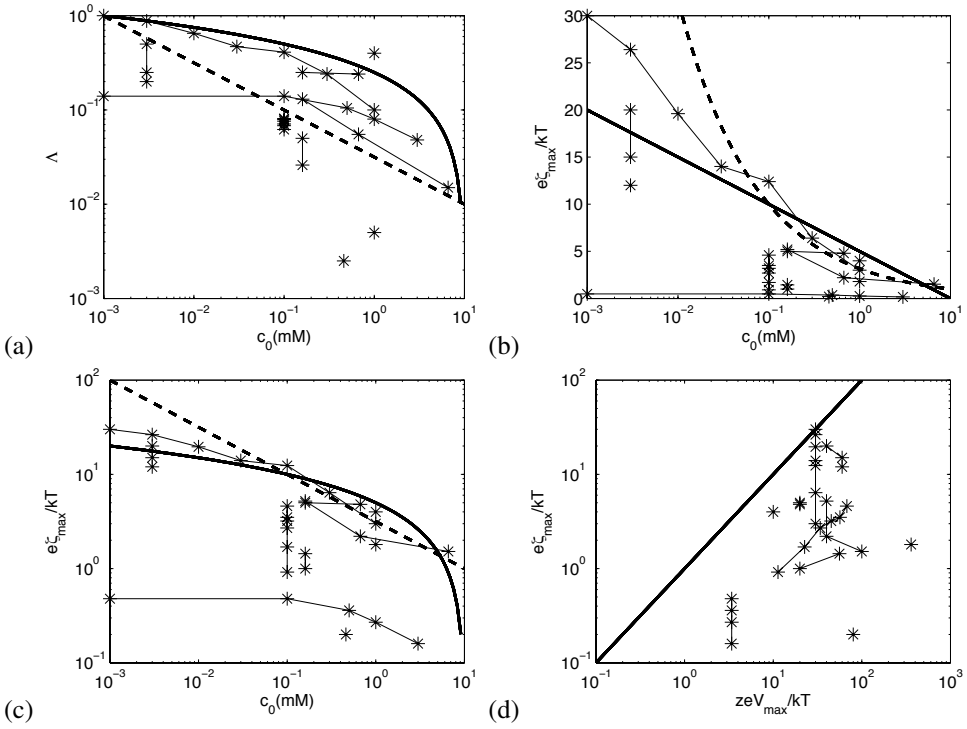

Figure 2: General trends in the under-prediction of ICEO flow velocity by the Standard Model from Table 1, compared with (solid and dashed) scaling curves, simply to guide the eye. (a) Log-log plot of Λ vs. c_0 compared with the curves $\Lambda = \sqrt{10^{-3}\mathrm{mM}/c_0}$ (dashed) and $= \ln_{10}(10\mathrm{mM}/c_0)/4$ (solid); (b) log-linear plot and (c) log-log plot of ζ_{max} vs. c_0 compared with the curves $e\zeta_{max}/kT = \sqrt{10\mathrm{mM}/c_0}$ (dashed) and $= 5\ln_{10}(10\mathrm{mM}/c_0)$ (solid); and (d) log-log plot of ζ_{max} vs. V_{max} compared to $\zeta_{max} = V_{max}$ (solid). Points from the same experiment (varying concentration or voltage) are connected by line segments.

predict the observed values of $\Lambda \ll 1$. In contrast, if we take the physical picture of a Stern monolayer literally, then h_S should be only a few Angstroms, and λ_S at most a few nanometers, so there is no way to justify the model. As noted in early papers by Brown et al. [30] and Green et al. [27] , it is clear that the effective diffuse-layer voltage (or induced zeta potential) is not properly described by the Standard Model under typical experimental conditions.

2.2.2. Electrolyte dependence

In addition to overestimating experimental velocities, the standard model fails to predict some important phenomena, even qualitatively. For example, ICEO flows have a strong sensitivity to solution composition, which is under-reported and unexplained. Most experimental work has focused on dilute electrolytes [30, 27, 120, 17]. (See Table 1.) Some recent experiments suggest a logarithmic decay of the induced electro-osmotic mobility, $b \propto \ln(c_c/c_0)$, with bulk concentration c_0 seen in KCl for ACEO micropumps [34, 37], in KCl and $CaCO_3$ for ICEO flows around metal posts [121], and in NaCl for ICEP motion of metallo-dielectric Janus particles [21]. This trend is visible to some extent at moderate concentrations in Fig. 2(b) over a wide range of experimental conditions, although a power-law decay also gives a reasonable fit at high salt concentrations. Two examples of different nonlinear electrokinetic phenomena (ACEO fluid pumping and ICEP particle motion) showing this unexplained decay with concentration are shown in Fig. 3.

In all experiments, such as those in Fig. 2, the flow practically vanishes for $c_0 > 10$ mM, which is two orders of magnitude below the salinity of most biological fluids and buffer solutions ($c_0 > 0.1$ M). Experiments with DC [122, 123] and AC [124, 112] field-effect flow control, where a gate voltage controls the zeta potential of a dielectric channel surface, have likewise been limited to low salt concentrations below 10 mM in a variety of aqueous solutions. Indeed, we are not aware of any reported observations of induced-charge electrokinetic phenomena at significantly higher salt concentrations.

The Standard Model seems unable to explain the decay of flow with increasing salt concentration quantitatively, although it does aid in qualitative understanding. Substituting the Debye-Hückel screening length for a binary $z:z$ electrolyte in (6) we obtain

$$\Lambda = \frac{1}{1+\sqrt{c_0/c_c}} \sim \sqrt{\frac{c_c}{c_0}} \quad \text{for } c_0 \gg c_c \tag{7}$$

where

$$c_c = \frac{kT}{2\varepsilon_b}\left(\frac{\varepsilon_S}{h_S z e}\right)^2 = \frac{\varepsilon_b kT}{2(ze)^2\lambda_S^2} \tag{8}$$

is a crossover concentration, above which the flow decays like the inverse square-root of concentration. As noted above, it is common to attribute the theoretical over-prediction of ICEO flows, even in very dilute solutions to a large voltage drop across the compact layer ($\delta \gg 1$), but this would imply a strong concentration dependence ($c_0 \gg c_c$) that is not observed. Alternatively, fitting the compact-layer capacitance to reproduce the transition from dilute to concentrated solution behavior ($c_0 \approx c_c$, $\delta \approx 1$) would eliminate the correction factor in dilute solutions ($\delta \ll 1$), making the theory again over-predict the observed velocities. For example, such difficulties are apparent in Ref. [51] where this argument applied to the data of Gangwal et al [21] for ICEP motion of metallo-dielectric Janus particles (Fig. 3(a)).

Beyond the dependence on salt concentration, another failing of dilute-solution theory is the inability to explain the experimentally observed ion-specificity of ICEO phenomena. At the same bulk concentration, it has been reported that ICEO flow around metal posts [121],

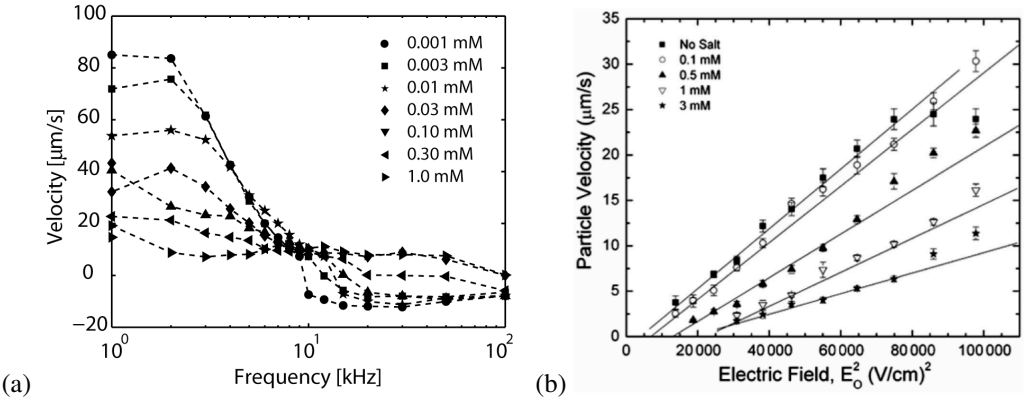

Figure 3: Typical experimental data (included in the estimates of Table 1) for two different types of nonlinear, induced-charge electrokinetic phenomena showing qualitative features not captured by the Standard Model, or the underlying electrokinetic equations of dilute solution theory. (a) Velocity of ACEO pumping of dilute aqueous solutions of KCl around a microfluidic loop by an asymmetric planar Au electrode array with the geometry of Refs [30, 34] versus AC frequency at constant voltage, 3 Volts peak to peak (V_{max} = 1.5 V), reproduced from Ref. [37]. The data exhibits the unexplained flow reversal at high frequency (10 – 100 kHz) and strong concentration dependence first reported in Ref. [34]. (b) Velocity of ICEP motion of 5.7 μm metallo-dielectric Janus particles versus field-squared at different concentrations of NaCl in water at constant 1kHz AC frequency, reproduced from Ref. [21]. The data shows a similar decay of the velocity with increasing bulk salt concentration, which becomes difficult to observe experimentally above 10mM, in both experiments.

ACEO pumping by electrode arrays [37] and AC-field induced interactions in colloids [125] depend on the ions. Comparing experiments under similar conditions with different electrolytes or different metal surfaces further suggests a strong sensitivity to the chemical composition of the double layer, although more systematic study is needed. In any case, none of these effects can be captured by the Standard Model, which posits that the ions are simply mathematical points in a dielectric continuum and that the surface is a homogeneous conductor or dielectric; all specific physical or chemical properties of the ions, solvent molecules, and the surface are neglected.

2.2.3. Flow reversal

In many situations of large induced voltages, the Standard Model does not even correctly predict the direction of the flow, let alone its magnitude. Flow reversal was first reported around tin particles in water [26], where the velocity agreed with the theory [15, 24] only for micron-sized particles and reversed for larger ones (90 – 400μm). The transition occured when several volts was applied across the particle and reversal was conjectured to be due to Faradaic reactions [26]. Flow reversal has also been observed at high voltage (> 2 V) and high frequency (10-100 kHz) in ACEO pumping by 10μm-scale planar electrode arrays for dilute KCl [34, 36, 37, 46], as shown in Fig. 3(b), although not for water in the same pump geometry [30, 36]. Non-planar 3D stepped electrodes [40] can be designed that do not exhibit flow reversal, as demonstrated for KCl [41], but certain non-optimal 3D geometries still reverse, as observed in deionized water [36]. In the latter case the frequency spectrum also develops a double peak with the onset of flow reversal around 3 Volts peak to peak. In travelling-wave electro-osmosis (TWEO) in aqueous electrolytes [44, 45], strong flow reversal at high voltage has also been observed, spanning all frequencies [45, 46, 126], and not yet fully understood.

Flow reversal of ACEO was first attributed to Faradaic reactions under different conditions of larger voltages (8-14 V) and frequencies (1-14 MHz) in concentrated NaCl solutions ($0.001 - 0.1$ S/m) with a 100μm-scale T-shaped electode pair composed of different metals (Pt, Al, Chromel) [127]. Indeed, clear signs of Faradaic reactions (gas bubbles) can always be observed at sufficiently large voltage, low frequency and high concentration [34, 127]. In recent TWEO experiments [126], signatures of Faradaic reactions have also been correlated with low-frequency flow reversal at high voltage. Under similar conditions another possible source of flow reversal is AC electrothermal flow driven by bulk Joule heating [128], which has been implicated in reverse pumping over planar electrode arrays at high salt concentrations [129]. Closer to standard ACEO conditions, e.g. at 1-2 V and 50-100 Hz in water with Au electrode arrays, flow reversal can also be induced by applying a DC bias voltage of the same magnitude as the AC voltage [130, 131]. Reverse ACEO flow due to "Faradaic charging" (as opposed to the standard case of "capacitive charging") is hypothesized to grow exponentially with voltage above a threshold for a given the electrolyte/metal interface [127, 131], but no quantitative theory has been developed.

Simulations of the standard low-voltage model with Butler-Volmer kinetics for Faradaic reactions have only managed to predict weak flow reversal at low frequency in ACEO [11, 38, 39] and TWEO [47, 116]. In the case of ACEO with a planar, asymmetric electrode array, this effect has recently been observed using sensitive (μm/s) velocity measurements in dilute KCl with Pt electrodes at low voltage (< 1.5 V) and low frequency (< 20 kHz) [132]. Faradaic reactions can also produce an oscillating quasi-neutral diffusion layer between the charged diffuse layer and the uniform bulk, due to the normal flux of ions involved in reactions, and recently it has been shown via a low-voltage, linearized analysis of TWEO that flow reversal can arise in the case of ions of unequal diffusivities due to enhanced diffusion-layer forces on the fluid [116]. However, current models cannot predict the strong ($> 100\mu$m/s), high-frequency (> 10 kHz) flow reversal seen in many ACEO and TWEO experiments [34, 36, 46, 37]. Faradaic reactions generally reduce the flow at low frequency by acting as a resistive pathway to "short circuit" the capacitive charging of the double layer [38, 47], and diffusion-layer phenomena are also mostly limited to low frequency. Resolving the apparent paradox of high-frequency flow reversal is a major motivation for our study.

2.3. Nonlinear dynamics in a dilute solution

Dilute-solution theories generally predict that nonlinear effects dominate at low frequency. One reason is that the differential capacitance C_D of the diffuse layer, and thus the "RC" time for capacitive charging of a metal surface, grows exponentially with voltage in nonlinear Poisson-Boltzmann (PB) theory. The familiar PB formula for the diffuse-layer differential capacitance of a symmetric binary electrolyte [5, 95],

$$C_D^{PB}(\Psi_D) = \frac{\varepsilon_b}{\lambda_D} \cosh\left(\frac{ze\Psi_D}{2kT}\right) \tag{9}$$

was first derived by Chapman [133], based on Gouy's solution of the PB model for a flat diffuse layer [134]. It has been shown that this nonlinearity shifts the dominant flow to lower frequencies at high voltage in ACEO [38] or TWEO [135] pumping. It also tends to suppress the flow with increasing voltage at fixed frequency, since there is not adequate time for complete capacitive charging in a single AC period.

At the same voltage where nonlinear capacitance becomes important, dilute-solution theory also predicts that salt adsorption [95, 97, 136] and tangential conduction [97, 137] by the diffuse

layer also occur and are coupled to (much slower) bulk diffusion of neutral salt, which would enter again at low frequency in cases of AC forcing. If concentration gradients have time to develop, then they generally alter the electric field ("concentration polarization") and can drive diffusio-osmotic slip [138, 7, 98] or even second-kind electro-osmotic flow [139, 98, 99] (if the bulk concentration goes to zero, at a limiting current). Concentration polarization has been demonstrated around electrically floating and (presumably) blocking metal posts in DC fields and applied to microfluidic demixing of electrolytes [140]. In nonlinear electrokinetics, diffusion-layer phenomena have begun to be considered in low-voltage, linearized analysis of TWEO with Faradaic reactions [116], but such effects are greatly enhanced in the strongly nonlinear regime and as yet unexplored. Including all of these effects in models of induced-charge electrokinetic phenomena presents a formidable mathematical challenge.

To our knowledge, such complete modeling within the framework of dilute solution theory has only been accomplished recently in the case of ACEO pumping (albeit without Faradaic reactions) by applying asymptotic boundary-layer methods to the classical electrokinetic equations in the thin-double-layer limit [39]. At least in this representative case, all of the nonlinear large-voltage effects in dilute solution theory tend to make the agreement with experiment worse than in the Standard Model. The flow is greatly reduced and shifts to low frequency, while the effects of salt concentration and ion-specificity are not captured. Similar conclusions have been reached by a recent numerical and experimental study of fixed-potential ICEO for DC bias of 9 Volts [112], where the correction factor is found to be $\Lambda = 0.005$ for the linear theory, but only $\Lambda = 0.05$ if nonlinear capacitance (9) and surface conduction from PB theory are included in the model (albeit without accounting for bulk concentration gradients).

Although more theoretical work is certainly needed on nonlinear dynamics in response to large voltages, especially in the presence of Faradaic reactions, we believe the time has come to question the validity of the underlying electrokinetic equations themselves. Based on experimental and theoretical results for induced-charge electrokinetic phenomena, we conclude that dilute solution theories do not properly describe the dynamics of electrolytes at large voltages. In the following sections, we consider some simple, fundamental changes to the Standard Model and the underlying electrokinetic equations. We review relevant aspects of mean-field concentrated-solution theories and develop some new ideas as well. Through a variety of model problems in nonlinear electrokinetics, we make theoretical predictions using modified electrokinetic equations, which illustrate qualitative new phenomena, not predicted by the Standard Model and begin to resolve some of the experimental puzzles highlighted above.

3. Crowding effects in a concentrated solution

3.1. Mean-field theory

3.1.1. Modified Poisson-Boltzmann models

All dilute solution theories, which describe point-like ions in a mean-field approximation, break down when the crowding of ions becomes significant, and steric repulsion and correlations potentially become important. If this can be translated into a characteristic length scale a for the distance between ions, then the validity of Poisson-Boltzmann theory is limited by a cutoff concentration $c_{max} = a^{-3}$, which is reached at a fairly small diffuse-layer voltage,

$$\Psi_c = -\frac{kT}{ze} \ln\left(\frac{c_{max}}{c_0}\right) = \frac{kT}{ze} \ln(a^3 c_0). \tag{10}$$

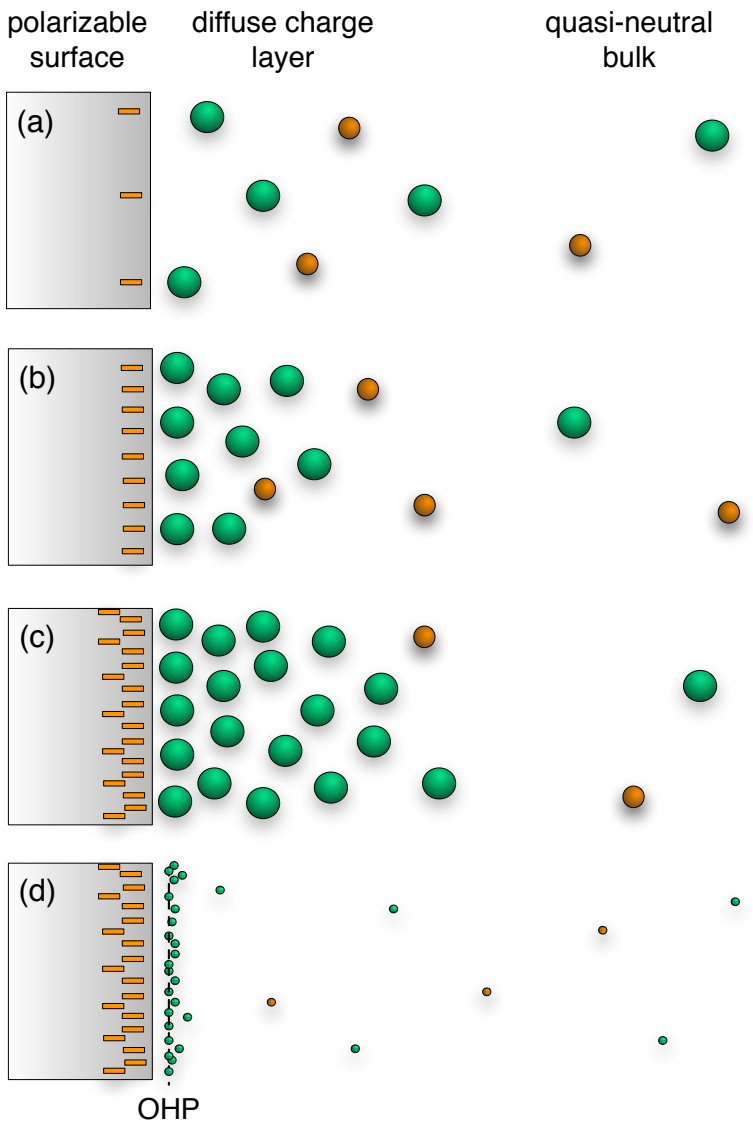

Figure 4: Sketch of solvated counterions (larger green spheres) and co-ions (smaller orange spheres) near a polarizable surface. (a) At small induced voltages, $\Psi_D \ll \Psi_c$, the neutral bulk is only slightly perturbed with a diffuse-charge layer of excess counterions at the scale of λ_D. (b) At moderate voltages, $\Psi_D \approx \Psi_c$, the diffuse layer contracts, as described by Poisson-Boltzmann (PB) theory. (c) At large voltages, $\Psi_D \gg \Psi_c$, the counterions inevitably become crowded, causing expansion of the diffuse layer compared to the predictions of the classical Gouy-Chapman-Stern model, sketched in (d), which is based PB theory for point-like ions with a minimum distance of approach, the "outer Helmholtz plane" (OHP), to model solvation of the surface.

where z is the valence (including its sign) and c_0 the bulk concentration of the counterions. In a dilute solution of small ions, this leads to cutoffs well below typical voltages for ICEO flows. For example, even if only steric effects are taken into account, with e.g. $a = 3$ Å(for solvated bulk K^+ - Cl^- interactions [141]), then $\Psi_c \approx 0.33V$ for $c_0 = 10^{-5}$ M and $z = 1$.

To account for the obvious excess ions in PB theory, Stern [142] long ago postulated a static compact monolayer of solvated ions [119]. A similar cutoff is also invoked in models of ICEO flows, where a constant capacitance is added to model the Stern layer and/or a dielectric coating, which carries most of the voltage when the diffuse-layer capacitance (9) diverges. However, it seems unrealistic that a monolayer could withstand most of the voltage drop in induced-charge electrokinetic phenomena (e.g. without dielectric breakdown [143], loss of solvation, or reactions). In any case, a *dynamical* model is required for a "condensed layer" that is built and destroyed as the applied field alternates. As sketched in Fig. 4, the condensed layer forms in the diffuse part of the double layer and thus should be described by the same ion transport equations.

A variety of "modified Poisson-Boltzmann" (MPB) theories have been proposed to describe equilibrium ion profiles near a charged wall (e.g. as reviewed in Refs. [56, 58, 144, 145, 146]), and we have recently extended some of these approaches to dynamical situations at large voltages [56, 96]. The starting point is a model for the excess electrochemical potential of an ion

$$\mu_i^{ex} = \mu_i - \mu_i^{ideal} = kT \ln f_i, \tag{11}$$

relative to its ideal value in a dilute solution,

$$\mu_i^{ideal} = kT \ln c_i + z_i e\phi, \tag{12}$$

where c_i is the mean concentration and f_i is the chemical activity coefficient. (Equivalently, one can write $\mu_i = kT \ln(\lambda_i) + z_i e\phi$, where $\lambda_i = f_i c_i$ is the absolute chemical activity [147].) In the mean-field approximation, the electrostatic potential ϕ self-consistently solves the MPB equation,

$$-\nabla \cdot (\varepsilon \nabla \phi) = \rho = \sum_i z_i e c_i, \tag{13}$$

with the mean charge density ρ. Time-dependent modified Poisson-Nernst-Planck equations then express mass conservation with gradient-driven fluxes [96].

In the asymptotic limit of thin double layers, it is often justified to assume that the ions are in thermal equilibrium, if the normal current is not too large and the nearby bulk salt concentration is not too low [148, 149], even in the presence of electro-osmotic flow [98, 99]. In terms of electrochemical potentials, the algebraic system $\{\mu_i = \text{constant}\}$ then determines the ion profiles c_i in the diffuse layer, which lead to effective surface conservation laws [137]. In dilute-solution theory, this procedure yields the Boltzmann distribution,

$$c_i(\psi) = c_i^0 \exp\left(\frac{-z_i e\psi}{kT}\right), \tag{14}$$

where $\psi = \phi - \phi_b$ is the potential relative to its bulk value ϕ_b just outside the double layer, and the Gouy-Chapman charge density,

$$\rho(\psi) = -2c_0 ze \sinh\left(\frac{ze\psi}{kT}\right), \tag{15}$$

for a symmetric binary electrolyte ($z_\pm = \pm z$).

In concentrated-solution theories [56, 58, 144, 150, 151], the choice of a model for μ_i^{ex} yields a modified charge density profile ρ, differing from (15) with increasing voltage. In this section, we focus on entropic contributions, where μ_i^{ex} depends on the ion concentrations (but not, e.g., explicitly on the distance to a wall [91, 152], as discussed below). In that case, the equilibrium charge density can be expressed as a function of the potential, $\rho(\psi)$, although the Boltzmann distribution (15) is generally modified for non-ideal behavior. For any such mean-field theory, by integrating the MPB equation and setting ε =constant, we obtain the electrostatic pressure, $p_e = \frac{1}{2}\varepsilon E^2$, at the inner edge of the diffuse layer,

$$p_e(\Psi_D) = \int_{\Psi_D}^{0} \rho(\psi) d\psi. \tag{16}$$

From the total diffuse charge per unit area,

$$q = -\mathrm{sign}(\Psi_D)\sqrt{2\varepsilon p_e(\Psi_D)}, \tag{17}$$

we then arrive at a general formula for the differential capacitance,

$$C_D(\Psi_D) = -\frac{dq}{d\Psi_D} = -\rho(\Psi_D)\sqrt{\frac{2\varepsilon}{p_e(\Psi_D)}}, \tag{18}$$

which reduces to (9) in a dilute solution.

3.1.2. The Bikerman-Freise formula

Since most MPB models are not analytically tractable, we first illustrate the generic consequences of steric effects using the oldest and simplest mean-field theory [142, 55, 153, 154, 56, 70]. This model has a long and colorful history of rediscovery in different communities and countries (pieced together here with the help of P. M. Biesheuvel, Wageningen). It is widely recognized that O. Stern in 1924 [142] was the first to cutoff the unphysical divergences of the Gouy-Chapman model of the double layer [134, 133] by introducing the concept of a "compact layer" or "inner layer" of solvent molecules (and possibly adsorbed ions) forming a thin mono-molecular coating separating an electrode from the "diffuse layer" in the electrolyte phase. The resulting two-part model of the double layer has since become ingrained in electrochemistry [119]. Over the years, however, it has somehow been overlooked that in the same groundbreaking paper [142], Stern also considered volume constraints on ions in the electrolyte phase and in his last paragraph, remarkably, wrote down a modified charge-voltage relation [his Eq. (2')] very similar to Eq. (21) below, decades ahead of its time. We have managed to find only one reference to Stern's formula, in a footnote by Freise [153].

Although Stern had clearly introduced the key concepts, it seems the first complete MPB model with steric effects in the electrolyte phase was proposed by J. J. Bikerman in 1942, in a brilliant, but poorly known paper [55]. (Bikerman also postulated forces on hydrated-ion dipoles in non-uniform fields, which we neglect here.) Over the past sixty years, Bikerman's MPB equation has been independently reformulated by many authors around the world, including Grimley and Mott (1947) in England [74, 75], Dutta and Bagchi (1950) in India [155, 156, 157, 158], Wicke and Eigen (1951) in Germany [159, 160, 161], Iglic and Kralj-Iglic (1994) in Slovenia [162, 163, 164, 165], and Borukhov, Andelman and Orland (1997) in Israel and France [154, 166, 167]. For an early review of electrolyte theory, which cites papers of Dutta, Bagchi, Wicke and Eigen up

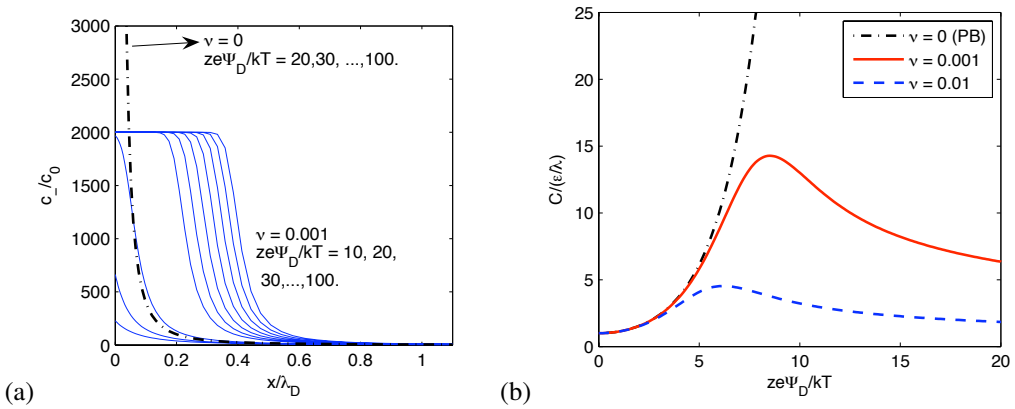

Figure 5: (a) The equilibrium distribution of counterions in a flat diffuse layer for large applied voltages $ze\Psi_D/kT = 10, 20, \ldots, 100$ predicted by Poisson-Boltzmann theory (PB) and Bikerman's modified theory (MPB) taking into account an effective (solvated) ion size a, where $\nu = 2a^3c_0 = 0.001$ is the bulk volume fraction of solvated ions. (b) The diffuse-layer differential capacitance C_D vs. voltage predicted by PB (9) ($\nu = 0$) and MPB (22) ($\nu > 0$), scaled to the low-voltage Debye-Hückel limit $\varepsilon/\lambda_D(c_0)$.

to 1954 (but not Bikerman or Freise, discussed below), see Redlich and Jones [168]. Unlike Bikerman, who applied continuum volume constraints to PB theory, all of these subsequent authors derived the same MPB model starting from the microscopic statistical mechanics of ions and solvent molecules on a cubic lattice of spacing a in the continuum limit, where the concentration profiles vary slowly over the lattice. While early authors were concerned with departures from PB theory in concentrated electrolytes [55, 155, 161] or ionic crystals [74, 75, 76], recent interest in the very same mean-field model has been motivated by modern applications to electrolytes with large ions [154, 166, 167], polyelectolytes [169, 170, 171], polymeric electrolytes [172], electrolytes confined in nanopores [64, 65], and solvent-free ionic liquids [70, 71, 73], in addition to our own work on simple electrolytes in large applied voltages [56, 96, 54].

In the present terminology, Bikerman's model corresponds to an excess chemical potential

$$\mu_i^{ex} = -kT \ln(1 - \Phi) \quad \text{(Bikerman)}\,, \tag{19}$$

associated with the entropy of the solvent, where $\Phi = a^3 \sum_i c_i$ is the local volume fraction of solvated ions on the lattice [58]. For now, we also assume a symmetric binary electrolyte, $c_+^0 = c_-^0 = c_0$, $z_\pm = \pm z$, to obtain an analytically tractable model. As shown in Fig. 5(a), when a large voltage is applied, the counterion concentration exhibits a smooth transition from an outer PB profile to a condensed layer at $c = c_{max} = a^{-3}$ near the surface. Due to the underlying lattice-gas model for excluded volume, the ion profiles effectively obey Fermi-Dirac statistics,

$$c_\pm = \frac{c_0 e^{\mp ze\psi/kT}}{1 + 2\nu \sinh^2(ze\psi/2kT)}, \tag{20}$$

where $\nu = 2a^3c_0 = \Phi_{bulk}$ is the bulk volume fraction of solvated ions. Classical Boltzmann statistics and the Gouy-Chapman PB model are recovered in the limit of point-like ions, $\nu = 0$.

For a flat double layer, similar results can be obtained with the even simpler Composite Diffuse Layer model of Kilic et al. [56] (also termed the "cutoff model" in Ref. [144]), where an

outer PB diffuse layer is abrubtly patched with an inner condensed layer of only counterions at the uniform, maximal charge density. This appealingly simple construction requires assumptions about the shape of the condensed layer (e.g. a plane), so its position can be determined only from its thickness or total charge. Even if it can be uniquely defined, the cutoff model introduces discontinuities in the co-ion concentration (which drops to zero in the condensed layer) and in the gradient of the counter-ion concentration, although the same is also true of Stern's original model of the compact layer. In this work we focus on Bikerman's model since it is the simplest general model of steric effects that remains analytically tractable; unlike the cutoff model, it predicts smooth ionic concentration profiles in any geometry and can be naturally extended to time-dependent problems [96].

For Bikerman's MPB theory, the charge-voltage relation for the diffuse layer (17) takes the form [56],

$$q_\nu = \mathrm{sgn}(\Psi_D) 2zec_0\lambda_D \sqrt{\frac{2}{\nu}\ln\left[1 + 2\nu \sinh^2\left(\frac{ze\Psi_D}{2kT}\right)\right]} \tag{21}$$

which was probably first derived by Grimley [75] in a lattice-gas theory of diffuse charge in ionic crystals, independent of Bikerman. Grimley's formula has the same form as Stern's surprising Eq. (2') noted above [142] but has all the constants correct and clearly derived. Recently, Soestbergen et al.[172] have given a slightly different formula approximating (21) that is easier to evaluate numerically for large voltages, and applied it to ion transport in epoxy resins encapsulating integrated circuits.

Although Stern and Grimley derived the modified form of the charge-voltage relation with volume constraints, they did not point out its striking qualitative differences with Gouy-Chapman dilute-solution theory. This important aspect was first clarified by Freise [153], who took the derivative of (21) and derived the differential capacitance (18) in the form

$$C_D^\nu = \frac{\frac{\varepsilon}{\lambda_D}\sinh(\frac{ze\Psi_D}{kT})}{[1 + 2\nu\sinh^2\left(\frac{ze\Psi_D}{2kT}\right)]\sqrt{\frac{2}{\nu}[1 + 2\nu\sinh^2\left(\frac{ze\Psi_D}{2kT}\right)]}}. \tag{22}$$

and pointed out that C_D^ν decays at large voltages. This is the opposite dependence of Chapman's formula (9) from dilute-solution theory, which diverges exponentially with $|\Psi_D|$. Since Chapman [133] is given credit in "Gouy-Chapman theory" for first deriving the capacitance formula (9) for Gouy's original PB model [134], we suggest calling Eq. (22) the "Bikerman-Freise formula" (BF), in honor of Bikerman, who first postulated the underlying MPB theory, and Freise, who first derived and interpreted the modified differential capacitance. By this argument, it would be reasonable to also refer to the general MPB model as "Bikerman-Freise theory", but we will simply call it "Bikerman's model" below, following Refs. [64, 65, 58].

As shown in Fig. 5(b), the BF differential capacitance (22) increases according to PB theory up to a maximum near the critical voltage $\Psi_D \approx \Psi_c$, and then *decreases at large voltages* as the square-root of the voltage,

$$C_D^\nu \sim \sqrt{\frac{ze\varepsilon_b}{2a^3|\Psi_D|}}, \tag{23}$$

because the effective capacitor width grows due to steric effects, as seen in Fig. 5(a). In stark contrast, the PB diffuse-layer capacitance diverges exponentially according to Eq. (9), since point-like ions pile up at the surface. Although other effects, notably specific adsorption of ions [119] (discussed below) can cause the capacitance to increase at intermediate voltages, this effect is

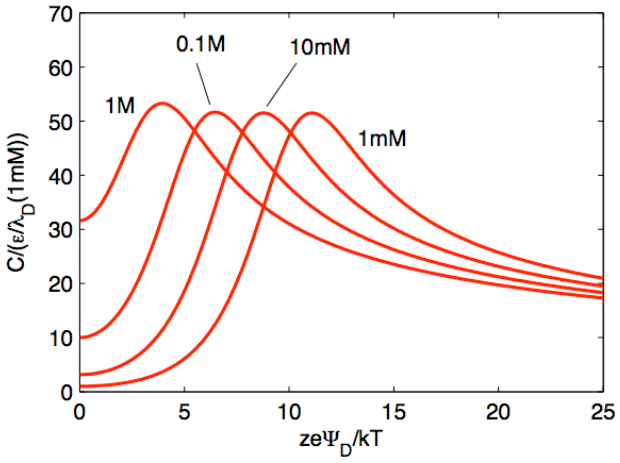

Figure 6: Differential capacitance C_D vs. voltage in Bikerman's MPB model (22) with $a = 4$Åfor ν values corresponding to $c_0 = 1, 10, 100$ mM. In contrast to Fig. 5(b), here C_D is scaled to a single constant, $\varepsilon/\lambda_D(1\text{mM})$, for all concentrations.

quite general. As long as the surface continues to block Faradaic current, then the existence of steric volume constraints implies the growth of an extended condensed layer at sufficiently large voltages, and a concomitant, universal decay of the differential capacitance. Indeed, this effect can be observed for interfaces with little specific adsorption, such as NaF and KPF_6 on Ag [173, 174] or Au [175], and fitted by models accounting for steric repulsion [150, 151]. The same square-root dependence at large voltage can also be observed in experiments [70] and simulations [71, 72] of ionic liquids at blocking electrodes, with remarkable accuracy. We conclude that the decay of the double-layer differential capacitance at large voltage is a universal consequence of the crowding of finite-sized, mobile charge carriers near a highly charged, blocking surface.

The BF formula (23) also illustrates another general feature of double-layer models with steric constraints, shown in Fig. 6: The differential capacitance at large voltages is *independent of bulk concentration, but ion specific* through z and a. This prediction is reminiscent of Stern's picture [142] of an inner, compact layer, which carries most of the double layer charge at large voltage, compared to the outer, diffuse layer described by dilute PB theory, as supported by Grahame's famous experiments on mercury electrodes [176]. The significant difference, however, is that the condensed layer forms continuously in the solution near the inner edge of the diffuse layer due to ion crowding effects in a general model of the electrolyte phase, which is not restricted to flat quasi-equilibrium double layers.

This approach provides a more natural basis to describe the dynamics of the electrolyte in response to the applied voltage. There is no need to introduce a separate model for ion transfer to an "outer Helmholtz plane" (OHP) of solvated ions near the surface, which are arbitrarily and discontinuously excluded from the rest of the electrolyte, as is commonly done to interpret electrochemical capacitance measurements [119]. All solvated ions are treated equally by a single model of their chemical potentials, and only activated processes of desolvation or electrochemical reactions can cause them to be removed from the electrolyte phase, such as Faradaic

reactions or specific adsorption to the "inner Helmholtz plane" on the surface (see below), which we neglect as a first approximation.

3.1.3. Hard-sphere liquid models

Although Bikerman's model describes steric effects in a convenient and robust analytical form, the bulk ionic volume fraction ν is best viewed as an empirical fitting parameter. For crystalline solid electrolytes, its microscopic basis in a lattice model is realistic, but even then, the thinness of the condensed layer, comparable to the lattice spacing at normal voltages, calls the continuum limit into question. For liquid electrolytes involved in electrokinetic phenomena, it would seem more realistic to start with the "restricted primitive model" of charged hard spheres in a uniform dielectric continuum [177] in developing better MPB models [57, 150, 58]. From this theoretical perspective, Bikerman's lattice-based model has the problem that it grossly underestimates steric effects in hard-sphere liquids; for example, in the case of a monodisperse hard-sphere liquid, the volume excluded by a particle is eight times its own volume [178, 179, 58]. Although we focus on electrolytes at large voltages, it is also interesting to consider the mean-field dynamics of charged hard spheres to model other systems, such as dense colloids [180, 181], polyelectrolytes [182, 183], and ionic liquids [70, 71].

Various approximations of μ_i^{ex} for hard-sphere liquids can be used to develop more sophisticated steric MPB models, which yield similar qualitative behavior of the diffuse-layer differential capacitance [150, 58], due to the generic arguments given above. For example, the Carnahan-Starling (CS) equation of state for a bulk monodisperse hard-sphere liquid corresponds to the following excess chemical potential [184, 6],

$$\frac{\mu_i^{ex}}{kT} = \frac{\Phi(8 - 9\Phi + 3\Phi^2)}{(1-\Phi)^3} \quad \text{(Carnahan-Starling)} \tag{24}$$

Although this algebraic form precludes analytical results, it is much simpler to evaluate numerically and incorporate into continuum models of electrokinetic phenomena than are more sophisticated MPB approximations, e.g. based on self-consistent correlation functions [67, 68, 69, 185] or density functional theory [186, 187, 188], which require solving nonlinear integro-differential equations, even for a flat double layer in equilibrium. As shown in Fig. 7(b), the simple CS MPB model predicts capacitance curves similar to Fig. 6 with Bikerman's model, respectively, only with more realistic salt concentrations [58]. In particular, the differential capacitance in Bikerman's model ressembles that of CS MPB if an unrealistically large hydrated ion size a (or large bulk volume fraction ν) is used, due to the under-estimation of liquid steric effects noted above.

In spite of similar-looking capacitance curves, however, there are important differences in the ionic profiles predicted by the two models. As shown in Fig 5(a), in Bikerman's model steric effects are very weak until the voltage becomes large enough to form a thin condensed layer at maximum packing. As such, the width of the diffuse layer at typical large voltages is still an order of magnitude smaller than the Debye length λ_D relevant for small voltages. In contrast, steric effects in a hard-sphere liquid are stronger and cause the diffuse layer to expand with voltage as shown in Fig. 7(c). The widening of the diffuse layer reduces its differential capacitance, but without forming the clearly separated condensed layer predicted by Bikerman's model. As shown in Fig. 7(d), the counterion density at the surface in the CS MPB model increases more slowly with voltage as compared to the Bikerman model. These differences will be important when we discuss the viscosity effects in Section 4.

An advantage of the hard-sphere approach to volume constraints is that it has a simple extension to mixtures of unequal particle sizes [189] which can be applied to general multicomponent

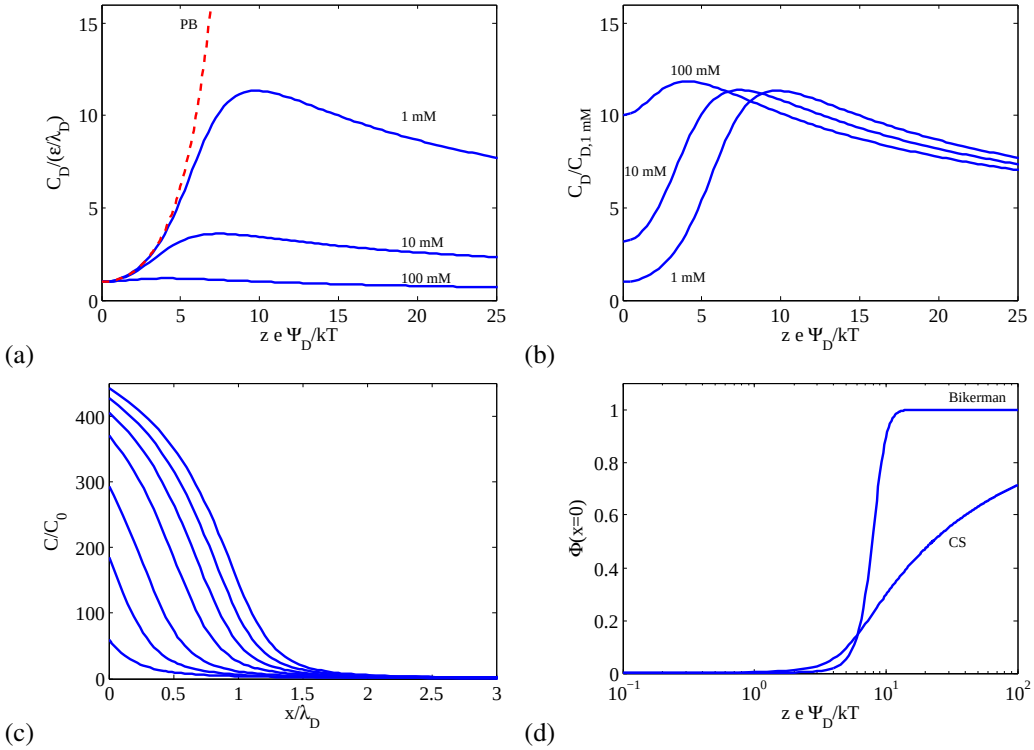

Figure 7: Modified Poisson-Boltzmann theory for a binary solution of charged hard spheres of diameter $a = 4$Åusing the Carnahan-Starling (CS) equation of state (24). (a,b) The diffuse-layer differential capacitance vs. voltage, analagous to Fig. 5 b and Fig. 6, respectively. (c) The counterion density profile in the diffuse layer at voltages $ze\Psi_D/kT = 5, 10, 20, 40, 60, 80, 100$ and concentration of $c_o = 10$ mM, analogous to Fig. 5(a). (d) The surface counterion density vs. voltage at $c_o = 10$ mM in the CS and Bikerman MPB models.

electrolytes [57, 58, 150, 183, 182]. According to the Boublik-Mansoori-Carnahan-Starling-Leland (BMCSL) equation of state [190, 191], the excess chemical potential of species i in a mixture of N species of hard spheres with different diameters $\{a_i\}$ is given by

$$\begin{aligned}\frac{\mu_i^{ex}}{kT} &= -\left(1+\frac{2\xi_2^3 a_i^3}{\Phi^3}-\frac{3\xi_2^2 a_i^2}{\Phi^2}\right)\ln(1-\Phi)+\frac{3\xi_2 a_i+3\xi_1 a_i^2\xi_0+a_i^3}{1-\Phi} \\ &+ \frac{3\xi_2 a_i^2}{(1-\Phi)^2}\left(\frac{\xi_2}{\Phi}+\xi_1 a_i\right)-\xi_2^3 a_i^3\frac{\Phi^2-5\Phi+2}{\Phi^2(1-\Phi)^3} \quad \text{(BMCSL)} \end{aligned} \tag{25}$$

where $\xi_n = \sum_{j=1}^{N}\Phi_j a_j^{n-3}$, Φ_j is the volume fraction of species j, and $\Phi = \sum_{j=1}^{N}\Phi_j$ is the total volume fraction of ions. Although this formula may seem complicated, it is an algebraic expression that can be easily expanded or evaluated numerically and thus is much simpler than statistical theories based on integral equations. The first BMCSL correction to dilute solution theory is simply,

$$\frac{\mu_i^{ex}}{kT} \sim \sum_{j=1}^{N}\left(1+\frac{a_i}{a_j}\right)^3\Phi_j \tag{26}$$

The BMCSL-MPB model for asymmetric electrolytes predicts the segregation of ions of different size and/or charge in the diffuse layer [58] and has been applied to adsorption phenomena in polyelectrolyte layers [183, 182]. The broken symmetry between ions of different sizes is an important qualitative effect, which we will show implies new electrokinetic phenomena at large voltages, regardless of the model.

3.1.4. Effective sizes for solvated ions

In order to interpret and apply our modified electrokinetic equations, it is important to stress that the effective diameter of a solvated ion is different from its bare atomic size and can exhibit very different trends. Smaller bare ions tend to be more heavily solvated and therefore have larger effective diameters [192]. Effective solvated ion sizes depend on the size and charge of the ions, the nature of the solvent, the ion concentration, and temperature – as well as the mathematical models used in their definitions. Table 2 compares bare ionic diameters in crystalline solids to effective solvated-ion diameters inferred from bulk properties [193] and "hard-sphere" diameters inferred from viscosity measurements [194], both in aqueous solutions. In these models used to interpret experimental data, the hard sphere radius is essentially a collision size, whereas the the effective solvated radius is an effective size for transport properties, similar to a Stokes radius. The effective solvated radius is generally larger than the hard sphere value. Both are greatly exceed the bare diameter and exhibit roughly opposite trends with the chemical identity of the ion.

What is the appropriate effective ion size a in our models? Unlike the models used to infer the various ion diameters in Table 2, our models seek to capture crowding effects in a highly charged double layer, rather than in a neutral bulk solution. As such, it is important to think of crowded counterions of the same sign and not a neutral mixture of oppositely charged ions (where our models reduce to the Standard Model in typical situations with dilute electrolytes). Below, we will argue that the crowding of counterions in large electric fields leads to some different physical effects. Among them, we can already begin to discuss solvation effects. In the bulk, ions cannot reach very high concentrations due to solubility limits, but a condensed layer of counterions cannot recombine and is unaffected by solubility (except for the possibility of

Ion	d_x (Å)	d_s (Å)	d_v (Å)
Li^+	1.20	7.64	4.2
Na^+	1.90	7.16	4.0
K^+	2.66	6.62	3.8
Cl^-	3.62	6.64	3.6

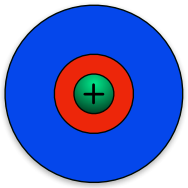

Table 2: Comparison of the bare ion diameter in a crystalline solid, d_x, with the effective solvated diameter d_s in water from bulk transport measurements (akin to a Stokes diameter) [193] and the "hard-sphere" diameter (akin to a collision cross section) inferred from viscosity data d_v in dilute aqueous solution [194] for some common ions used in nonlinear electrokinetic experiments. The figure depicts an ion with its effective hard-sphere and solvation shells, in red and blue respectively. Note that the effective sizes d_s and d_v in solution are much larger than the bare ion size d_x and exhibit different trends. In the text, we argue that the appropriate effective ion size a in our models of highly charged double layers may be approximated by d_s, and possibly larger.

electron transfer reactions near the surface). Moreover, like-charged ions cannot easily "share" a solvation shell and become compressed to the hard-sphere limit, since the outer surfaces of the polarized solvation shells have the same sign and yield electrostatic repulsion. Therefore, we propose that the "ion size" in our models is an effective solvated ion size at high charge density, which is much larger than the bare crystalline and hard-sphere ion sizes in Table 2 and may also exceed the solvated ion size inferred from bulk transport models. This physical intuition is borne out by the comparisons between theory and experiment below for nonlinear electrokinetics and in some recent electrochemical studies of double-layer capacitance [150, 151], although we will not claim to reach any quantitive molecular-level conclusions.

3.2. Implications for nonlinear electrokinetics

The decrease of diffuse-layer capacitance at large voltages for blocking surfaces is robust to variations in the model and has important consequences for nonlinear electrokinetics. Here, we provide two examples of nonlinear electrokinetic phenomena, where any MPB theory with volume constraints is able to correct obvious failures of PB theory. These results suggest that incorporating crowding effects into the electrokinetic equations may be essential in many other situations in electrolytes or ionic liquids, whenever the voltage or salt concentration is large.

3.2.1. High-frequency flow reversal of AC electro-osmosis

Steric effects on the double-layer capacitance alone suffice to predict high-frequency flow reversal of ACEO pumps, without invoking Faradaic reactions. Representative results are shown in Fig. 8, and the reader is referred to Ref. [63] for a more detailed study. Numerical simulations of a well studied planar pump geometry [30, 34, 36, 37] with the Standard Model in the linearized low-voltage regime [10, 11, 31, 40] predicts a single peak in flow rate versus frequency at all voltages. If the nonlinear PB capacitance (9) is included [38, 39], then the peak is reduced and shifts to much lower frequency (contrary to experiments), due to slower charging dynamics at large voltage [95, 97]. As shown in Fig. 8, the BF capacitance for Bikerman's MPB model of steric effects (22) reduces the peak shift and introduces flow reversal similar to experiments.

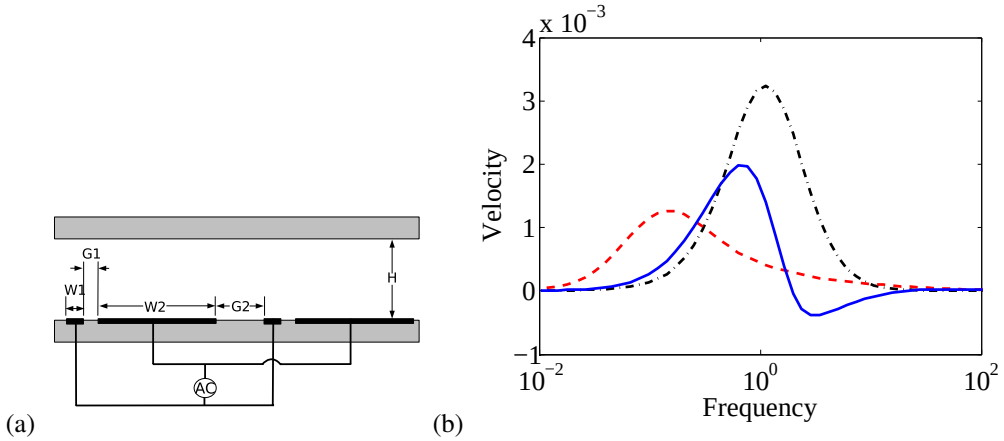

Figure 8: (a) One period of an asymmetric array of planar microelectrodes in an ACEO pump studied in experiments [30, 34, 36, 37] and simulations with the low-voltage model [30, 31, 38, 40] with $W1 = 4.2\,\mu$m , $W2 = 25.7\,\mu$m, $G1 = 4.5\,\mu$m , and $G2 = 15.6\,\mu$m. (b) The dimensionless flow rate versus frequency for different models. In the low-voltage limit $V \ll kT/e = 25$ mV, low-voltage models predict a single peak (black dash-dot line). For a typical experimental voltage, $V = 100kT/e = 2.5$ V, PB theory breaks downs and its capacitance (9) shifts the flow to low frequency (red dashed line) and Stern capacitance is needed to prevent the capacitance from diverging. Accounting for steric effects (22) with $\nu = 0.01$ (solid blue line) reduces the shift and predicts high frequency flow reversal, similar to experiments [34, 37].

This result is the first, and to our knowledge the only, theoretical prediction of high-frequency flow reversal in ACEO. The physical mechanism for flow reversal in our model can be easily understood as follows: At low voltages, the pumping direction is set by the larger electrode, which overcomes a weaker reverse flow driven by the smaller electrode. At large voltages, however, the more highly charged, smaller electrode has its *RC* charging time reduced by steric effects, so at high frequency it is able to charge more fully in a single AC period and thus pump harder than the larger electrode.

As shown in Fig. 9, the MPB model is able to reproduce experimental data for ACEO pumping of dilute KCl rather well, including the dependence on both voltage and frequency. Through Fig. 9, we compare simulations to experimental data at two different concentrations. In the left column we show experimental data and on the right we show the corresponding simulations using Bikerman's MPB theory for the double later capacitance. As in experiments, the flow reversal arises at 10-100 kHz frequency and high voltage, without shifting appreciably the main peak below 10 kHz frequency (which is hard to see in experiments at high voltage due to electrolysis). This is all the more remarkable, since the model has only one fitting parameter, the effective ion size a, and does not include any additional Stern-layer capacitance. As seen in 9 (a) and (b), the magnitude of the flow is over-estimated by a roughly a factor of two ($\Lambda \approx 0.4$), but this is much better than in most predictions of the Standard Model (in Table 1), which fail to predict flow reversal under any circumstances.

In spite of this success, we are far from a complete understanding of flow reversal in ACEO. One difficulty with these results is that the effective ion size in Bikerman's model needed to fit the data is unrealistically large. For the simulations to reproduce the experiments we seem to typically require $\nu = 0.001 - 0.01$, which implies an overly small bulk ion spacing $l_0 = (2c_0)^{-1/3} = \nu^{-1/3}a$, or overly large ion size a. For example, for the $c_0 = 0.1$ mM KCl data shown

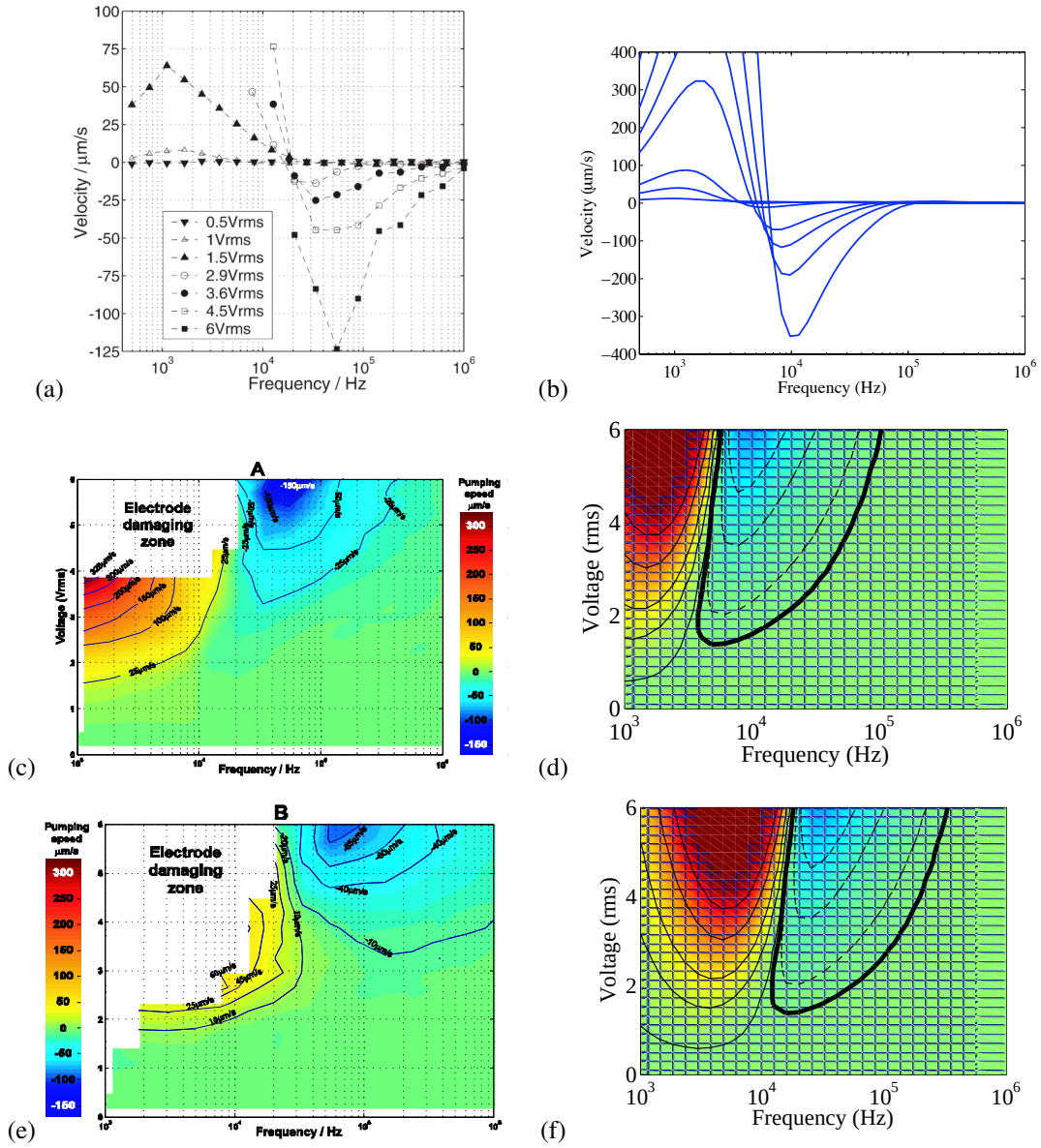

Figure 9: (a) Velocity of ACEO pumping in 0.1mM KCl by a planar electrode array around a microfluidic loop versus frequency at different voltages from the experiments of Studer et al. [34]. (b) Simulations by Storey et al. [63] of the same flow using the Standard Model with Bikerman's MPB theory (22) for the double-layer differential capacitance with only one fitting parameter, $a = 4.4$ nm or $\nu = 0.01$. Countour plots of ACEO pumping velocity contours in frequency-voltage space for (c) 0.1 mM and (e) 1.0 mM KCl from experiments of Studer et al. [34], compared to simulations under the same conditions using Bikerman's MPB theory with $\nu = 0.01$ in (d) and (f), respectively. Red indicates forward flow and blue reverse flow. The solid contour lines show positive velocity contour and the dashed show reverse flow. The heavy solid contour is the zero velocity contour in the simulations.

in Fig. 9 (a) and (b), we use $a = 4.4$ nm in the model, which is clearly unphysical. As noted above and shown in Fig. 7, this can be attributed at least in part to the signficant under-estimation of steric effects in a liquid by the simple lattice approximation behind Bikerman's model.

Indeed, hard-sphere liquid models tend to improve the agreement betweeen simulation and experiment, and this increases our confidence in the physical mechanism of ion crowding at large voltage. Using the CS MPB model for monodisperse charged hard spheres in the same simulations of ACEO pumping allows a smaller value of the ion size. For example, the 0.1 mM KCl shown in Fig. 9 (a) can be fit by using $a = 2.2$ nm (instead of 4.4 nm for Bikerman), and the magnitude of the velocity also gets closer to the experimental data ($\Lambda \approx 0.7$). Assuming a reduced permittivity in the condensed layer could further yield $a \approx 1$ nm (≈ 10 atomic diameters) [63]. This value is more realistic but still considerably larger than the bulk hydrated ion sizes in KCl and NaCl. For the commonly used electrolytes in ICEO experiments (see Table 1), the cation-anion radial distribution function from neutron scattering exhibits a sharp hard-sphere-like first peak at 3Å, although the water structure is strongly perturbed out to the second neighbor shell (up to 1nm), as if under electrostriction. Anion-anion correlations are longer ranged and softer, with peaks at 5 Åand 7 Å, but unfortunately such data is not available for crowded like charges within the double layer at high voltage. Perhaps under such conditions the effective hard-sphere radius grows due to strong correlations, beyond the mean-field approximation.

It is interesting to note that similar oversized hard-sphere radii have also recently been inferred by Di Caprio et al [150, 151] in fitting MPB models to differential capacitance curves ressembling Figs. 5-7 for electrochemical interfaces with little specific adsorption [173, 174, 175]. Hard-sphere MPB models give good qualitative predictions, but effective ion radii over 1.2 nm are required to fit the data [150] (without adding parameters for specific ion-ion interactions [151]). The fact that we reach similar conclusions in the completely different context of ACEO pumping suggests that various neglected effects, such as correlations, solvent interactions, and surface roughness, may be extending the apparent scale for crowding effects in MPB models, as discussed below.

In addition to overly large ion sizes, an additional problem is that the simulated results in Fig. 9 (d) and (f), are reproducing data from two different concentrations using the same value of $\nu = 0.01$ in Bikerman's MPB theory. Since the concentration varies between the two experiments by a factor of 10, the simulations are using different values of the ion size, a; 4.4 nm at 0.1 mM and 2 nm at 1 mM. Physically, it would make sense to use the same ion size in the model regardless of concentration. If we use the same ion size to fit data from both concentrations, the comparison worsens significantly, representing one of the key difficulties of fitting model to experimental data.

The steric models can thus provide good qualitative agreement between the measured and predicted frequency responses. However, the models can not predict the proper frequency response as we change concentration and hold the ion size fixed. In the model calculations, the frequency response at high voltage always shows regions of forward and reverse flow. As concentration changes, features in the modeled frequency response (e.g. forward and reverse peaks, crossover frequency) shift along the frequency axis as the RC charging time changes with concentration. Since the capacitance of the double layer is insensitive to bulk concentration at high voltage (see Fig. 6), the RC charging time depends on concentration through the bulk resistance. Thus the location of peaks on the frequency response should vary approximately linearly with concentration; experiments at high voltage indicate a much weaker dependence. It is likely that the difficulty in matching the frequency response of experiments to simulations is due to the neglect of Faradaic reactions. Faradaic reactions can reduce the resistance in the RC charging

time, thus shifting the oberved frequency response to higher frequency. Faradaic reactions are addressed in a later section.

At least at a qualitative level, changes in the double-layer charging time due to crowding effects likely also play a role in the sensitivity of ACEO flow to the solution chemistry. For example, flow reversal in our models is related to an ion-specific scale for crowding effects. In cases of asymmetric electrolytes, there may also be two different frequency responses at large voltages, one for positive and another for negative charging of the double layer. Perhaps this effect is responsible for the double-peaked frequency spectrum of ACEO pumping in water with non-planar electrodes at high voltage [36]. In multicomponent electrolytes, the situation is even more complicated, since large voltages can induce segregation of different counterions, opposite to PB predictions, e.g. with smaller ions condensing closest to the surface, even if the larger ions have high bulk concentration or carry more charge. These effects can be predicted by MPB models [58, 150, 151] using expressions for μ_i^{ex} for hard-sphere mixtures [190, 191] consistent with x-ray reflectivity measurements on mixed double layers [195, 196], so there is hope that applying such models in our weakly nonlinear formalism for ACEO may also be fruitful.

3.2.2. Field-dependent electrophoretic mobility

In the classical theory of electrophoresis [7, 5], the electrophoretic mobility b_{ep} of a homogeneous particle with thin double layers is a material constant, given by Smoluchowski's formula,

$$b_{ep} = b = \frac{\varepsilon_b \zeta}{\eta_b}. \tag{27}$$

In particular, the electrophoretic mobility does not depend on the background field E_b or the shape or size of the particle. These are consequences of the assumption of fixed surface charge, or constant zeta potential. For polarizable particles, the theory must be modified to account for ICEO flows [16], which produce a shape-sensitive ICEP velocity scaling as $U \propto \varepsilon_b R E_b^2/\eta_b$, where R is the particle size [13, 19, 20]. Transverse ICEP of metallo-dielectric Janus particles in AC fields has recently been observed in experiments [21] up to fairly large induced double-layer voltages $E_b R \approx 15kT/e$.

ICEP theories aimed at AC fields tend to assume zero total charge, but ICEO flows can also alter the DC electrophoretic mobility of a charged, polarizable particle (the "Stotz-Wien effect" [62]). In the limit of weak fields $E_b \ll kT/eR$, A. S. Dukhin first showed that an ideally polarizable sphere with equilibrium zeta potential ζ_0 and radius R has a field-dependent electrophoretic mobility,

$$b_{ep}(E_b) \sim \frac{\varepsilon_b}{\eta_b}\left(\zeta_0 - \frac{3}{8}\frac{C_D'(\zeta_0)}{C_D(\zeta_0)}(E_b R)^2 + \ldots\right) \tag{28}$$

if the diffuse-layer differential capacitance is voltage dependent [61]. This general correction has only been applied in the context of PB theory, Eq. (9), which predicts decreased mobility, $\Delta b_{ep} < 0$ since $dC_D/d\psi > 0$ for $\zeta_0 > 0$. This correction has also been derived as the small field limit of a general PB analysis for thin double layers by Yariv [111].

The basic physics of this nonlinear effect is illustrated in Fig. 10(a-b). If the double-layer voltage varies enough to cause spatial variations in its differential capacitance, then counterions aggregate with varying density (per area) around the surface of the particle upon polarization by the applied field, and this nonlinearity breaks symmetry in polarity with respect to the mean voltage. For example, if the positively charged part of the diffuse layer (relative to the mean charge) is less dense (e.g. due to larger or less charged cations than anions), it will cover more

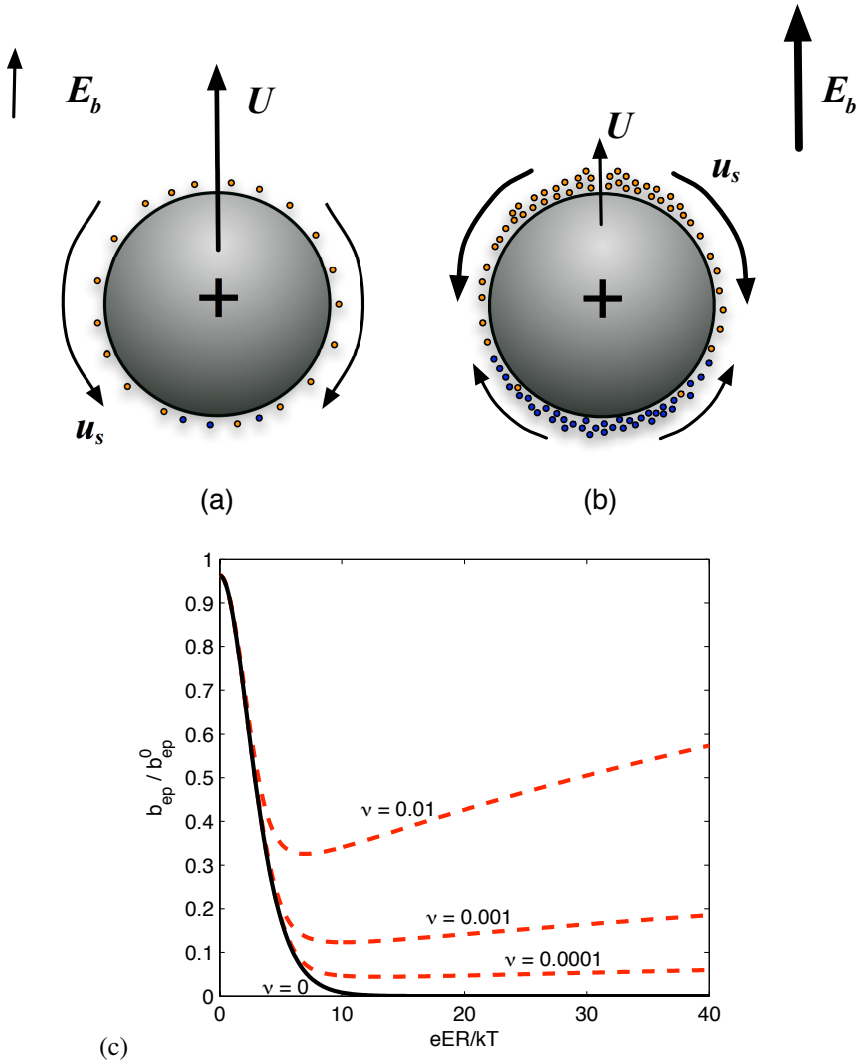

Figure 10: Field-depenent electrophoretic velocity U of an ideally polarizable, charged sphere of radius R with thin double layers in a background field E_b. (a) In small fields, the mobility $b_{ep} = U/E_b$ is set by the uniformly distributed double-layer charge. (b) In large fields, $E_b \gg kT/eR$, the dipolar induced charge overwhelms the pre-existing charge and alters b_{ep}, if cations and anions do not condense at the same density and must redistribute to conserve total charge. (c) In PB theory, the unphysical collapse of point-like ions to the surface causes exponential decay of $b_{ep}(E_b)$ via Eq. (30); finite-size effects in Bikerman's MPB model (Fig. 5) prevent this decay and lead to the opposite trend: increase of mobility in large fields via Eq. (33).

of the surface than the negatively charged part; cations are then more likely to dominate in regions of large tangential field near the equator and thus make an enhanced contribution to the electrophoretic mobility of the particle, regardless of its true surface charge. Other effects can also be important (see below), but this one is particularly sensitive to MPB models for the double layer.

Dukhin's formula (28) can be derived from the general weakly nonlinear formalism of Refs. [16, 19] for ideally polarizable particles with thin double layers (yielding the same result as Ref. [61]). In the low-frequency or DC limit, the background field E_b causes nonuniform polarization of the double layer around the particle to screen the bulk electric field $\mathbf{E} = -\nabla\phi$, which thus solves Laplace's equation $\nabla^2\phi = 0$ with the effective boundary condition, $\hat{n} \cdot \mathbf{E} = 0$. If we let ϕ_0 denote the *induced* potential of the particle, relative to the background applied potential, then $\Delta\phi(\mathbf{r}) = \phi_0 - \phi(\mathbf{r})$ is the non-uniform voltage across the double layer, which enters the electro-osmotic slip formula, either the HS formula (5) or one of its generalizations below. For a sphere with HS slip, the electrophoretic mobility is simply $b_{ep} = \varepsilon_b\phi_0/\eta_b$.

The crucial step is to determine the particle's potential ϕ_0, after polarization of the double layers, which generally differs from its initial equilibrium value, ζ_0, due to nonlinearity of the charging process. (This phenomenon, first noted by Dukhin [61], was overlooked in Refs. [13, 14, 20, 19].) /Using the mathematical formalism of Ref. [19], the potential of the particle must adjust to maintain the same total charge Q, which can be related to the differential capacitance of the double layer as follows:

$$Q = \oint\left(\int_0^{\zeta_0} C_D(\psi)d\psi\right)dA = \oint\left(\int_0^{\phi_0-\phi(\mathbf{r})} C_D(\psi)d\psi\right)dA, \tag{29}$$

for a given initial zeta potential ζ_0, bulk polarization $\phi(\mathbf{r})$, and (total) double layer differential capacitance, $C_D(\psi)$. For simplicity, we assume the diffuse layer carries all the double-layer voltage, but a compact Stern layer can be easily included in Eq. (29) by replacing $\Delta\phi$ with $\Delta\phi/(1+\delta)$. Regardless of the particle shape, the assumption of a uniform, constant C_D implies $\phi_0 = \zeta_0 = Q/(C_D A)$ (where A is the surface area), and thus no impact of polarization on the electrophoretic mobility in the case of a sphere [19]. With a nonlinear differential capacitance, however, Equation (29) is a nonlinear algebraic equation for ϕ_0, and thus b_{ep}, in terms of ζ_0 and E_b. In the geometry of a sphere, Dukhin's formula (28) can be derived by asymptotic analysis in the limit of small fields, $E_b \ll kT/eR$ for any choice of $C_D(\psi)$ [16], and for some models exact solutions and the large-field limit can also be derived [197].

Using this mathematical formalism with our MPB models, we predict that steric effects in the electrolyte can signficantly influence the mobility of polarizable particles in large applied fields and/or highly concentrated solutions. Here, we focus on new qualitative phenomena predicted by the theory. (More details can be found in Ref. [197].) From Fig. 5 and Eq. (22), we see that the mobility of a highly charged particle $|\zeta_0| \gg kT/e$ can increase with the field squared in Dukhin's formula (28) since $dC_D/d\psi < 0$, which is the opposite prediction of PB theory. The mobility is also clearly sensitive to the ionic species through C_D.

The discrepancy with PB theory becomes more dramatic in a large applied field, $E_b \gg kT/eR$, even if the particle is not highly charged $|\zeta_0| \approx kT/e$. Previous authors have only considered weak fields [62, 61], so it was apparently not noticed until Refs. [111, 197] that PB theory (9) leads to a surprising prediction, shown in Fig. 10(c): The mobility of a charged, ideally polarizable, spherical particle vanishes exponentially in the limit $E_b \gg kT/eR$ (=100 V/cm for

$R = 2.5\mu$m),

$$b_{ep}^{PB} \sim \frac{3\varepsilon_b}{\eta_b} \sinh\left(\frac{ze\zeta_0}{2kT}\right) E_b R\, e^{-3zeE_bR/4kT}, \tag{30}$$

which is the large-voltage limit of an exact solution for the ICEP mobility of an ideally polarizable sphere with thin double layers in PB theory,

$$b_{ep}^{PB} = 2\frac{kT}{ze} \sinh^{-1}\left[\frac{3zeE_bR}{4kT}, \frac{\sinh(ze\zeta_0/2kT)}{\sinh(3zeE_bR/4kT)}\right] \tag{31}$$

The mechanism for this seemingly unphysical effect is the massive overcharging of the diffuse layer in PB theory at large voltages in Fig. 5(b), which causes the anti-symmetric induced charge (not causing motion) to overwhelm the symmetric pre-existing charge (giving rise to mobility). We view this prediction as another failure of PB theory, since we are not aware of any evidence that polarizable particles lose their electrophoretic mobility so strongly in such fields, which are routinely applied in electrophoresis experiments. (Note that $kT/eR = 100$ V/cm for a 5μm diameter particle at room temperature.) The PB prediction of vanishing mobility is closely tied to the unphysical pile-up of point-like ions near a highly charged surface in PB theory.

Indeed, the situation is completely different and more physically reasonable in any mean-field theory with finite-sized ions, regardless of the model. Using our general MPB formula (18), the mobility in large fields $E_b \gg kT/eR$ can be expressed as

$$b_{ep} \sim \frac{3\varepsilon_b E_b R\, q(\zeta_0)}{2\eta_b\, q\left(\frac{3}{2}E_bR\right)} \tag{32}$$

and typically grows as $b_{ep}^{\nu} \propto \sqrt{E_b}$. For example, in Bikerman's model the BF formula (22) yields

$$b_{ep}^{\nu} \sim \frac{\varepsilon_b}{\eta_b}\sqrt{\frac{3\nu kT E_b R}{4ze}}. \tag{33}$$

As shown in Fig. 10(c), the mobility b_{ep}^{ν} rapidly decreases in weak electric fields until PB theory breaks down, and then gradually increases in larger fields [197]. Physically, steric effects prevent overcharging of the double layer in PB theory, thus preserving the asymmetry of the initial charge distribution.

A related general consequence is that asymmetry in the electrolyte, e.g. ions of different effective sizes, can affect a particle's electrophoretic mobility. Remarkably, an uncharged particle can acquire a nonzero mobility in an asymmetric electrolyte in a large applied field ($\zeta_0 = 0$ but $b_{ep} \neq 0$). An asymmetric field-dependence of the double-layer capacitance is enough to predict such exotic effects on very general grounds.

As a first approximation for the weakly nonlinear regime using MPB theory, we simply postulate two different (homogeneous) ion sizes $a_\pm$ for positive and negative polarization of the diffuse layer,

$$C_D(\Psi_D) = \begin{cases} C_D(\Psi_D; \nu = \nu^+) & \text{for } \Psi_D > 0 \\ C_D(\Psi_D; \nu = \nu^-) & \text{for } \Psi_D < 0 \end{cases} \tag{34}$$

where $\nu^\pm = 2a_\pm^3 c_0$ (or $\Phi^\pm$ for hard sphere models). This may seem like a crude approximation, but it is quite accurate for a binary electrolyte at large voltages since the diffuse layer mostly contains counterions of one sign; at low voltages, where all species are present in a dilute mixture, the ion sizes play no role. Inserting (34) into (29) yields the results shown in Figure 11 for the

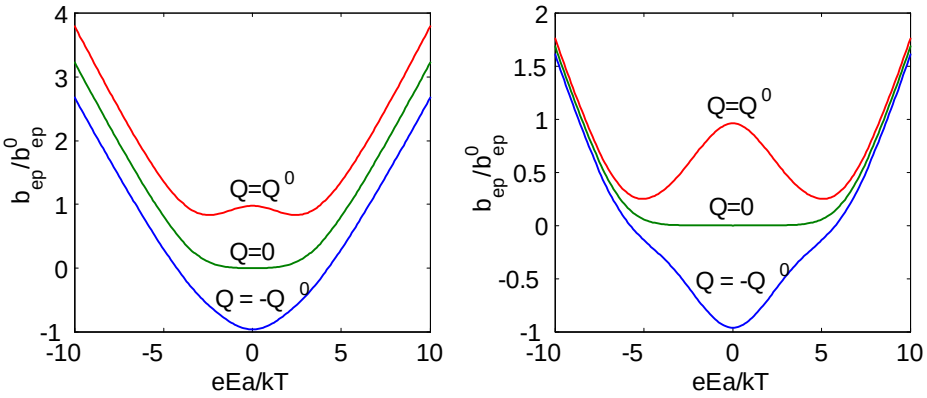

Figure 11: Electrophoretic mobility b_{ep} of an ideally polarizable sphere of total charge Q in an asymmetric binary $z:z$ electrolyte, scaled to $b^0_{ep} = \varepsilon_b kT/ze\eta_b$, in the weakly nonlinear limit of thin double layers. The case of an uncharged particle $Q = 0$ is compared to those of total charge $Q = \pm Q^0$ where $Q^0 = \varepsilon_b kT/ze\lambda_D$. Using the approximation (34), the mobility is calculated with Bikerman's MPB model (22) for an effective volume ratio $(a_-/a_+)^3 = 10$ in two cases: (a) high salt concentration with $\nu_- = 0.1$ and $\nu_+ = 0.01$ and (b) moderate salt concentration with $\nu_- = 10^{-3}$ and $\nu_+ = 10^{-4}$. At small electric fields and/or low salt concentrations, the size asymmetry is irrelevant, and the predictions of PB theory from Fig 10 are apparent; at large fields and/or low concentrations, the particle acquires an apparent positive charge, due to the covering of more of the particle's area by the larger cations, regardless of its true surface charge;

(weakly nonlinear) mobility of a charged, ideally polarizable sphere in a DC field. Interestingly, at large voltages, positive or negative, the mobility tends to a $|E|$ scaling, set by the ratio a_+/a_-, independent of the total charge of the particle Q. We also see that an uncharged particle with $Q = 0$ can still have a nonzero mobility, once nonlinear charging of the double layers sets in.

We stress that all the calculations of this paper consider the weakly nonlinear limit of thin double layers, where the bulk concentration remains uniform and surface conduction is neglected. As such, the trends we predict for PB and MPB models are meaningful at moderate voltages, but may need to be significantly modified at large voltages for strongly nonlinear dynamics. Moreover, even in the weakly nonlinear regime, we will now argue that at least one more physical important effect should be considered.

4. Viscoelectric effect in a concentrated solution

4.1. Mean-field theory

4.1.1. Modified Helmholtz-Smoluchowski slip formulae

There is a considerable literature on electrokinetic phenomena at highly charged surfaces with large (but constant) zeta potential [5, 4, 198, 199, 9]. In this context, it is well known that the linear electrophoretic mobility departs from Smoluchowski's formula at large surface potentials, $\Psi > \Psi_c$, and decreases at large voltage, due to effects of surface conduction (large Dukhin number). Using PB theory for thin double layers, Dukhin and Semenikhin [198] derived a formula for the electrophoretic mobility of a highly charged, non-polarizable sphere, which was famously verified by O'Brien and White [200] via numerical solutions of the full electrokinetic equations for a dilute solution. This established the mathematical validity of the formula, but in

this article we are questioning the *physical validity* of the underlying equations at large induced voltages and/or high salt concentrations.

As described in section 2, recent experiments on induced-charge electrokinetic phenomena reveal a strong decay of electro-osmotic mobility with increasing salt concentration at highly charged surfaces, which cannot be explained by the standard model, based on the HS formula (5), even if corrected for strongly nonlinear effects perturbing the salt concentration. Continuum electrohydrodynamics, however, does not require the HS formula, even for thin double layers, but instead provides a general expression for the electro-osmotic mobility [5],

$$b = \int_0^{\Psi_D} \frac{\varepsilon}{\eta} d\Psi \tag{35}$$

as an integral over the potential difference Ψ entering the diffuse layer from the bulk. This allows us to derive "modified Helmholtz-Smoluchowski" (MHS) formulae for $b(\Psi_D, c_0, \ldots)$ based on general microscopic electrokinetic equations.

The standard way to interpret electrokinetic measurements is in terms of the effective zeta potential,

$$\zeta_{eff} = \frac{b\eta_b}{\varepsilon_b}, \tag{36}$$

but we view this as simply a measure of flow generated in units of voltage, and not a physically meaningful electrostatic potential. One can also use PB theory for the hypothetical "mobile" part of the double layer to express the mobility in terms of an effective "electrokinetic charge" [9, 5], e.g. using the Gouy-Chapman solution for a symmetric binary electrolyte,

$$q_{ek} = 2\lambda_D zec_0 \sinh\left(\frac{ze\zeta_{eff}}{2kT}\right) \tag{37}$$

which measures the observed flow in units of charge.

It is well known that the classical theory tends to overpredict experimentally inferred zeta potentials ($|\zeta_{eff}| < |\Psi_D|$ or $|q_{ek}| < |q|$), and the discrepancy is often interpretted in terms of a "slip plane" or "shear plane" separated from the surface by a molecular distance $d \geq 0$, where the no-slip boundary condition is applied [201, 9]. If the low-voltage theory with $\varepsilon = \varepsilon_b$ and $\eta = \eta_b$ is applied beyond this point, then ζ_{eff} acquires physical meaning, as the potential of the slip plane relative to the bulk. Behind the slip plane, the fluid is assumed to be "stagnant" with effectively infinite viscosity, although it may still have finite ionic surface conductivity [9].

As in the case of effective hydrodynamic slip ($d < 0$) over hydrophobic surfaces [202, 203] the slip-plane concept, although useful, obscures the true physics of the interface. In particular, it has limited applicability to nonlinear electrokinetic phenomena, where the double layer responds non-uniformly to a large, time-dependent applied voltage. We have already argued this leads to signficant changes in the structure of the double layer, and clearly it must also have an impact on its rheology. Without microscopic models of how *local* physical properties, such as viscosity and permittivity, depend on local variables, such as ion densities or electric field, it is impossible to predict how the effective electro-osmotic slip depends on the *global* double-layer voltage or bulk salt concentration. This is also true in complicated geometries, such as nanochannels or porous structures, where the concept of a flat "slip plane" is not realistic.

4.1.2. The viscoelectric effect

Based on Eq. (35), there are good reasons to expect reduced mobility at large voltage, $|\Psi_D| > \Psi_c$, compared to the HS formula, $\zeta_{eff} = \Psi_D$, based only on field-dependent properties of a polar

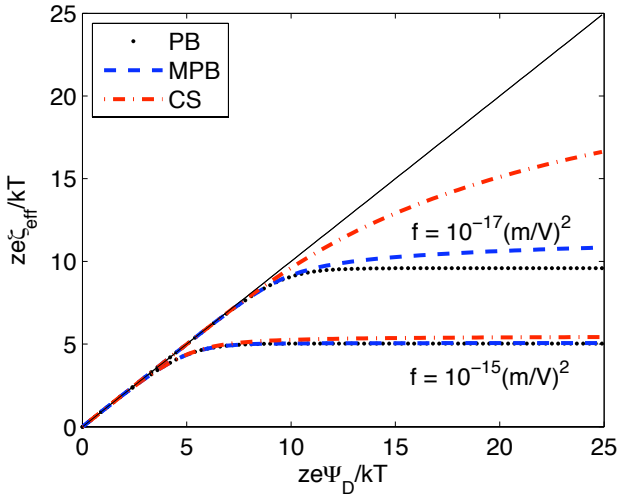

Figure 12: Modified Helmholtz-Smoluchowski (MHS) slip formulae assuming a charge-independent viscoelectric effect in the polar solvent (38). This example assumes a bulk concentration $c_0 = 1$ mM of $z:z$ electrolyte using different models of double-layer structure. The Lyklema-Overbeek (LO) model, based on Poisson-Boltzmann (PB) theory of point-like ions, is compared to MHS slip with the Bikerman (MPB) and Carnahan-Starling (CS) modified PB theories, using an effective ion size of $a = 4$Å. The viscoelectric coefficient is set to the value $f = 10^{-15}\mathrm{m}^2\mathrm{V}^{-2}$ suggested by LO for water as well as a smaller value $f = 10^{-17}\mathrm{m}^2\mathrm{V}^{-2}$, which reduces the viscoelectric effect.

solvent [5]. The large normal electric fields in a highly charged double layer can decrease the permittivity, by aligning the solvent dipoles. The viscosity can also increase [204, 192], through viscoelectric thickening of a dipolar liquid with polarization transverse to the shear direction.

Focusing on the viscoelectric effect in water, Lyklema and Overbeek [59, 60] proposed the first (and perhaps the only) microscopic electro-rheological model leading to an MHS slip formula. They assumed a field-squared viscosity increase in dilute-solution theory,

$$\eta = \eta_b \left(1 + fE^2\right), \tag{38}$$

and were able to integrate (35) to obtain an analytical (although cumbersome) MHS formula. Physically, their model predicts that b saturates to a constant value at large $|\Psi_D|$, which decays with increasing c_0. The saturation in the LO model, however, is tied to the unphysical divergence of the counterion concentration (and thus E) in PB theory, and thus should be revisited with steric effects.

It is straightforward to use the LO postulate (38) for the viscoelectric effect in our modified PB models to obtain corresponding MHS slip relations, although the integration of (35) cannot be done analytically. Numerical results for a typical case are shown in Fig. 12, using the value $f = 10^{-15}\mathrm{m}^2\mathrm{V}^{-2}$ suggested by LO for water [59, 60]. It is interesting to note that this choice makes all three models of double layer structure, PB, Bikerman MPB, and CS MPB, yield very similiar electro-osmotic mobility versus voltage, in spite of completely different ion density profiles. The reason is that the viscoelectric effect sets in so quickly with increasing voltage that the shear plane is effectively still in the dilute, outer part of the diffuse layer, where all theories reduce to PB. Indeed, as shown in the figure, more differences become apparent we if choose a smaller value,

$f = 10^{-17}\mathrm{m}^2\mathrm{V}^{-2}$. The reduction in normal electric field due to crowding-induced expansion of the inner diffuse layer leads to slower saturation of ζ_{eff} compared to PB theory, especially in the CS MPB model, since it has stronger steric effects than the Bikerman MPB model.

What this exercise shows is that the inner part of a highly charged double layer is effectively frozen by field-dependent viscosity in a similar way regardless of the model for the diffuse-charge profile. The LO model attributes this effect entirely to the solvent (water), independent of the local diffuse charge density or ionic currents, but this hypothesis does not seem entirely satisfactory. An implication is that water is effectively immobilized within a few molecular layers of the surface near a charged surface, even if there is no added salt. This effect seems to contradict recent experimental and theoretical literature on hydrodynamic slip [202, 205, 206, 203] which has shown that shear flow in water persists down to the atomic scale with a no-slip boundary condition for smooth hydrophilic surfaces and with significant slip lengths (up to tens of nanometers) on hydrophobic surfaces [207, 208, 209]. If the viscosity is a property of pure water (as opposed to the local electrolytic solution), then the field dependence should also be observable in the bulk, but we are not aware of any experiments or simulations showing that bulk de-ionized water becomes rigid in fields larger than $f^{-1} = 30\mathrm{V}/\mu\mathrm{m}$. Of course, it is hard to apply such fields in the bulk at low frequency, due to capacitive screening by the double layers and Faradaic reactions, but the LO model is time-independent and should also apply at high frequency where these effects are reduced.

Molecular dynamics (MD) simulations of electrokinetic phenomena in nanochannels generally imply a local viscosity increase close to a charged surface, although its origin and mathematical description are not well understood. An early MD simulation of Lyklema et al. [89] showed a stagnant monolayer of water, which could pass ions freely, with a surface conductivity comparable to the bulk, but subsequent MD simulations of electro-osmosis have shown motion of the liquid (both ions and solvent) down to the atomic scale near the wall [90, 91, 152, 210, 92, 93, 94], albeit with an apparent viscosity often smoothly increasing across the closest molecular layers. We are not aware of any MD simulations of electro-osmosis in a large transverse voltage ($\gg kT/e$), but it seems that the presence of crowded counterions near the surface (described in section 3) must affect the apparent viscosity, since the liquid no longer resembles the pure bulk solvent.

4.1.3. Charge-induced thickening

A natural physical hypothesis, sketched in Figure 13, is that the crowding of counterions in a highly charged diffuse layer increases the local viscosity, not only through the viscoelectric effect of the bare solvent, but also through the presence of a large volume fraction of like-charged ions compressed against the surface. For now, we neglect explicit field dependence, such as (38), to focus on effects of large charge density. In a very crude attempt at a model, we consider an electrolyte with solvated ions of finite size and postulate that ε/η diverges as a power law,

$$\frac{\varepsilon}{\eta} = \frac{\varepsilon_b}{\eta_b}\left[1 - \left(\frac{|\rho|}{\rho_j^{\pm}}\right)^{\alpha}\right]^{\beta} \tag{39}$$

as the local charge density approaches a critical value, $\rho_j^{\pm}$, which generally must depend on the polarity $\mathrm{sign}(\rho) = \pm$ in an asymmetric electrolyte.

A natural choice is to postulate diverging viscosity (jamming) at the steric limit, $\rho_j = \rho_{max}^{\pm} = |z_{\pm}|ec_{max}^{\pm}$. In that case, similar exponents α and β controlling the singularity also arise in the

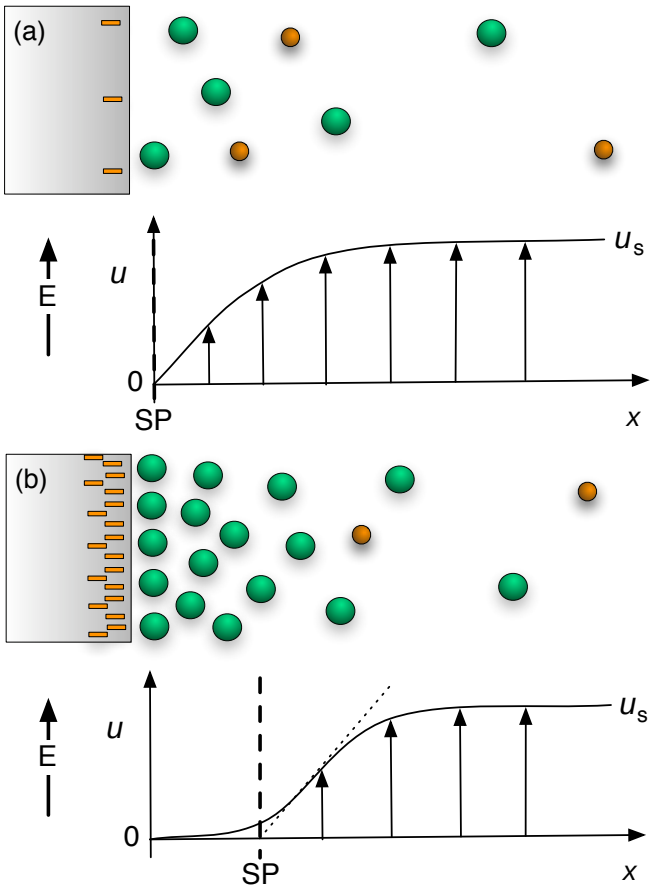

Figure 13: Sketches of finite-sized hydrated ions near a polarizable surface as in Fig. 4, showing the solution velocity u profile in response to a tangential electric field. (a) At small induced voltages, the no-slip boundary condition holds at the surface, and the effective electro-osmotic slip u_s builds up exponentially across the diffuse layer. (b) At large voltages, crowding of hydrated ions increases the viscosity of the condensed layer, and the apparent slip plane "SP" (dashed line) moves away from the surface with increasing voltage.

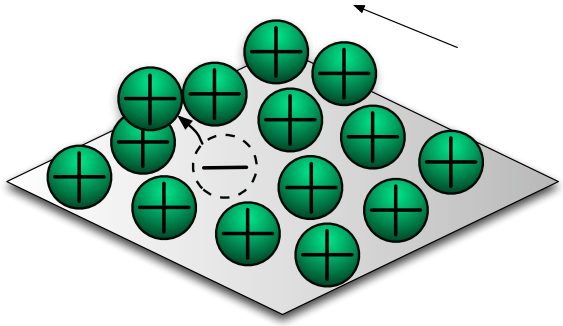

Figure 14: Sketch of a physical mechanism for charge-induced thickening due to electrostatic correlations. A condensed layer of solvated counterions (spheres) is confined against a highly charged surface by the normal electric field. Shear of the fluid (arrow) causes an ion to leave its local equilibrium position in a Wigner-like crystal of like charges, but its motion is inhibited by a strong attraction back to its oppositely charged "correlation hole" (dashed).

rheology of dense granular materials [211]. If we also assume $\alpha = \beta = 1$, then there are no new fitting parameters,

$$\frac{\varepsilon}{\eta} = \frac{\varepsilon_b}{\eta_b}\left(1 - \frac{|\rho|}{\rho^{\pm}_{max}}\right) \tag{40}$$

since the steric constraints $\rho^{\pm}_{max}$ come from the MPB model. In our original letter [53], we considered only this postulate with Bikerman's model for steric effects and thus assumed an even simpler form,

$$\frac{\varepsilon}{\eta} = \frac{\varepsilon_b}{\eta_b}\left(1 - \frac{a^3|\rho|}{ze}\right) \tag{41}$$

The resulting electrokinetic model is extremely simple in that it only involves one parameter beyond dilute-solution theory, the effective ion size, a. As such, it lacks flexibility to fit multiple sets of experimental data, but we will use it in our analytical calculations below to further understand the general consequences of steric constraints.

The general model (39) also allows for other types of behavior. With $\rho^{\pm}_j > \rho^{\pm}_{max}$, there is a finite maximum viscosity in the condensed layer, or effectively some flow behind the slip plane. With $\rho^{\pm}_j < \rho^{\pm}_{max}$, the model postulates flow arrest at high charge density before the close-packing limit is reached (and $\eta = \infty$ for $|\rho| > \rho^{\pm}_j$). The new parameters $\rho^{\pm}_j$, α and β allow some flexibility to fit experiments or simulations, in addition to the ion sizes $a_{\pm}$ from the MPB models above.

The arbitrary choice (39) is motivated by a number of possible physical effects:

- *Jamming against a surface.* In a bulk colloid [6], the maximum density corresponds to random close packing at the jamming point [212], where the shear modulus becomes finite [213] and the viscosity diverges [211]. Molecular dynamics simulations of soft disks in a periodic box have recently established a viscosity divergence of the form (39) with $\alpha = 1$ and $\beta = 1.7$. In an electrolyte, strong electrostatic compression of solvated counterions against a (typically rough) surface may cause some transient local jamming of the condensed layer, and thus increased viscosity at high charge density.

- *Electrostatic correlations.* Condensed counterions at large voltages ressemble a Wigner crystal [214, 215] (or glass) of like charges. Discrete Coulomb interactions [146, 216] may

contribute to increased viscosity, e.g. through the attraction between a displaced ion and its "correlation hole", which effectively carries an opposite charge. (See Fig. 14.) We are not aware of attempts to predict the rheological response of sheared Wigner crystals or glasses, let alone discrete, correlated counterion layers, but we expect that electrostatic correlations will generally contribute to charge-induced thickening in electrolytes and ionic liquids.

- *Solvent effects.* Several molecular dynamics simulations of linear electro-osmosis (at low voltages) have infered $\approx 5\times$ greater viscosity within 1 nm of a flat surface [90, 91], which grows with surface charge [210] and surface roughness [217] (but decreases with hydrophobicity [93]). Aligning water dipoles near a highly charged surface reduces the electro-osmotic mobility by lowering ε, but in the presence of crowded ions, solvation forces and confined hydrogen-bond networks may further reduce ε/η. The latter effect may be related to local electrostriction, which compresses the second hydration shell around certain cations (K^+ and Na^+, also used in ICEO experiments, Table 1) [141].

Of course, this electrohydrodynamic model is rather simple. In general, we expect that ε and η will depend independently on both the local field E and the solution composition. We have already mentioned the different physical effects affecting ε and η in a pure dipolar solvent, and the situation only becomes more complicated with large ion densities. In order to model general phenomena such as diffusio-osmosis or surface conduction, it is necessary to provide separate functional forms for ε and η, since these variables no longer only appear as the ratio ε/η. In that case, we would propose viewing (39) as a model for η with $\varepsilon = \varepsilon_b$ fixed, since molecular dynamics simulations of electro-osmosis predict smaller changes in permittivity than in viscosity near a charged surface, even within a few molecular diameters [90, 91]. This is also analytically convenient because variable ε is a major complication in MPB models (although progress can be made [197]). Finally, our neglect of explicit field-dependence such as (38), in favor of charge-density dependence (which is more closely related to our modeling of crowding effects), does not affect the modeling of quasi-equilibrium double layers, since the dominant normal field can be expressed in terms of the charge-density, and vice versa, in any MPB model. In more general models, however, it may be important to also include a field-dependent viscoelectric effects.

Our basic picture of charge induced thickening is consistent with prior models for the increase of viscosity with salt concentration in neutral bulk solutions [204, 192, 194]. Traditionally, the viscosity of electrolytes has been described empirically using the Dole-Jones correlations [218, 219, 220], but more recent theories based on molecular models take a more fundamental approach. Like our hypothesis, these models also postulate infinite viscosity as the hard sphere solvated volume fraction approaches unity [194]. In a neutral bulk electrolyte, such high volume fractions are never reached due to limits of solubility, though a factor of ten increase in viscosity has been observed for some systems at high salt concentration [221]. The effective hard-sphere diameters (see Table 2) inferred from these viscosity models may also have relevance for our models, although there is an important difference: We neglect crowding effects in a neutral bulk solution and focus instead on crowding of like-charged counter-ions. As discussed above, at high charge density in a large electric field, various physical effects could significantly increase the viscosity compared to what would be observed in a neutral solution at the same concentration. Moreover, solubility limits are not relevant for like-charged ions, so higher concentrations approaching packing limits can more easily be reached, as we have postulated in response to a large voltage.

Regardless of the specific form of our model, its key feature is that the concentrated solution of counterions near a highly charged surface is thickened with voltage, compared to the bulk,

although it can still flow slowly. This picture is consistent with molecular dynamics simulations of electro-osmosis [90, 91, 210, 93, 217, 222], which do not observe a truly stagnant layer, even at low surface potentials. As sketched in Fig. 13, from a macroscopic point of view, there is an apparent slip plane separated from the surface, which depends on the ion density profiles and thus external conditions of voltage and bulk solution composition. At low voltage, near the point of zero charge, there is no change in the local viscosity, aside from any pure solvent interactions with the surface, e.g. due to hydrophobic or hydrophilic effects (which we neglect). At high voltage, the crowding of counterions leads to thickening and an apparent movement of the slip plane away from the surface. Without a microscopic model, it would not be possible to predict this dependence or derive a functional form for fitting.

The picture of a thin layer near the surface with different electro-rheological properties also appears in models of electrokinetics with porous or soft surfaces [223, 224], which build on the Zukowski-Saville [225, 226] and Mangelsdorf-White [227, 228, 229] theories of the "dynamical Stern layer". In these models, ions are allowed to move within a flat Stern monolayer, while the diffuse layer is described by the standard electrokinetic model. Recently, López-Garcia, Grosse and Horno have extended these models to allow for some fluid flow in a thicker dynamical surface layer, and this allows more flexibility in fitting (linear) electrical and electrokinetic measurements [230]. In the case of a flat surface with an equilibrium double layer, this is similar to our picture, if the surface layer is ascribed a higher viscosity, but in our model there is no need to postulate a sharp plane where properties of the solution change. Instead, by modifying the electrokinetic equations everywhere in the solution, its electro-rheology changes continuously as a function of local contiuum variables.

The concept of charge-induced viscosity increase may be widely applicable in nano-scale modeling of electrolytes, in conjunction with modified theories of the ions densities. The general modified electrokinetic equations are summarized in section 5. Now, let us consider generic consequences of this hypothesis for electrokinetic phenomena with thin double layers and make some explicit calculations using Eq. (39).

4.2. Implications for nonlinear electrokinetics

4.2.1. Electro-osmotic slip at large voltages in concentrated solutions

To describe electro-osmotic flows with thin double layers, we can use our microscopic models to derive modified Helmholtz-Smoluchowski (MHS) slip formulae, which depend nonlinearly on double-layer voltage (or surface charge) and bulk salt concentration. Such predictions could perhaps be directly tested experimentally by field-effect flow control of electro-osmosis in microfluidic devices [122, 123, 124], if a nearly constant double-layer voltage could be maintained along a channel and then varied systematically for different electrolytic solutions. Alternatively, one could compare with molecular dynamics simulations of electro-osmotic flow in nanochannels with oppositely and highly charged walls, leading to large induced double-layer voltages.

A general MHS slip formula — If we assume $\varepsilon = \varepsilon_b$ in Eq. (40) with $\alpha = \beta = 1$ (an arbitrary choice for analytical convenience), then for any MPB model with $|\rho^{\pm}_{max}| < \infty$ we can integrate Eq. (35) obtain an MHS formula for the effective electro-osmotic slip outside the double layer,

$$\zeta_{eff} = \Psi_D \pm \frac{p_e(\Psi_D)}{\rho^{\pm}_j} = \Psi_D \pm \frac{q(\Psi_D)^2}{2\varepsilon_b \rho^{\pm}_j} \tag{42}$$

where $\pm = \mathrm{sign}(q) = -\mathrm{sign}(\Psi_D)$ and $p_e(\Psi_D)$ and $q(\Psi_D)$ are given by (16) and (17), respectively. This simple and general expression reduces to the HS formula ($\zeta_{eff} = \Psi_D$) in the limit of point-like ions ($\rho^{\pm}_{max} \to \infty$) and/or small voltages ($\Psi_D \ll kT/e$). At large voltages, $|\zeta_{eff}|$ is always

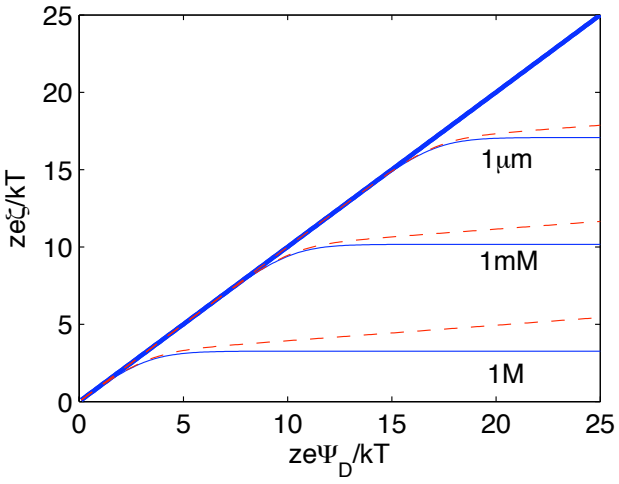

Figure 15: MHS slip formula (45) using Bikerman's model with ion size $a = 4$Å and charge-induced thickening (39) with $\alpha = 1 = \beta = 1$ at different bulk concentrations, $c_0 = 1\mu$M, 1 mM, and 1M. The viscosity is postulated to diverge either at a mean ion spacing $a_j = a$ (solid curves), in which case the condensed layer in Fig. 5(a) is effectively rigid, or at $a_j = 0.9a$ (dashed curves), in which case it flows with a large, but finite viscosity.

reduced, depending on how the model for μ_i^{ex} imposes volume constraints or other contributions to the excess chemical potential.

In any MPB model, such as Bikerman's, where counterions ($\pm$) form nearly uniform condensed layers with $c_\pm \approx c_{max}^\pm$ and $\eta \gg \eta_b$ from Eq. (39), the apparent zeta potential (42) either saturates to a constant,

$$\zeta_{eff} \sim \Psi_c^\pm = -\frac{kT}{z_\pm e} \ln\left(\frac{c_{max}^\pm}{c_0}\right) \tag{43}$$

if the condensed layer is stagnant ($\rho_j^\pm = \rho_{max}^\pm$) or switches to a slower linear dependence

$$\zeta_{eff} \sim \Psi_D - \left[1 - \left(\frac{a_j^\pm}{a_\pm}\right)^3\right](\Psi_D^\pm - \Psi_c^\pm) \tag{44}$$

if the condensed layer has a finite viscosity, as shown in Fig. 15. The former case (43) ressembles the logarithmic concentration dependence of equilibrium zeta potential observed in many microfluidic systems [201], as well as the decay of ICEO flow noted above. The latter case allows for intermediate behavior between strong saturation of $\zeta_{eff} \sim \Psi_c^\pm$ and the HS limit $\zeta_{eff} = \Psi_D$.

MHS slip with Bikerman's model — The reduction of ζ_{eff} arises in different ways depending on the diffuse-layer model. In Bikerman's model for a symmetric electrolyte [53], the limiting behavior is reached fairly suddenly. In that case the integral (41) can be performed analytically to obtain a simple formula:

$$\zeta_{eff}^v = \Psi_D \pm \frac{kT}{ze}\left(\frac{a_j}{a}\right)^3 \ln\left[1 + 4a^3 c_0 \sinh^2\left(\frac{ze\Psi_D}{2kT}\right)\right], \tag{45}$$

illustrated in Fig. 15. For a rigid condensed layer, this model predicts a simple logarithmic decay of ICEO flow with concentration, Eq. (43). If the condensed layer has a large, but finite viscosity, the decay is slower and more complex via Eq. (44). A general feature of even these very simple models is that ICEO flow becomes concentration-dependent and ion-specific at large voltages and/or high salt concentrations, through $z_\pm$, $a_\pm$, $a_j^\pm$,and c_0.

It is interesting to compare Eq. (45) to the only previous MHS formula of Lyklema and Overbeek [59, 60], based on the viscoelectric effect (38) in the context of PB dilute-solution theory. As shown in Figures 12 and 15, the two formulae make similar predictions of saturation of the zeta potential with voltage with $a_j = a$, but our formula (45) is simpler and more amenable to mathematical analysis, as illustrated below. (In contrast, the LO formula takes several lines to write down in closed form [60].) The parameter a is also more constrained on physical grounds, to be of order the hydrated ion size, than the empirical viscoelectric constant f. Qualitatively, the LO formula based on PB theory does not offer any explanation of the experimental fact that ICEO flows depend on the particular ions, even in different solutions of the same ionic valences, $\{z_i\}$ (such as NaCl and KCl), although we do not claim that our Bikerman MHS formula correctly captures any specific trends.

MHS slip in a hard-sphere liquid — As noted above, hard-sphere liquid models show qualitative differences with Bikerman's lattice-based model, beyond just allowing the use of more realistic, smaller effective ion sizes. As shown in Fig. 7, steric effects are stronger in a hard-sphere liquid. The ion density approaches close packing as the voltage is increased much more slowly with the Carnahan-Starling model when compared to Bikerman's model, as shown in Fig. 7(d). When the CS model is used to compute the effective zeta potential with $\rho_j^\pm = \rho_{max}^\pm$ and $\alpha = \beta = 1$ in Eq. (39) as shown in Fig. 16, the effective zeta potential does not saturate as with Bikerman's model, and the layer continues to flow until extremely high voltages are reached, albeit much more slowly than in the classical HS model without charge-induced thickening.

However, at this time we have no reason to assume that $\alpha = \beta = 1$ in Eq. (39). The crucial exponent controlling the viscosity divergence is β. If we set $\beta = 4$, then the divergence is fairly strong as shown by the dashed curves in Fig. 16. Here, we find a strong saturation of ζ_{eff}, similar to what is predicted by Bikerman's model (Fig. 15), which more easily forms a condensed layer. A range of possible MHS slip behavior is possible with a given MPB model for the ion density profile, depending on the precise postulate for charge-induced thickening.

It is important to note the validity of the CS model at high volume fractions must also be questioned. From Eq. 24 and Fig. 7(d) we see that the chemical potential diverges at a volume fraction of 1, but the physical maximum for random close packing for bulk hard spheres is $\Phi \approx 0.63$ [212, 213, 211]. Moreover, crowding in the double layer occurs against a hard wall, which removes geometrical degrees of freedom and thus reduce the accessible local volume fraction for random close packing of hard spheres [231]. It is therefore not even clear what the proper value of $\rho_{max}^\pm$ should be. At this stage, we must consider all of the parameter choices above arbitrary. The development of accurate models of the local rheology of highly charged double layers should ideally be guided by atomistic theories and simulations. We simply give a range of examples to show what kind of qualitative behavior can be predicted by various simple MPB/MHS models, which are suitable for macroscopic theory and simulation of electrokinetic phenomena.

Comparison to compact-layer models. For completeness, we briefly discuss how the general liquid-state models we develop above compare to the traditional approach of dividing the double layer into two parts, a flowing diffuse layer and a rigid compact layer, and assuming a constant viscosity and permittivity everywhere, leading to the HS formula. First we consider the classical

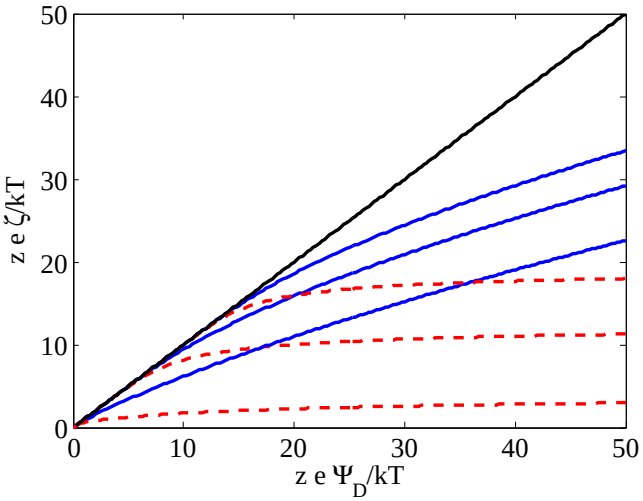

Figure 16: Effective zeta potential ζ_{eff} versus diffuse-layer voltage Ψ_D at different bulk concentrations using the Carnahan-Starling MPB model for charged hard spheres of diameter $a = 4$Å from Fig. 7. The concentration are $c_0 = 1\mu$M, 1 mM, and 1 M from top to bottom. The solid curves use the MHS slip formula (39) with $\alpha = \beta = 1$ and $\rho_j = \rho_{max}$, and the dashed curves change to $\beta = 4$.

Gouy-Chapman-Stern model which postulates an uncharged dielectric monolayer of solvent of constant effective thickness λ_S in contact with a diffuse layer of point-like ions obeying PB theory. The nonlinear charge-voltage relation [95],

$$\Psi = \Psi_D + 2\frac{kT\lambda_D}{ze\lambda_S}\sinh\left(\frac{ze\Psi_D}{2kT}\right), \tag{46}$$

then implies that only a logarithmically small diffuse-layer voltage Ψ_D contributes to the zeta potential at large total voltage Ψ applied to the double layer,

$$\zeta = \Psi_D \sim \frac{kT}{ze}\ln\left(\frac{\varepsilon_b\Psi^2}{2kT\lambda_S^2 c_0}\right)\left[1 - \frac{kT}{ze\Psi} + \ldots\right]. \tag{47}$$

This HS model also predicts that the zeta potential decays logarithmically with concentration and somewhat resembles our MHS models, as shown in Figure 17.

Although the thin-dielectric compact-layer hypothesis leads to some reasonable predictions, it is not fully satisfactory either. As noted above, the saturation of zeta depends on the pileup of point-like ions, albeit reduced by transferring most of the voltage to the compact layer. This can be avoided by using an MPB model with steric constraints, such as Bikerman's model, together with a Stern layer and HS slip. As shown in Fig. 17(a), this tends to reduce the Stern-layer effect, since the diffuse layer is able to carry more voltage due to its reduced capacitance. With increasing δ, however, the Stern layer always carries most of the voltage, and the difference between PB and MPB models on HS slip with the Stern model is eventually lost, as shown in Fig. 17(b) for $\delta = 10$.

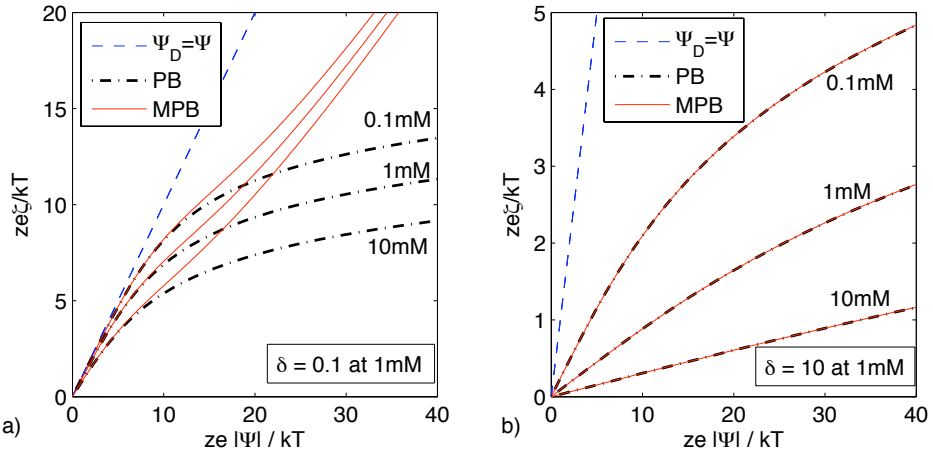

Figure 17: Compact layer effects in traditional HS slip theory assuming a thin dielectric coating between the surface and the diffuse layer, whose importance is controlled by the parameter $\delta = \lambda_S/\lambda_D(c_0) = C_D(c_0)/C_S$ defined in Eq. (6). Both PB (dot-dash curves) and Bikerman's MPB (solid curves) models are considered for the diffuse layer. The zeta potential, equal to the diffuse-layer voltage $\zeta = \Psi_D$, is plotted versus the total double layer voltage Ψ at different values of the bulk salt concentration c_0 (labeled) for $\delta = 0.1$ in (a) and $\delta = 10$ in (b).

This exercise shows that some concentration and voltage effects on slip can be captured by the classical Stern model and HS slip formula, but we are left with the same general criticisms made above for charging dynamics. The model places most of the large voltage across a region for which no detailed physical model is assumed, without attempting to account for liquid-state properties, salt concentration, surface roughness, liquid-surface interactions, etc. It is also not clear that a hypothetical Stern monolayer of solvent could withstand several Volts, while leaving a dilute diffuse layer with a small voltage, and some model for dynamical effects in response to applied voltages should be required.

We have already seen in section 2 that the classical model is unable to predict all the trends in nonlinear electrokinetics. Except in the case of a true dielectric coating (e.g a native oxide on a metal electrode), it seems more physically realistic to discard the the concept of the compact layer and ascribe all the behavior to the dynamics of the liquid state, as described by an appropriate modified theory that approximates the compact layer through strong molecular interactions, as sketched in Fig. 13. At least in this work, we have shown that it is possible to describe a variety of nonlinear effects in charging dynamics and electro-osmotic flow at large voltages and/or large salt concentrations without resorting to lumping the errors from dilute solution theory in a hypothetical compact layer outside the continuum model. Perhaps a more accurate theory would combine the ideas of this paper for the liquid phase with boundary conditions representing a compact interfacial phase, along the lines of the dynamical Stern layer model [225, 227, 230].

4.2.2. Ion-specific electrophoretic mobility

We have already noted that induced-charge electrokinetic phenomena are sensitive to the solution composition in our models, via both the nonlinear capacitance and the effective zeta potential. There are some surprising, general consequences, which are well illustrated by ICEP

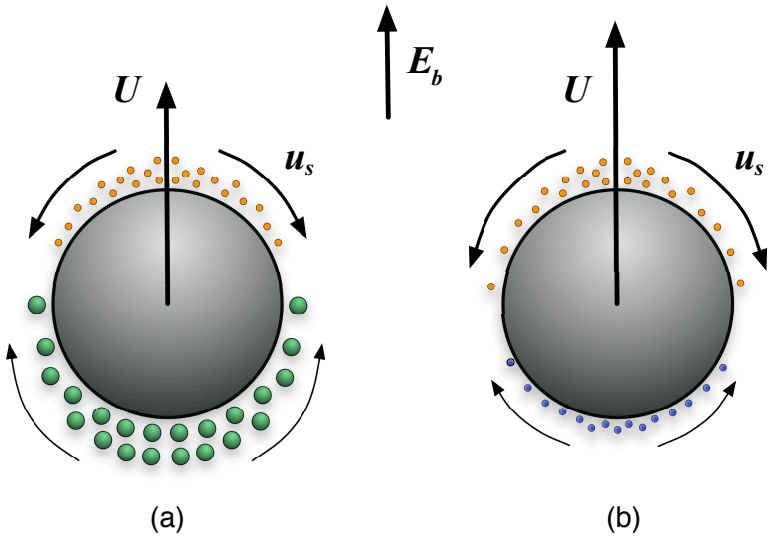

Figure 18: Mechanisms for DC electrophoretic motion U of an uncharged metallic sphere in an asymmetric electrolyte (48) due to saturated ICEO flow (43) in a large field $E_b \gg kT/eR$. (a) Larger cations (below) in a $z:z$ electrolyte ($a_+ > a_-$, $z_+ = |z_-|$) pack at lower density than smaller anions (above) and thus cover more of the sphere, but produce less slip due to greater crowding. (b) Divalent cations (below) cover less area and also produce less slip than monovalent anions of the same size ($a_+ = a_-$, $z_+ > |z_-|$). In both examples, the sphere has an *apparent* positive charge ($U > 0$).

of an uncharged metallic sphere. It has been predicted using low-voltage models [13, 19, 20] and observed [232, 21] that asymmetric polarizable particles in a uniform field have an ICEP velocity scaling as E_b^2, but it is widely believed that linear velocity scaling, $U = b_{ep}E_b$, implies nonzero total charge. For non-polarizable particles with thin double layers, this is the case, unless the particle has both asymmetric shape and a non-uniform charge density [233, 234]. For polarizable particles, our models predict that a nonzero mobility b_{ep} can result simply from *broken symmetry in the electrolyte*, even for a perfectly symmetric particle.

Consider an ideally polarizable, uncharged sphere of radius R in an asymmetric binary electrolyte with ions of unequal effective sizes $a_\pm$ and charges $z_\pm e$, subject to a uniform DC background field E_b. The first effect to consider is the shift in the potential $\phi_0(E_b)$ of the particle (relative to the applied background potential) due to its asymmetric nonlinear capacitance, since the induced charge (which must integrate to zero) is more dense on one side than the other, as shown in Fig. 18. As noted above, this already yields a nonzero mobility with the HS formula, $b_{ep} = \varepsilon_b\phi_0/\eta_b$.

The effect of zeta saturation (43) provides a different dependence on the solution composition, which dominates in large fields, $E_b \gg kT/eR$. Since $|\phi_0(E_b)| \ll E_bR$, the change in polarity of the induced charge occurs near the equator, around which there is only a narrow region with $|\zeta_{eff}| < |\Psi_c^\pm|$. In this limit, therefore, we approximate one hemisphere with uniform $\zeta_{eff} = \Psi_c^+$ and the other with Ψ_c^-, which yields the ion-dependent mobility

$$b_{ep} \sim \frac{1}{2}\frac{\varepsilon_b}{\eta_b}\frac{kT}{e}\ln\left[\frac{(a_+^3c_0)^{1/z_+}}{(a_-^3c_0)^{1/|z_-|}}\right] \tag{48}$$

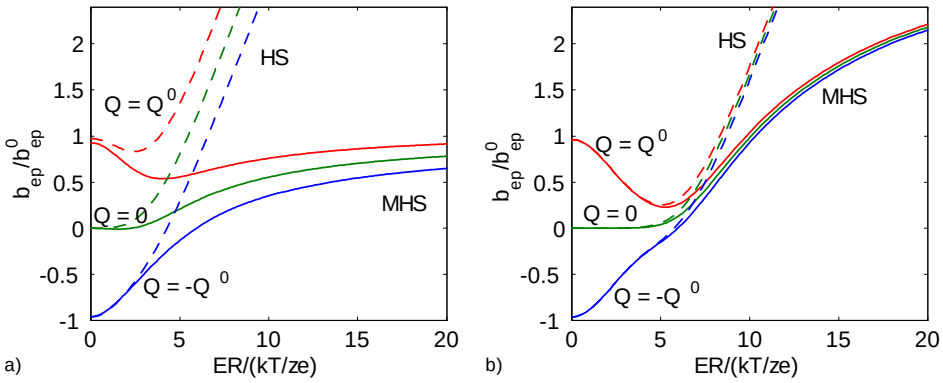

Figure 19: Electrophoretic mobility of an ideally polarizable sphere of total charge Q in an asymmetric electrolyte with $(a_-/a_+)^3 = 10$ from Fig. 11 with HS slip (dashed curves) compared to the same calculations redone with MHS slip (45) for (a) high salt concentration $\nu_- = 0.1$ and $\nu_+ = 0.01$ and (b) moderate salt concentration $\nu_- = 10^{-3}$ and $\nu_+ = 10^{-4}$. Charge-induced thickening has the opposite effect of nonlinear capacitance, since it gives more weight to smaller and/or more highly charged counterions in determining the electrophoretic mobility. This significantly reduces the apparent charge of the particle at large fields and/or high salt concentrations, but not enough to change its sign.

The apparent zeta potential from a DC electrophoresis measurement $\zeta_{ep} = \eta_b b_{ep}/\varepsilon$, tends to a constant of order $\approx kT/e$, independent of E_b and R. In a $z:z$ electrolyte, the limiting value

$$\zeta_{ep} \sim \frac{3}{2}\frac{kT}{ze}\ln\frac{a_+}{a_-} \tag{49}$$

is set by the size ratio a_+/a_- and does not depend on the bulk concentration c_0. With equal sizes $a_+ = a_- = a$, the limiting apparent zeta potential

$$\zeta_{ep} \sim \frac{1}{2}\frac{kT}{\bar{z}e}\ln(a^3 c_0) \tag{50}$$

is set by harmonic mean of the valences, $\bar{z} = z_+ z_-/(z_+ + z_-)$, if $z_+ + z_- \neq 0$.

An interesting feature of this nonlinearity is that the limiting mobility is set by properties of the electrolyte and is independent of the true charge of the particle. As sketched in Fig. 18, the induced viscosity increase alone causes the neutral sphere to have an apparent charge whose sign is that of the ions which condense at a lower potential (larger z and/or larger a). For consistency, however, we should also include the nonlinear capacitance effect, which can act in the opposite direction, making the apparent charge that of the ions which pack less densely (smaller z and/or smaller a). As shown in Fig. 19, it turns out that the nonlinear capacitance effect is stronger and determines the sign of the apparent charge of the particle in large fields and/or high salt concentrations. Nevertheless, the charge-induced thickening effect significantly reduces the mobility in this regime and introduces a strong decay with salt concentration.

By now, it should be clear that ICEP of charged, asymmetric, polarizable particles can have a very complicated dependence on the solution chemistry in large electric fields and/or high salt concentrations. We must stress again that we do not include strongly nonlinear effects such as surface conduction and salt adsorption by the double layers, so the predictions of this paper only pertain to moderate voltages and thin double layers in the weakly nonlinear regime. Nevertheless,

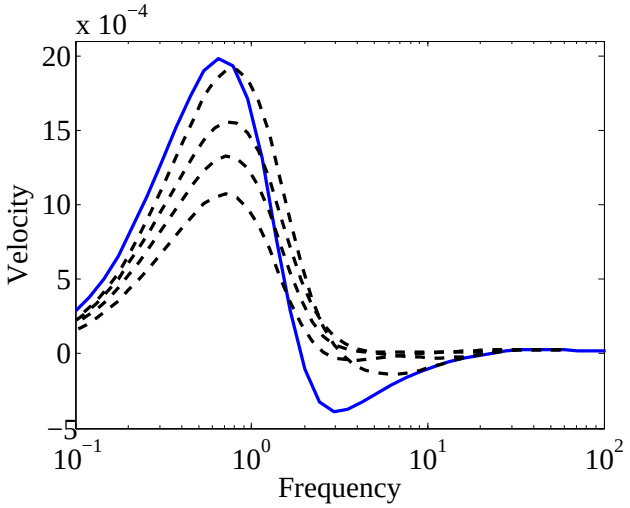

Figure 20: Frequency response of ACEO pumping with MHS slip and Bikerman's model of steric effects. Data are shown in dimensionless form where frequency is scaled by the RC time of the equivalent circuit and the velocity is scaled by $\varepsilon V^2/\eta L_0$ [38]. The values of $\nu = 2c_o a^3$ used in (45) are 0, 10^{-10}, 10^{-6}, 10^{-4}, and 10^{-2}, from top to bottom. Even at the extremely low values of ν, this model of charge induced thickening essentially removes the prediction of reverse flow. For the steric effects, $\nu = 0.01$, in the Bikerman model was used for all cases.

we already see some interesting new qualitative features predicted by the modified models. Our examples also show that the electrophoretic mobility of a homogeneous polarizable particle need not provide a reliable measure of its total charge, contrary to common wisdom.

4.2.3. Concentration dependence of AC electro-osmosis

Next we revisit the weakly nonlinear analysis of ACEO pumping by adding the effect of charge-induced thickening via the MHS slip formula (45) in a symmetric electrolyte. In Fig. 20 we show predictions of an ACEO pump including steric effects (Bikerman) and the simplest MHS, Equation 45 with $a_j/a = 1$. In interpreting these data, it is useful to remember that our simple model predicts the effective zeta potential to be the same as the voltage across the double layer up to a critical voltage whereafter the effective zeta potential saturates, see Fig. 15. At high frequency, there is insufficient time for the double layers to fully charge and therefore the cutoff voltage is not reached and the slip is uneffected. At low frequency and high volatge, the double layers fully charge and the saturated zeta-potential severly limits the flow. Thus the MHS model acts as a high-pass filter for electroosmotic slip. This effect can be seen in Fig. 20 as the ion size decreases (thus the cutoff voltage increases). The upper dashed curve, given the physical interpretation of the model would require an ion size of 0.1 angstroms at 0.1 mM concentration. For more realistic ion sizes (at 0.1 mM and $a = 3$ angstroms, $\nu = 7 \times 10^{-6}$) we find that the viscoelectric effect essentially eliminates the prediction flow reversal from Bikerman's model. To date we have not successfully predicted flow decay with concentration and high frequency reversal in ACEO with a single, unified model though work continues in this direction.

Figure 21 shows results applying the MHS model, (45), to the ACEO pumps of Urbanski *et*

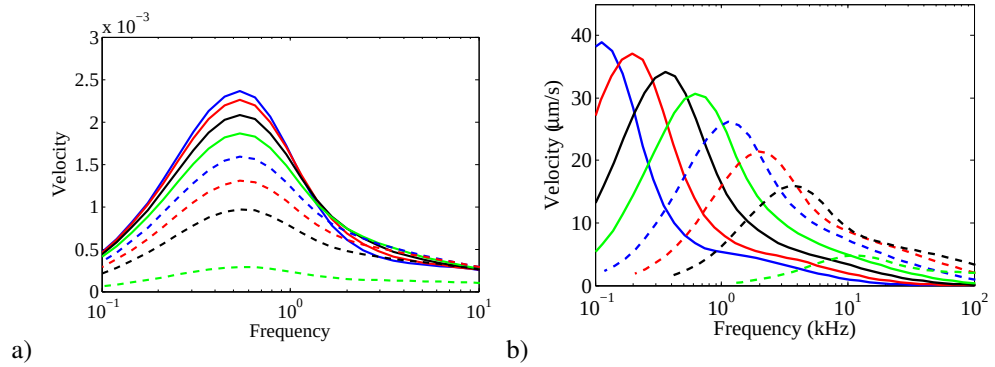

Figure 21: Predicted frequency response of the ACEO pump of Urbanski *et al* [36] from Fig. 3(a) with an MPB double-layer model also accounting for MHS slip with charge-induced thickening. In (a) we show the dimensionless frequency response of the pump as we change concentration (C = 0.001, 0.003, 0.01, 0.03, 0.1 0.3, 1, and 10 mM from top to bottom). In (b) the same data are plotted in dimensional form. The model of charge-induced thickening uses a constant ion size of 4 nm. The response is computed with the Bikerman model using a constant value of $\nu = 0.01$, though no high-frequency flow reversal is predicted at this voltage.

al [36]. We see a decay in the maximum flow velocity with concentration that is reminiscent of experiments, Fig. 3, when we view the data in dimensionless form. Figure 21 (a) shows the dimensionless frequency response as we change concentration as in the experiments using a fixed ion size of 4 nm. As with the predictions of flow reversal in ACEO, it seems that the ion size that best fits the experiments is an order of magnitude larger than we would expect. The simulated data show the promise of a simple charge-induced thickening model to predict decay of flow with concentration. It is interesting to note that at the relatively low voltage of these experiments (3 Vpp $\approx$ 1 Vrms) there is no flow reversal predicted even when the viscoelectric effect is relatively weak, contrary to the experimental observations.

We show the data in dimensional form in Figure 21 (b) for a direct comparison to experiments. We again see one of the key discrepancies which occurs in all models be they based in classical electrokinetic theory or based on the modified models presented here. All the models assuming blocking electrodes predict that the features in the frequency response are strongly concentration dependent, while the data show relative insensitivity to concentration. As discussed in Section 3.2.1, we hypothesize this discrepancy is due to neglect of Faradaic reactions though this remains an area for future study.

These simple models are capable of reproducing at least in qualitative way the general experimental trends of ACEO. The Standard Model which does not account for charge induced thickening does not predict a strong flow decay as concentration is increased as all ACEO experiments have shown. We should also emphasize that our models are surely oversimplified, and various neglected effects, such as specific solvent-mediated forces or electrostatic correlations can effectively increase the range of crowding effects (to allow the use of realistic ion sizes) and change their form in ways that may improve the ability to fit experimental data.

5. Mathematical modeling of electrokinetics in a concentrated solution

5.1. Nanoscale physics

The fundamental difficulty in modeling all electrokinetic phenomena is that complex molecular-scale phenomena at the electrified interface give rise to macroscopic fluid motion. The modified models above attempt to take into account some new physics – steric effects for finite-sized ions and charge-dependent visco-electric effects - but these are just simple first steps away from dilute-solution theory in electrokinetics. In this section, we develop a general theoretical framework for modeling electrokinetic phenomena in concentrated solutions (including large applied voltages in dilute solutions).

We begin by discussing various neglected effects in our models above that might need to be incorporated into the general theory, some of which were anticipated (qualitatively) by J. J. Bikerman decades ago [235, 236]. In some sense, what we are attempting is to model part of the "compact layer" in microscopic detail using the *same* continuum equations that describe the "diffuse layer" and the bulk electrolyte. The hypothetical partitioning of the interface between diffuse and compact parts has become entrenched in electrokinetics and had many successes, at least in describing linear phenomena with non-polarizable surfaces of fixed charge. In such cases, it usually suffices to define an effective slip plane, which marks the sharp transition from a dilute solution to a stagnant [201, 9] or dynamical [225, 227, 230] compact layer, whose fixed position can be fit to electrokinetic measurements. At large induced voltages or concentrated solutions, however, we believe it is necessary to describe the nanoscale rheology of the liquid in more detail, since it is otherwise not clear how to shift the effective shear plane with voltage or concentration, as sketched in Fig. 13. As in prior work, it may still be useful to maintain the theoretical construct of a separate "compact layer" via effective boundary conditions on the continuum region, but crowding effects, which vary with the local electric field and ionic concentrations, should also be included in modified electrokinetic equations.

The following are some nanoscale physical effects, other than steric and viscoelectric effects, that we have neglected or included only heuristically, which may be important in nonlinear electrokinetics and other situations discussed below. In some cases, simple continuum models are available but have not yet been applied to electrokinetic phenomena as part of a coherent theoretical framework. Setting the stage for such modeling is the goal of this section.

- *Electrostatic correlations.* To our knowledge, all mathematical models in electrokinetics are based on the mean-field approximation, where each ion only feels an electrostatic force from the mean charge density of all the other ions In reality, ions are discrete charges that exert correlated forces on each other, which become especially important with increasing valence [146, 145]. The breakdown of the mean-field approximation for multivalent ions can lead to counterion condensation on the surface, effectively leading to a correlated two-dimensional liquid (or glass) resembling a Wigner crystal of like charges in the limit of strong coupling [216].

  In addition to this effect, a promising direction for continuum modeling (discussed below) may be to build on MPB equation of Ref. [237], which describes the effective restoring force acting on an ion that tries to fluctuate from its local electrostatic equilibrium position, only to be drawn back toward its correlation hole. We conjecture that this effect may not be so important at very high charge densities in large applied voltages, where simple crowding becomes dominant and flattens out any oscillations in the charge-density profiles. Some evidence comes from recent molecular simulations of the double-layer capacitance of ion

liquids [72], which verify the square-root scaling of MPB theory with steric effects discuss above.

On the other hand, electrostatic correlations may be crucial for the dynamics of highly charged double layers under mechanical shear stress, which to our knowledge has never been studied. We have conjectured above that the correlation hole interaction may effectively enhance the viscosity of the solution and lead to charge-induced thickening. Electrostatic correlations may also effectively increase the critical length for crowding effects, and we have noted elsewhere that the Bjerrum length $\ell_B = e^2/4\pi\varepsilon_b kT$ is at the same scale as the effective ion size required in our steric MPB models of ACEO, especially if corrected for reduced permittivity in large field [56, 96, 63]. The electrostatic correlation length λ_c (defined below) is approximately $\lambda_c = z^2\ell_B$ for a $z:z$ electrolyte, so ion-ion correlations are particularly important for multivalent ions.

The relative importance of corrections to mean-field theory due to electrostatic ion-ion correlations is controlled by the dimensionless parameter,

$$\begin{aligned} \delta_c &= \frac{\lambda_c}{\lambda_D} \\ &= \frac{\ell_B z^2}{\lambda_D} = \frac{(ze)^2(2c_0)^{1/2}}{4\pi(\varepsilon_b kT)^{3/2}} \quad (z:z \text{ electrolyte}) \end{aligned} \tag{51}$$

which grows with bulk salt concentration like $\sqrt{c_0}$, as the Debye screening length shrinks. The Bjerrum length in bulk water is $\ell_B \approx 7$Å, so we expect strong correlation effects on electrochemical transport and electrokinetics when $\lambda_D > 7z^2$Å which is 7Å, 1.4 nm, and 2.8 nm for monovalent, divalent, and trivalent ions, respectively. The condition of "intermediate coupling" $\delta_c = O(1)$ is met in many concentrated aqueous solutions, so it may be necessary to include correlation effects in theories of nonlinear electrokinetics and double-layer charging dynamics. Below, we discuss a possible modification of Poisson's equation, based on Ref. [237], which could provide a starting point.

- *Specific ion-ion interactions.* In addition to entropic effects such as hard-sphere repulsion and long-range electrostatic forces, ions can interact via more complicated short-range forces, due to direct molecular interactions or solvent-mediated effective forces. DiCaprio et al. [151] recently expressed the excess free energy density of an electrolyte as the sum of a hard-sphere entropic contribution (e.g. the CS model above, or its generalization to polydisperse mixtures) plus the first, quadratic terms in a Taylor expansion in the ionic concentrations. In our theoretical framework, the latter corresponds to an additional linear, enthalpic contribution to the excess chemical potential

$$\mu_i^{ex} = kT \sum_j a_{ij} c_j \quad \text{(specific ion-ion interactions)} \tag{52}$$

where the coupling coefficients a_{ij} (with units of volume) are assumed to be concentration independent. These terms effectively "soften" the hard-sphere interactions by introducing further short-range forces. For example, if $a_{ii} > 0$ (or < 0), then like-charged ions experience an additional repulsion (or attraction) within a volume a_{ii}, and this increases (or decreases) the effective hard-sphere radius for crowded counterions. (More complicated concentration-dependent enthalpic terms have also been postulated for ions intercalated in

crystalline solids in rechargeable battery electrodes [238].) Specific interactions may also contribute to dynamical friction coefficients between different ionic species, e.g. leading to off-diagonal elements in the mobility tensor (see below), which could be important in large ac fields [136] where oppositely charged ions must quickly pass each other upon polarization reversal.

- *Specific ion-wall interactions.* Just as ions in the liquid phase can have short-range interactions with each other, beyond the mean-field electrostatic force and hard-sphere repulsion, so too can they have specific interactions with molecules comprising a phase boundary, such as a solid wall. The simplest of these result from hard-sphere ordering and solvent-mediated forces which produced correlations near the flat wall. Indeed, molecular simulations taking into account the solvent (beyond the primitive model) reveal strong density oscillations near a wall [239, 240, 241, 90, 91]. This solvent-induced layering can be described by MPB models, by simply adding an effective external potential $V_w(x)$ to the excess chemical potential [91, 152, 93],

$$\mu_i^{ex} = V_w(x) = -kT \ln\left(\frac{\rho_s(x)}{\rho_b}\right) \tag{53}$$

  which can be expressed in terms of the statistical density profile (pair correlation function) $\rho_s(x)$ of the solvent molecules near the wall, relative to their bulk density ρ_b [241]. Stern's original model of a solvation monolayer separating ions from the surface [142] is of this type, since he essentially postulated an infinite chemical potential $V_w(x)$ for ions in the monolayer. Of course, it is more realistic to allow for smooth oscillations in the ion-wall correlation function over several molecular diameters, but at least Stern's model is easily incorporated into a boundary condition [95] (see below).

- *Surface heterogeneity.* Discrete surface charges contribute to electrostatic correlations [216], but chemical heterogeneities can also play an important role in the structure of the double layer and electrokinetic phenomena [242, 243]. In the context of PB theory, the effect of surface roughness on the differential capacitance of the double layer depends on the correlation length of the roughess relative to the Debye length [244, 245]. With finite-size ions, roughness could have a much stronger effect, not only on capacitance, but also on slip generation. Molecular dynamics simulations of electro-osmosis over atomically rough surfaces have revealed departures from PB theory [217], but large induced voltages have yet to be studied. Given the arguments of the previous section, the charge-induced viscosity increase is likely to be enhanced by roughness, since the electrostatic compression of hydrated ions against molecular scale asperities should thicken the fluid and make the apparent ion size seem larger.

- *Specific adsorption of ions.* Another effect we have neglected is the specific adsorption of ions, which break free of solvation and come into direct molecular contact with a surface, under sufficiently large normal electric fields, which is related to the phenomenon of "charge regulation" or "potential regulation" of a charged surface [242]. This effect is widely invoked in electrochemistry to explain the increase of differential capacitance of the double layer at high voltage observed in many experimental situations, since the distance between plates of the equivalent capacitor effectively shrinks from the "outer Helmholtz plane" to the "inner Helmholtz plane", and a number phenomenological models are available [119, 246]. Some results combining specific adsorption with MPB models of the

diffuse layer are in Ref. [197]. Of course, at very large voltages with steric effects included, the differential capacitance at blocking electrodes must eventually decrease, once the IHP and OHP both become saturated with ions, as we have argued above. This regime of universal square-root decay is often inaccessible at low frequency due to Faradaic reactions, but our modeling of ACEO flow reversal above suggests that it can be probed at high frequency.

- *Normal current and Faradaic reactions.* Most models in nonlinear electrokinetics assume blocking surfaces in order to focus on capacitive double-layer charging and simple ICEO flow. As noted in section 2, however, there is growing evidence that Faradaic charge-transfer reactions play a major role, especially at low frequency and high voltage (as in Fig. 9). This leads to normal currents, which can perturb the equilibrium structure of the double layer. Lacoste et al. [18] have recently noted that reverse ICEO flows can arise even at low voltages in a mean-field theory of biological membranes passing a normal ionic current, in the Helmholtz limit of a thick dielectric layer ($\delta \to \infty$). Since this limit corresponds to a large "correction factor" in the Standard Model as inferred from most experiments (see section 2), it may be that non-equilibrium double-layer structure in the presence of Faradaic reactions is involved in the low-frequency, high-voltage flow reversal in ACEO and TWEO, in addition to effects of diffusion-layer electroconvection [116]. Below, we note that the mathematical description of Faradaic reactions may also need to be modified for large voltages or concentrated solutions.

In the next section, we summarize a general mathematical framework for the dynamics of electrolytes and ionic liquids, which naturally allows the incorporation of some of these effects.

5.2. Modified electrokinetic equations

5.2.1. Electrochemical transport

Until now we have focused on situations with thin double layers and integrated over the double-layer structure to obtain modified effective boundary conditions on the quasi-neutral bulk fluid, namely the MPB differential capacitance in section 3 and MHS slip in section 4. In this section, we summarize the modified continuum electrokinetic equations corresponding to these models, which could be applied to arbitrary geometries with thin or thick double layers in nonlinear electrokinetics. A few examples of this approach been developed for linear electrokinetics [64, 65] and electrochemical dynamics [96, 172]. Such modified continuum equations aim to capture more of the essential physics of nanoscale electrokinetics, while remaining much simpler and widely applicable than brute-force molecular dynamics [89, 90, 91, 92, 93, 94] or more complex statistical approaches [247, 248, 66], and could have broad applicability beyond the problems considered here.

We have made the case for modified electrokinetic equations based on experimental and theoretical arguments in nonlinear electrokinetics, but similar issues also arise in other fields. We have already noted that Bikerman's model has recently been adapted to model the double layer in ionic liquids [70, 71, 72], but mainly to predict the differential capacitance for use in RC circuit models. We are not aware of any attempt to describe electrokinetics or non-equiilibrium dynamics of ionic liquids, so our general approach below may have some relevance, in the limit of very high salt concentration, approaching a molten salt. Steric effects in polyelectrolytes have also been described by Bikerman's model [171] as well as the CS and BMCSL hard-sphere models [183, 182], and this is another interesting area to consider electrokinetics with crowding effects.

Even in the more familiar context of electrolytes, there has been a recent explosion of interest in nanofluidics [77, 78], since the high surface-to-volume ratio of nanochannels amplifies the importance of transport phenomena occurring in confined geometries, effectively inside double layer. In recent years, the classical electrokinetic equations for a dilute solution have been used extensively (and exclusively) to model nanochannel phenomena such as ion selectivity [79, 80, 81, 82] and mechanical-to-electrical power conversion [83, 84, 85, 86, 87, 88], but quantitative agreement with experiments often requires fitting "extra" compact-layer properties. As noted in the introduction, Liu et el. [66] have recently considered correlations and crowding effects in steady nanochannel transport via a continuum MPB theory, based on more complex statistical models than those considered here [67, 68, 69]. This approach incorporates more physics than we have considered above, but this comes at the expense of sacrificing some generality and mathematical simplicity, since it assumes equilibrium charge profiles and requires numerical integration of coupled integral equations to determine the self-consistent charge density in Poisson's equation. Instead, we build on the simpler models of nanochannel transport with steric effects developed by Cervera et al. [64, 65].

Here, we describe a general modeling framework based on electrochemical potentials, which applies to non-equilibrium situations and includes the simple cases considered above. In principle, one could start with the full theory of non-equilibrium thermodynamics of multicomponent systems [249, 250], but we develop a simpler phenomenological theory for electrokinetics in an isothermal concentrated solution. Our general starting point is to postulate a continuum model for the electrochemical potential of an ion of species i (possibly including a solvation shell, depending on the model), decomposed into ideal-gas, electrostatic, and excess contributions as follows:

$$\mu_i = kT \ln c_i + z_i e\phi + \mu_i^{ex}(x, \{c_j\}, \phi, \{\nabla c_j\}, \nabla\phi, \ldots) \tag{54}$$

The thermodynamic meaning of μ_i is the Gibbs free energy difference upon adding a particle of species i (and replacing other particles or empty space) within a continuum element, viewed as a local open system in quasi-equilibrium with the reservoir of nearby elements. Its gradient $-\nabla\mu_i$ acts as a mean "thermodynamic force" on each particle, driving the system toward local equilibrium. In (54), we have defined μ_i^{ex} as the excess chemical potential of ion i relative to a dilute solution, expressed in terms of local continuum variables, such as the position x (e.g. distance from a surface), ionic concentrations $\{c_j\}$ and their gradients (to approximate non-local contributions), electrostatic potential ϕ and field $E = -\nabla\phi$, etc. The fundamental significance of electrochemical potentials is emphasized by Newman [147], who also questions validity of the mean electrostatic potential ϕ at the molecular level in a multi-component concentrated solution. Nevertheless, it is necessary to separate long-range electrostatic forces from short-range chemical interactions to develop continuum equations for electrokinetics, so we proceed with the phenomenological decomposition in (54). From this perspective, we can view $\mu_i^{ex} = kT \ln f_i$ as defining the chemical activity coefficient f_i in terms of the mean-field approximation for ϕ.

In principle, the excess chemical potential μ_i^{ex} can be derived from microscopic statistical models or by fitting to molecular dynamics simulations or experiments. For example, throughout this article, we have focused on two simple models of μ_i^{ex} for steric effects of excluded volume for solvated ions, namely Bikerman's lattice-based model (19) and the Carnahan-Starling hard-sphere-liquid model (24). Above in this section, we noted some other possible contributions. Simple mean-field models are also available for specific solvent-mediated ion-wall interactions (53) and ion-ion interactions (52). More complicated effects of statistical correlations can also be included in μ_i^{ex} by making it a non-local functional of the complete ion density-profiles and

the self-consistent electrostatic potential [247], although mathematical analysis is clearly simpler for local models which lead to partial differential equations, where μ_i^{ex} is only a function of the concentrations and potential and possibly their gradients, in a Taylor expansion of non-local effects.

In non-equilibrium thermodynamics [249, 250, 147], the mass flux densities $\mathbf{F}_i$ are obtained from the phenomenological hypothesis of linear response:

$$\mathbf{F}_i = c_i \mathbf{u} - \sum_j L_{ij} c_j \nabla \mu_j \tag{55}$$

where $\mathbf{f}_j = -c_j \nabla \mu_j$ is the thermodynamic force density (force/volume) acting on species j and L_{ij} is the (symmetric, positive definite) Onsager mobility tensor converting these forces into mean drift velocities in the frame moving with the mass-averaged velocity $\mathbf{u}$. The mobility tensor is related to the diffusivity tensor by the Einstein relation, $D_{ij} = L_{ij} kT$, and is usually assumed to be be diagonal, $D_{ij} = D_i \delta_{ij}$, but this can only be justified for a dilute solution. In a highly concentrated solution, the mobility tensor (or its inverse, the friction tensor) may have significant off-diagonal elements [249, 250].

Conservation of mass implies

$$\frac{\partial c_i}{\partial t} + \nabla \cdot \mathbf{F}_i = r_i \tag{56}$$

where r_i is the reaction rate density for production (or removal) of ion i, which is usually (but not always [251]) set to zero for electrolytes. With these further assumptions, the modified Nernst-Planck equations take the form,

$$\frac{\partial c_i}{\partial t} + \nabla \cdot (c_i \mathbf{u}) = \nabla \cdot \left\{ D_i \left[\nabla c_i + c_i \nabla \left(\frac{z_i e \phi + \mu_i^{ex}}{kT} \right) \right] \right\} \tag{57}$$

5.2.2. Electrostatics

The system of modified PNP equations [96] is usually closed by making the mean-field approximation, in which the electrostatic potential self-consistently satisfies Poisson's equation

$$-\nabla \cdot (\varepsilon \nabla \phi) = \rho = \sum_i z_i e c_i \tag{58}$$

where ρ is the mean charge density. The permittivity ε of a polar solvent like water is usually taken as a constant in (58). The permittivity is believed to decrease in large fields, especially within a few molecular diameters of a highly charged surface (within the compact layer) due to the alignment of solvent dipoles [119], although a recent modified PB theory of ions and solvent dipoles predicts an increase in electrolyte permittivity with field intensity near a charged surface, due to an increase in the dipole density [252]. The permittivity may also vary with temperature, due to Joule heating or reactions, but here we only consider isothermal systems.

We are not aware of any attempts to go beyond the mean-field approximation (58) in dynamical problems of ion transport or electrokinetics. This would require a simple continuum treatment of correlation effects, ideally leading to a general modification of (58). Recently, Santangelo [237] derived a simple modified PB equation accounting for ion-ion electrostatic correlations near a charged wall in the relevant regime of "intermediate coupling", $\delta_c = \lambda_c / \lambda_D = O(1)$, which suggests modifying Poisson's equation with an additional term,

$$\left(\lambda_c^2 \nabla^2 - 1 \right) \nabla \cdot (\varepsilon \nabla \phi) = \rho \tag{59}$$

where λ_c is the electrostatic ion-ion correlation length, set by the balance of thermal energy and Coulomb energy in the dielectric medium. Physically, the extra term roughly accounts for interactions between an ion and its correlation hole during thermal fluctuations. The higher derivative of the correction term introduces the possibility of oscillations in the ion densities at the scale of the correlation length. (It also requires additional boundary conditions, discussed below.) The relative importance of the correction term in (59) is measured by the dimensionless parameter $\delta_c = \lambda_c/\lambda_D$ introduced above, which takes the form $\delta_c = z^2\ell_B/\lambda_D$ for a $z:z$ electrolyte. Since $\delta_c = O(1)$ for concentrated aqueous solutions (and increases if local permittivity decreases), correlation effects could be important in electrokinetics, and Santangelo's equation may provide a useful starting point for analysis. For ionic liquids, correlation effects are even more important, since the diffuse layer shrinks to the molecular scale ($\delta_c \gg 1$).

5.2.3. Electrochemical hydrodynamics

To determine the mass-averaged solution velocity, $\mathbf{u}$, we enforce the conservation of linear momentum

$$\rho_m \frac{\partial \mathbf{u}}{\partial t} + \nabla \cdot \mathbf{T} = \mathbf{f} \tag{60}$$

where ρ_m is the total solution mass density (which can be set to its bulk value in most cases), $\mathbf{T}$ is the hydrodynamic stress tensor (arising from mechanical friction), and $\mathbf{f} = \sum_i \mathbf{f}_i$ is the thermodynamic force density (acting on all the ions, independent of fluid flow). The nonlinear inertial convection term $\mathbf{u}\cdot\nabla\mathbf{u}$ could be added to (60), but it is typically negligible in nonlinear electrokinetics due to a very small Reynolds number. For the stress tensor, the first approximation is the Newtonian form, $\mathbf{T} = p\mathbf{I} - \mathbf{T}^{(v)}$ with contributions from the dynamic pressure p (to satisfy incompressibility, $\nabla\cdot\mathbf{u} = 0$) and the viscous stress tensor,

$$T^{(v)}_{ij} = \eta\left(\frac{\partial u_i}{\partial x_j} + \frac{\partial u_j}{\partial x_i}\right). \tag{61}$$

As explained in section 4, there may be significant local changes in viscosity near a highly charged surface. For example, the following empirical form combines the viscoelectric effect (38) and charge-induced thickening (39),

$$\eta = \eta_b\left[1 - \left(\frac{\rho}{\rho_j^{\pm}}\right)^2\right]^{-\beta}\left(1 + fE^2\right)^{\gamma}. \tag{62}$$

For simplicity, one could typically set $\gamma = 0$, since E tends to grow with ρ in a similar way, via the MPB equations, as noted above. Alternatively, one could set $\beta = 0$, but that removes any explicit dependence on the effective ion sizes or other modified interactions.

The thermodynamic force $\mathbf{f}$, which acts as a source of momentum in (60), can be simplified, if we assume small departures from local thermal equilibrium. We also neglect heat transfer and assume isothermal conditions. In that case, the Gibbs free energy density, $g = \sum_i c_i\mu_i$, varies as

$$\delta g = \delta p_0 + \sum_i \mu_i\,\delta c_i + \rho\,\delta\phi = \sum_i (c_i\delta\mu_i + \mu_i\,\delta c_i) \tag{63}$$

where p_0 is the hydrostatic pressure. Taking the variation between adjacent continuum elements, we obtain

$$-\mathbf{f} = \sum_i c_i\nabla\mu_i = \nabla p_0 + \rho\nabla\phi \tag{64}$$

which is a form of the Gibbs-Duhem relation [249, 147], adapted for an isothermal charged system. Note that p_0 includes the osmotic pressure that balances concentration gradients, which takes the form, $kT\sum_i c_i$, in a dilute solution upon inserting (12) into (64). In a concentrated solution, the osmotic pressure can take a more complicated, possibly non-algebraic form, but its gradient should still uphold the local Gibbs-Duhem relation(64) near thermal equilibrium.

Since we assume incompressible flow, we can insert (64) into (60) and absorb p_0 into the dynamical pressure p. In this way, we arrive at the familiar form of the unsteady Stokes equation,

$$\rho_m \frac{\partial \mathbf{u}}{\partial t} + \nabla \cdot \mathbf{T} = \mathbf{f}_e \tag{65}$$

with an electrostatic force density, $\mathbf{f}_e = -\rho\nabla\phi$. The unsteady term $\partial\mathbf{u}/\partial t$ in (65) is often overlooked, but it can be important in nonlinear electrokinetics, e.g. for oscillating momentum boundary layers and vortex shedding in response to AC forcing [14, 39].

The Stokes equation (65) is the standard description of fluid mechanics at low Reynolds number, which is normally applied in to a dilute solution, but we see that it also holds for an isothermal, concentrated solution near equilibrium, regardless of the form of μ_i^{ex}. In their theory of non-equilbrium thermodynamics, De Groot and Mazur [249] instead assert (65) as the fundamental expression of momentum conservation, where the "external" or "long-ranged" force $\mathbf{f}_e$ acts as the source of momentum flux in a continuum element, whose internal "short-ranged" forces are described by $\mathbf{T}$. Here, we show the equivalence of starting with (60) based on the full thermodynamic force $\mathbf{f}$ for a concentrated solution and deriving (65) as the quasi-equilibrium limit, where only the external (electrostatic) force $\mathbf{f}_e$ produces momentum. In this limit, which is consistent with the assumption of linear response (55) for the mass fluxes, all other the "chemical" interactions in $\mathbf{f} - \mathbf{f}_e$ only contribute to the (osmotic) pressure.

Non-equilibrium thermodynamics can be extended to account for the electrical polarizability of a concentrated solution [249]. For a linear dielectric medium with variable permittivity ε, the electrostatic force density can be expressed in the familiar form, $\mathbf{f}_e = -\nabla\cdot\mathbf{T}^{(e)}$, where

$$T_{ij}^{(e)} = \varepsilon\left(E_iE_j - \frac{1}{2}|E|^2\delta_{ij}\right) \tag{66}$$

is the Maxwell stress tensor [253]. As noted above, in polar solvents, the permittivity should generally decrease in large fields. Various phenomenological models for $\varepsilon(E)$ can be incorporated into the theory of electrokinetics for concentrated solutions, but they complicate analysis and can introduce seemingly unphysical oscillations or singularities in the concentration profiles [197] and are perhaps best avoided, or included only heuristically in the boundary conditions.

5.3. Modified boundary conditions

5.3.1. Electrostatic boundary conditions

For Poisson's equation in the mean-field approximation (58), the electrostatic boundary conditions at a dielectric surface require continuity of the tangential electric field $\mathbf{E}_t$ and equate the jump in normal electric displacement $\varepsilon\mathbf{E}$ across the interface to the free charge q_S (which is related to the equilibrium zeta potential) [253]. For a low-dielectric surface with a fixed surface charge density, the internal electric field can often be neglected, yielding the standard boundary condition,

$$\varepsilon\,\hat{n}\cdot\nabla\phi = q_S\,. \tag{67}$$

Alternatively, for a metal surface, one can simply fix the potential $\phi = \phi_0$ or allow for a thin dielectric layer (or compact Stern layer) on the surface through the mixed boundary condition [148, 23, 110, 18],

$$\Delta\phi_S = \phi - \phi_0 = \lambda_S \hat{n} \cdot \nabla\phi - \frac{q_S}{C_S}, \tag{68}$$

where $\lambda_S = \varepsilon h_S / \varepsilon_S$ is an effective thickness of the layer, equal to the true thickness h_S by the ratio of permittivities of the solution ε and the layer ε_S, and $C_S = \varepsilon_S / h_S$ is its capacitance. The boundary condition can also be generalized for voltage-dependent surface capacitance, which makes the surface-layer voltage drop $\Delta\phi_S$ a nonlinear function of the normal electric field [148]. When applying (68) to a metal electrode, one can set $q_S = 0$ to model the Stern layer as a thin dielectric coating of solvent molecules, while specific adsorption of ions would lead to $q_S \neq 0$.

The preceding boundary conditions can be imposed on the mean-field Poisson equation (58), but the modified equation for electrostatic correlations (59) introduces a fourth derivative term and requires one more boundary condition on each surface. Charge conservation requires the following boundary condition

$$\hat{n} \cdot \left[\left(\lambda_c^2 \nabla^2 - 1 \right) \varepsilon \nabla\phi \right] = q_S \tag{69}$$

where brackets indicate the jump across the boundary. For consistency with the derivation of (59), Santangelo sets the second term (jump in mean dielectric displacement) to zero and thus equates the surface charge to the jump in the curvature of the field [237]. For an insulating surface of fixed charge density, this would imply replacing (67) with two boundary conditions

$$\hat{n} \cdot \nabla\phi = 0 \quad \text{and} \quad \hat{n} \cdot \lambda_c^2 \nabla^2 \left(\varepsilon \nabla\phi \right) = q_S \tag{70}$$

For a metal surface with a compact Stern layer modeled as a thin dielectric coating (with a uniform electric field), we would replace (68) with

$$\phi - \phi_0 = \lambda_S \hat{n} \cdot \nabla\phi \quad \text{and} \quad \hat{n} \cdot \lambda_c^2 \nabla^2 \left(\varepsilon \nabla\phi \right) = q_S . \tag{71}$$

This mathematical model provides an interesting opportunity for analysis of correlation effects in electrochemical dynamics and electrokinetics, although it is only a first approximation.

5.3.2. Electrochemical boundary conditions

Standard boundary conditions for the concentration fields equate normal ionic fluxes with Faradaic reaction rates

$$\hat{n} \cdot \mathbf{F}_i = R_i(\{c_i\}, \phi, \{\mu_i\}, \ldots), \tag{72}$$

which vanish for inert ions ($R_i = 0$). The flux boundary condition can also be generalized for a dynamical Stern layer, which supports tangential ionic fluxes [225, 227, 230], although some effects of this type are already captured by the modified electrokinetic equations, as noted above. The proper mathematical description of Faradaic reactions is complex and not fully understood [119]. The standard approach in electrochemistry is the Butler-Volmer equation, usually applied across the entire double layer under conditions of electroneutrality [147]. Applying an analogous expression at the molecular level has better theoretical justification and introduces the "Frumkin correction" for diffuse-layer voltage variations [254, 255]. For example, for the redox reaction $R \leftrightarrow O + ne^-$, this model asserts Arrhenius kinetics for the forward (anodic) and backward (cathodic) reaction rates,

$$R = k_a c_R e^{-\alpha_O ne\Delta\Phi_S / kT} - k_c c_O e^{\alpha_R ne\Delta\phi_S / kT}, \tag{73}$$

where k_a and k_c are rate constants for the anodic and cathodic reactions, c_R and c_O are concentrations of species R and O, and α_R and α_O are transfer coefficients defined below ($\alpha_R + \alpha_O = 1$) . The bias voltage $\Delta\phi_S$ can be interpreted as the Stern-layer voltage in models of the type we have considered here [149, 256, 257, 255]. This approach has been used to model ACEO [38] and TWEO [116] at reacting electrode arrays in dilute solutions. It is straightforward to include nonlinear differential capacitance of the Stern layer, $C_S(\Delta\phi_S)$, as well [149], but more significant modifications may be needed for concentrated solutions and large voltages.

For consistency with our statistical thermodynamical framework, following Ref. [258], the reaction rate should properly be expressed in terms of the electrochemical potentials,

$$R = k_0 \left(e^{(\mu_R - \mu_{TS}^{ex})/kT} - e^{(\mu_O - \mu_{TS}^{ex})/kT} \right), \tag{74}$$

where μ_R and μ_O are the complete electrochemical potentials of the reaction complex in the reduced and oxidized states, and μ_{TS}^{ex} is the excess electrochemical potential in the transition state, and k_0 is an arbitrary rate constant (which can be set by shifting μ_{TS}^{ex}). The Butler-Volmer equation (73) follows from dilute-solution theory ($\mu_R^{ex} = \mu_O^{ex} = 0$) and a purely electrostatic model for the activation barrier which is a linear combination of the electrostatic energy of the reduced and oxidized states, weighted by the transfer coefficients:

$$\mu_{TS}^{ex} = E_a + \alpha_R q_R \phi + \alpha_O (q_O \phi - ne\phi_0) \tag{75}$$

where E_a is a composition-independent activation energy barrier, absorbed into the rate constants k_a and k_c, and q_R and $q_O = q_R + ne$ are the charges of the reduced and oxided states. The general expression (74) can be derived from statistical transition-state theory in a hypothetical local open system [258], and it contains a variety of possible non-electrostatic influences on the reaction rate, via the excess contributions to the chemical potentials. This approach was recently introduced in the context of ion intercalation in rechargeable-battery materials, where the chemical potential in the electrode, and thus the reaction rate, depends on gradients in the ion concentration [238]. Steric effects were also recently considered in the context of fuel-cell membranes , and a form of (74) was effectively applied. In nonlinear electrokinetics, it may also be necessary to consider more general forms of the reaction rate in (74), whenever the voltage is large enough to breakdown the dilute-solution approximation.

5.3.3. Hydrodynamic boundary conditions

Until recently, almost all theoretical studies in electrokinetics have assumed the no-slip boundary condition for the liquid velocity, $\mathbf{u} = \mathbf{U}$, where $\mathbf{U}$ is the velocity of the surface. With the emergence of microfluidics [205], the phenomenon of hydrodynamic slip has been studied extensively in simple, Newtownian fluids [202, 203, 206] and interpreted in terms of the Navier boundary condition [259],

$$\Delta\mathbf{u} = \mathbf{u} - \mathbf{U} = b\,\hat{n} \cdot \nabla\mathbf{u}, \tag{76}$$

where the slip $\Delta\mathbf{u}$ is proportional to the shear strain rate via the slip length b. Flow past smooth hydrophilic surfaces has been shown to be consistent with the no-slip hypothesis, but b can reach tens of nanometres for hydrophobic surfaces [207, 208, 209] or even several microns over superhydrophobic textured surfaces with trapped nanobubbles [260, 261, 262, 263, 264].

The study of electrokinetic phenomena in the presence of slip was perhaps first pursued by the group of N. V. Churaev [265, 266]. For electro-osmotic flow in a microchannel, Kiseleva et al. [265] considered the effect of exponentially varying viscosity $\eta(x)$ near a wall, increasing

toward a hydrophilic surface or decreasing toward a hydrophobic surface, and Muller et al. [266] studied the impact of the slip boundary condition (76), which enhances the flow by a factor $(1 + b/\lambda_D)$ at low voltage [203]. This enhancement of electro-osmosis was recently analyzed and demonstrated by Joly et al. [93] via molecular dynamics simulations and extended to diffusio-osmosis by Ajdari and Bocquet [267]. The possibility of slip-enhanced (linear) electro-osmotic flows has generated considerable excitement in nanofluidics [88, 268], but so far it has only been analyzed with the classical electrokinetic equations and the simple, purely viscous boundary condition (76).

We suggest using a modified Navier slip boundary condition [269],

$$\Delta \mathbf{u} = \mathbf{M}\,(\mathbf{T} \cdot \hat{n}), \tag{77}$$

where $\mathbf{T} \cdot \hat{n}$ is the total normal traction on the surface due to short-range forces (force/area) and $\mathbf{M}$ is an interfacial mobility tensor (velocity×area/force), which is non-diagonal for anisotropic surfaces. For an isotropic, impermeable surface, the mobility matrix is diagonal, $\mathbf{M} = M\mathbf{I}$, with zero elements for normal flow, and then Eq. (76) is recovered from (77) with $b = M\eta$.

Using these models, it would be interesting to study the competition of viscoelectric effects (62) and hydrodynamic slip (76) or (77) in nonlinear electrokinetic phenomena at polarizable, hydrophobic surfaces in large applied voltages and/or concentrated solutions. The amplification factor $(1 + b/\lambda_D(c_0))$ associated with (76) increases with concentration and becomes appreciable when the diffuse-layer thickness becomes smaller than the slip length, so this may counteract the effect of increasing viscosity very close to the surface and allow induced-charge electro-kinetic phenomena to be observed at higher concentrations and voltages. We pose this as an interesting open question for future work.

5.4. Thin double layers and diffusion layers

The modified electrokinetic equations and boundary conditions above may be useful in modeling nanoscale electrokinetic phenomena, e.g. taking into account steric effects of finite ion sizes, but at larger scales, where the double layers become thin, asymptotic analysis can be used to systematically integrate out the diffuse layer and derive effective boundary conditions on the quasineutral bulk. First, we briefly summarize the results in the typical situation where the voltage is not strong enough to drive the double layer out of equilibrium or fully deplete the bulk salt concentration, due to diffusion limitation. In that case, the ion transport equations (56) remain unchanged in the bulk, but Poisson's equation (58) is replaced by the condition of electroneutrality, $\sum_i z_i e c_i = 0$. The fluid equations are also unchanged, and bulk viscosity variations can usually be neglected.

As noted above, chemical potentials are approximately constant (or "quasi-equilibrium" holds) in the normal direction across a thin double layer. For the ionic concentrations, the boundary conditions then take the form of surface conservation laws [137],

$$\frac{\partial \Gamma_i}{\partial t} + \nabla_s \cdot \mathbf{F}_i^{(s)} = \hat{n} \cdot \mathbf{F}_i - R_i, \tag{78}$$

where $\Gamma_i(\Psi_D, \{c_i\})$ is the excess concentration of species i per unit area, $\nabla_s \cdot \mathbf{F}_i^{(s)}(\Psi_D, \{c_i\})$ is the surface divergence of the integrated tangential flux in the diffuse layer, $\hat{n} \cdot \mathbf{F}_i$ is the normal flux from the bulk, and $R_i(\Psi_D, \{c_i\})$ is the Faradaic reaction rate density at the surface, evaluated in terms of the bulk variables. (See Ref. [137] for expressions using Bikerman's model, neglecting convective fluxes.) Equation (78) generalizes the RC boundary condition (2).

Integrating over the diffuse-layer also yields a "first kind" effective slip boundary condition for the bulk fluid velocity,

$$\mathbf{u}_s = b^{(eo)}\,\mathbf{E}_t - \sum_i b_i^{(do)}\,kT\nabla_t \ln c_i, \tag{79}$$

where the first term describes electro-osmosis driven by the bulk tangential field with $b^{(eo)}(\Psi_D, \{c_i\})$ given by (35) and various approximations above. The second term describes diffusio-osmosis in response to tangential bulk salt concentration gradients [198, 138, 98]. The diffusio-osmotic mobilities $b_i^{(do)}(\Psi_D, \{c_i\})$ can be systematically derived following the asymptotic analysis of Prieve et al. [138] or Rubinstein and Zaltzman [98, 99], although this can be cumbersome with the modified equations [197]. For concentrated solutions or large voltages, similar methods can express the effective slip boundary condition in terms of bulk electrochemical potential gradients, $\{\nabla_t \mu_i\}$.

In our many examples of induced-charge electrokinetic phenomena with blocking surfaces, we have assumed "weakly nonlinear" dynamics [95, 97], where the bulk concentration is not significantly perturbed. Under "strongly nonlinear" dynamics at large voltages, even with blocking electrodes [270, 136], strong bulk concentration gradients can develop, and the other terms in Equations (78) and (79) become important [198, 98, 99]. Although steric effects generally reduce the importance of surface conduction (smaller Dukhin-Bikerman number) compared to dilute solution theory, since there are not nearly as many ions in the double layer [56], diffusio-osmosis, concentration polarization, and diffusion-layer electro-convection [116] are affected less and could be significant. All of the problems we have considered above should be revisited in the strongly nonlinear regime to better understand the predictions of the modified models, but this is beyond the current scope.

As noted in section 2, the effects of Faradaic reactions or other mechanisms for normal ionic flux are still poorly understand in nonlinear electrokinetics, even for thin double layers. Normal currents can disturb the quasi-equilibrium structure of the double layer, even at small currents (in the Helmholtz limit $\delta \to 0$), and lead to seemingly reverse ICEO flows [18]. Concentration gradients can also develop due to normal ionic fluxes under diffusion limitation. If the bulk salt concentration approaches zero, at a limiting current, the quasi-equilibrium diffuse layer expands into a non-equilibrium space charge layer and drives second-kind electro-osmotic flows [199] and hydrodynamic instability [139, 99]. The classical electrokinetic equations suffice in that case, since the decreasing concentration only helps to validate dilute solution theory. In the case of induced-charge electrokinetic phenomena, however, the strongly nonlinear regime is just beginning to be explored and may require modeling with modified electrokinetic equations.

6. Conclusion

We have provided a critical review of recent work in nonlinear electrokinetics, comparing theory to experiment for the first time across a wide range of phenomena to extract general trends. In doing so, we were naturally led to question the theoretical foundations of the field and then develop modified models for concentrated solutions at large voltages. This undertaking also involved a substantial review component to bring out important work in modeling electrolytes from other fields, where fluid flow is neglected.

We have argued that (at least) two generic new phenomena arise in electrokinetic phenomena at large induced voltages: (i) Crowding effects decrease the differential capacitance (Fig. 5) which may explain high frequency flow reversal in ACEO pumps (Fig. 8) and imply ion-specific mobility of polarizable particles in large fields (Fig. 10); (ii) a charge-induced viscosity increase

upon ion crowding reduces the effective zeta potential (Fig. 15), which implies flow decay with increasing concentration and an additional source of ion-specificity (Fig. 18). In order to illustrate these phenomena, we have derived analytical formulae based a variety of microscopic models, ranging from lattice-gas (Bikerman) to hard-sphere (CS) approximations for steric effects, as well as various postulates of charge-induced thickening leading to modified (MHS) slip.

We have also developed a general theoretical framework for nonlinear electrokinetics, starting from any modified mean-field theory with volume constraints, which can be refined and extended in future work, e.g. to account for solvent structure near the surface, specific adsorption of ions, surface roughness, and Faradaic reactions. Especially for multivalent ions, it may also be necessary to account for electrostatic correlations, beyond the mean-field approximation. The challenge to describe ICEO flow over more than three decades of double-layer voltage from $kT/e = 25$ mV to ≈ 10 V. The upper limit corresponds to a new regime for the theory of electro-osmosis, where counterions become condensed near a highly charged surface. Nanoscale experiments and atomic-level simulations will be crucial to further develop the theory. Once properly validated, simple, modified mathematical models can allow us to advance our basic understanding and better predict experimental observations.

This research was supported by the National Science Foundation, under Contract DMS-0707641. AA acknowledges the hospitality of MIT and financial help from ANR grant Nanodrive. MZB acknowledges the hospitality of ESPCI and support from the Paris Sciences Chair. MZB and MSK also thank A. Ramos for helpful discussions, made possible by the MIT-Spain program, and P. M. Biesheuvel for key references and a critical reading of the manuscript.

References

[1] T. M. Squires, S. R. Quake, Microfluidics: fluid physics on the nanoliter scale, Rev. Mod. Phys. 77 (2005) 977–1026.
[2] M. Z. Bazant, Nonlinear electrokinetic phenomena, in: D. Li (Ed.), Encyclopedia of Microfluidics and Nanofluidics, Vol. Part 14, Springer, 2008, pp. 1461–1470.
[3] J. Lyklema, Electrokinetics after Smoluchowski, Colloids and Surfaces A 222 (2003) 5–14.
[4] R. J. Hunter, Foundations of Colloid Science, Oxford University Press, Oxford, 2001.
[5] J. Lyklema, Fundamentals of Interface and Colloid Science. Volume II: Solid-Liquid Interfaces, Academic Press Limited, San Diego, CA, 1995.
[6] W. B. Russel, D. Saville, W. R. Schowalter, Colloidal Dispersions, Cambridge University Press, Cambridge, England, 1989.
[7] J. L. Anderson, Colloid transport by interfacial forces, Annu. Rev. Fluid Mech. 21 (1989) 61–99.
[8] S. S. Dukhin, Electrochemical characterization of the surface of a small particle and nonequilibrium electric surface phenomena, Adv. Colloid Interface Sci. 61 (1995) 17–49.
[9] A. Delgado, F. González-Caballero, R. Hunter, L. Koopal, J. Lyklema, Measurement and interpretation of electrokinetic phenomena, J. Colloid Interface Sci. 309 (2007) 194–224.
[10] A. Ramos, H. Morgan, N. G. Green, A. Castellanos, AC electric-field-induced fluid flow in microelectrodes, J. Colloid Interface Sci. 217 (1999) 420–422.
[11] A. Ajdari, AC pumping of liquids, Phys. Rev. E 61 (2000) R45–R48.
[12] M. Z. Bazant, AC electro-osmotic flow, in: D. Li (Ed.), Encyclopedia of Microfluidics and Nanofluidics, Vol. Part 1, Springer, 2008, pp. 8–14.
[13] M. Z. Bazant, T. M. Squires, Induced-charge electro-kinetic phenomena: Theory and microfluidic applications, Phys. Rev. Lett. 92 (2004) 066101.
[14] T. M. Squires, M. Z. Bazant, Induced-charge electro-osmosis, J. Fluid Mech. 509 (2004) 217–252.
[15] V. A. Murtsovkin, Nonlinear flows near polarized disperse particles, Colloid Journal 58 (1996) 341–349.
[16] M. Z. Bazant, Electrokinetic motion of polarizable particles, in: D. Li (Ed.), Encyclopedia of Microfluidics and Nanofluidics, Vol. Part 5, Springer, 2008, pp. 522–529.

[17] J. A. Levitan, S. Devasenathipathy, V. Studer, Y. Ben, T. Thorsen, T. M. Squires, M. Z. Bazant, Experimental observation of induced-charge electro-osmosis around a metal wire in a microchannel, Colloids and Surfaces A 267 (2005) 122–132.
[18] D. Lacoste, G. I. Menon, M. Z. Bazant, J. F. Joanny, Electrostatic and electrokinetic contributions to the elastic moduli of a driven membrane, European Physical Journal E 28 (2009) 243–264.
[19] T. M. Squires, M. Z. Bazant, Breaking symmetries in induced-charge electro-osmosis and electrophoresis, J. Fluid Mech. 560 (2006) 65–101.
[20] E. Yariv, Induced-charge electrophoresis of nonspherical particles, Phys. Fluids 17 (2005) 051702.
[21] S. Gangwal, O. J. Cayre, M. Z. Bazant, O. D. Velev, Induced-charge electrophoresis of metallo-dielectric particles, Phys. Rev. Lett. 100 (2008) 058302.
[22] S. K. Thamida, H.-C. Chang, Nonlinear electrokinetic ejection and entrainment due to polarization at nearly insulated wedges, Phys. Fluids 14 (2002) 4315.
[23] G. Yossifon, I. Frankel, T. Miloh, On electro-osmotic flows through microchannel junctions, Phys. Fluids 18 (2006) 117108.
[24] N. I. Gamayunov, V. A. Murtsovkin, A. S. Dukhin, Pair interaction of particles in electric field. 1. features of hydrodynamic interaction of polarized particles, Colloid J. USSR 48 (1986) 197–203.
[25] V. A. Murtsovkin, G. I. Mantrov, Steady flows in the neighborhood of a drop of mercury with the application of a variable external electric field, Colloid J. USSR 53 (1991) 240–244.
[26] N. I. Gamayunov, G. I. Mantrov, V. A. Murtsovkin, Study of flows induced in the vicinity of conducting particles by an external electric field, Colloid J. 54 (1992) 20–23.
[27] N. G. Green, A. Ramos, A. González, H. Morgan, A. Castellanos, Fluid flow induced by nonuniform ac electric fields in electrolytes on microelectrodes. I. experimental measurements, Phys. Rev. E 61 (2000) 4011–4018.
[28] A. González, A. Ramos, N. G. Green, A. Castellanos, H. Morgan, Fluid flow induced by non-uniform ac electric fields in electrolytes on microelectrodes. II. a linear double-layer analysis, Phys. Rev. E 61 (2000) 4019.
[29] N. G. Green, A. Ramos, A. González, A. Castellanos, H. Morgan, Fluid flow induced by nonuniform ac electric fields in electrolytes on microelectrodes. III. observation of streamlines and numerical simulation, Phys. Rev. E 66 (2002) 026305.
[30] A. B. D. Brown, C. G. Smith, A. R. Rennie, Pumping of water with ac electric fields applied to asymmetric pairs of microelectrodes, Phys. Rev. E 63 (2000) 016305.
[31] A. Ramos, A. González, A. Castellanos, N. G. Green, H. Morgan, Pumping of liquids with ac voltages applied to asymmetric pairs of microelectrodes, Phys. Rev. E 67 (2003) 056302.
[32] V. Studer, A. Pépin, Y. Chen, A. Ajdari, Fabrication of microfluidic devices for ac electrokinetic fluid pumping, Microelec. Eng. 61 (2002) 915–920.
[33] M. Mpholo, C. G. Smith, A. B. D. Brown, Low voltage plug flow pumping using anisotropic electrode arrays, Sens. Actuators B 92 (2003) 262–268.
[34] V. Studer, A. Pépin, Y. Chen, A. Ajdari, An integrated ac electrokinetic pump in a microfluidic loop for fast tunable flow control, Analyst 129 (2004) 944–949.
[35] S. Debesset, C. J. Hayden, C. Dalton, J. C. T. Eijkel, A. Manz, An AC electroosmotic micropump for circular chromatographic applications, Lab on a Chip 4 (2004) 396–400.
[36] J. P. Urbanski, J. A. Levitan, M. Z. Bazant, T. Thorsen, Fast AC electro-osmotic pumps with non-planar electrodes, Applied Physics Letters 89 (2006) 143508.
[37] M. Z. Bazant, J. P. Urbanski, J. A. Levitan, K. Subramanian, M. S. Kilic, A. Jones, T. Thorsen, Electrolyte depenence of AC electro-osmosis, in: J. L. Viovy, P. Tabeling, S. Descroix, L. Malaquin (Eds.), Micro Total Analysis Systems 2007, Vol. 1, Chemical and Biological Microsystems Society, 2007, pp. 285–287.
[38] L. H. Olesen, H. Bruus, A. Ajdari, AC electrokinetic micropumps: the effect of geometrical confinement faradaic current injection and nonlinear surface capacitance, Phys. Rev. E 73 (2006) 056313.
[39] L. H. Olesen, AC electrokinetic micropumps, Ph.D. thesis, Danish Technical University (2006).
[40] M. Z. Bazant, Y. Ben, Theoretical prediction of fast 3d AC electro-osmotic pumps, Lab on a Chip 6 (2006) 1455–1461.
[41] J. P. Urbanski, J. A. Levitan, D. N. Burch, T. Thorsen, M. Z. Bazant, The effect of step height on the performance of AC electro-osmotic microfluidic pumps, Journal of Colloid and Interface Science 309 (2006) 332–341.
[42] B. Weiss, W. Hilber, R. Holly, P. Gittler, B. Jakoby, K. Hingerl, Dielectrophoretic particle dynamics in alternating-current electro-osmotic micropumps, Applied Physics Letters 92 (18) (2008) 184101.
[43] W. Hilber, B. Weiss, M. Mikolasek, R. Holly, K. Hingerl, B. Jakoby, Particle manipulation using 3d ac electro-osmotic micropumps, Journal of Micromechanics and Microengineering 18 (6) (2008) 064016 (6pp).
[44] B. P. Cahill, L. J. Heyderman, J. Gobrecht, A. Stemmer, Electro-osmotic streaming on application of traveling-wave electric fields, Physical Review E 70 (2004) 036305.
[45] A. Ramos, H. Morgan, N. G. Green, A. Gonzalez, A. Castellanos, Pumping of liquids with traveling-wave electro-osmosis, Journal of Applied Physics 97 (2005) 084906.

[46] P. García-Sanchez, A. Ramos, N. G. Green, H. Morgan, Experiments on AC electrokinetic pumping of liquids using arrays of microelectrodes, IEEE Transactions on Dielectrics and Electrical Insulation 13 (2006) 670–677.
[47] A. Ramos, A. González, P. García-Sánchez, A. Castellanos, A linear analysis of the effect of faradaic currents on traveling-wave electroosmosis, J. Colloid Interface Sci. 309 (2007) 323–331.
[48] C. K. Harnett, J. Templeton, K. A. Dunphy-Guzman, Y. M. Senousya, M. P. Kanouff, Model based design of a microfluidic mixer driven by induced charge electroosmosis, Lab on a Chip 8 (2008) 565–572.
[49] K. A. Rose, J. G. Santiago, Rotational electrophoresis of striped metallic microrods, Physical Review E 75 (2006) 197–203.
[50] D. Saintillan, E. Darve, E. S. G. Shaqfeh, Hydrodynamic interactions in the induced-charge electrophoresis of colloidal rod dispersions, Journal of Fluid Mechanics 563 (2006) 223–259.
[51] M. S. Kilic, M. Z. Bazant, Induced-charge electrophoresis near an insulating wall, arXiv:0712.0453v1 [cond-mat.mtrl-sci].
[52] M. Z. Bazant, M. S. Kilic, A. Ajdari, A theory of electrokinetics at highly charged surfaces, ELKIN International Electrokinetics Meeting, Nancy, France, 25-29 June 2006.
[53] M. Z. Bazant, M. S. Kilic, B. D. Storey, A. Ajdari, Nonlinear electrokinetics at large voltages, arXiv:cond-mat/0703035v2 [cond-mat.other] (2007).
[54] M. Z. Bazant, M. S. Kilic, B. Storey, A. Ajdari, Nonlinear electrokinetics at large voltages, New Journal of Physics accepted, to appear.
[55] J. J. Bikerman, Structure and capacity of the electrical double layer, Philosophical Magazine 33 (1942) 384.
[56] M. S. Kilic, M. Z. Bazant, A. Ajdari, Steric effects in the dynamics of electrolytes at large applied voltages: I double-layer charging, Phys. Rev. E 75 (2007) 033702.
[57] L. Lue, N. Zoeller, D. Blankschtein, Incorporation of nonelectrostatic interactions in the PoissonBoltzmann equation, Langmuir 15 (1999) 3726–3730.
[58] P. M. Biesheuvel, M. van Soestbergen, Counterion volume effects in mixed electrical double layers, Journal of Colloid and Interface Science 316 (2007) 490–499.
[59] J. Lyklema, J. T. G. Overbeek, On the interpretation of electrokinetic potentials, Journal of Colloid and Interface Science 16 (1961) 501–512.
[60] J. Lyklema, On the slip process in electrokinetics, Colloids and Surfaces A: Physicochemical and Engineering Aspects 92 (1994) 41–49.
[61] A. S. Dukhin, Biospecific mechanism of double layer formation and peculiarities of cell electrophoresis, Colloids and Surfaces A 73 (1993) 29–48.
[62] A. S. Dukhin, S. S. Dukhin, Aperiodic capillary electrophoresis method using alternating current electric field for separation of macromolecules, Electrophoresis 26 (2005) 2149–2153.
[63] B. D. Storey, L. R. Edwards, M. S. Kilic, M. Z. Bazant, Steric effects on ac electro-osmosis in dilute electrolytes, Phys. Rev. E 77 (2008) art. no. 036317.
[64] J. Cervera, J. A. Manzanares, S. Mafé, Ion size effects on the current efciency of narrow charged pores, Journal of Membrane Science 191 (2001) 179187.
[65] J. Cervera, V. García-Morales, J. Pellicer, Ion size effects on the electrokinetic flow in nanoporous membranes caused by concentration gradients, J. Phys. Chem. B 107 (2003) 8300–8309.
[66] Y. Liu, M. Liu, W. M. Lau, J. Yang, Ion size and image effect on electrokinetic flows, Langmuir 24 (2008) 2884–2891.
[67] C. Outhwaite, L. Bhuiyan, Theory of the electric double layer using a modified Poisson-Boltzmann equation, J. Chem. Soc., Faraday Trans. 2 76 (1980) 1388–1408.
[68] C. Outhwaite, L. Bhuiyan, An improved modified Poisson-Boltzmann equation in electric-double-layer theory, J. Chem. Soc., Faraday Trans. 2 78 (1983) 707–718.
[69] L. Bhuiyan, C. Outhwaite, Comparison of the modified Poisson-Boltzmann theory with recent density functional theory and simulation results in the planar electric double layer, Phys. Chem. Chem. Phys. 6 (2004) 3467–3473.
[70] A. A. Kornyshev, Double-layer in ionic liquids: Paradigm change?, J. Phys. Chem. B 111 (2007) 5545–5557.
[71] M. V. Federov, A. A. Kornyshev, Towards understanding the structure and capacitance of electrical double layer in ionic liquids, Electrochimica Acta 111 (2008) in press.
[72] M. V. Fedorov, A. A. Kornyshev, Ionic liquid near a charged wall: Structure and capacitance of electrical double layer, Journal of Physical Chemistry B 112 (38) (2008) 11868–11872.
[73] K. B. Oldham, A Gouy-Chapman-Stern model of the double layer at a metal/ionic liquid interface, Journal of Electroanalytical Chemistry 613.
[74] T. B. Grimley, N. F. Mott, The contact between a solid and a liquid electrolyte, Discussions of the Faraday Society 1 (1947) 3–11.
[75] T. B. Grimley, The contact between a solid and an electrolyte, Proceedings of the Royal Society of London, Series A 201 (1950) 40–61.
[76] J. R. Macdonald, Layered lattice gas model for the metal-electrolyte interface, Surface Science 116 (1982) 135–

147.
[77] J. Eijkel, A. van den Berg, Nanofluidics: what is it and what can we expect from it?, Microfluidics and Nanofluidics 1 (3) (2005) 249–267.
[78] R. B. Schoch, J. Han, P. Renaud, Transport phenomena in nanofluidics, Reviews of Modern Physics 80 (3) (2008) 839–883.
[79] Z. Zheng, D. J. Hansford, A. T. Conlisk, Effect of multivalent ions on electroosmotic flow in micro- and nanochannels, Electrophoresis 24 (2003) 3006–3017.
[80] S. Pennathur, J. G. Santiago, Electrokinetic transport in nanochannels. 1. theory, Analytical Chemistry 77 (2005) 6772–6781.
[81] S. Pennathur, J. G. Santiago, Electrokinetic transport in nanochannels. 2. experiments, Analytical Chemistry 77 (2005) 6782–6789.
[82] F. Baldessari, J. G. Santiago, Electrophoresis in nanochannels: brief reivew and speculation, J. Nanobiotechnology 4 (2006) 12.
[83] F. A. Morrison, J. F. Osterle, Electrokinetic energy conversion in ultrafine capillaries, J. Chem. Phys. 43 (1965) 2111–2115.
[84] S. H. Yao, J. G. Santiago, Porous glass electroosmotic pumps: theory, Journal of Colloid and Interface Science 268 (1) (2003) 133–142.
[85] H. Daiguji, P. D. Yang, A. J. Szeri, A. Majumdar, Electrochemomechanical energy conversion in nanofluidic channels, Nano Letters 4 (12) (2004) 2315–2321.
[86] F. H. J. van der Heyden, D. J. Bonthuis, D. Stein, C. Meyer, C. Dekker, Electrokinetic energy conversion efficiency in nanofluidic channels, Nano Letters 6 (10) (2006) 2232–2237.
[87] F. H. J. van der Heyden, D. J. Bonthuis, D. Stein, C. Meyer, C. Dekker, Power generation by pressure-driven transport of ions in nanofluidic channels, Nano Letters 7 (4) (2007) 1022–1025.
[88] S. Pennathur, J. C. T. Eijkel, A. van den Berg, Energy conversion in microsystems: is there a role for micro/nanofluidics?, Lab on a Chip 7 (10) (2007) 1234–1237. doi:10.1039/b712893m.
[89] J. Lyklema, S. Rovillard, J. De Coninck, Electrokinetics: The properties of the stagnant layer unraveled, Langmuir 14 (20) (1998) 5659–5663.
[90] J. Freund, Electroosmosis in a nano-meter scale channel studied by atomistic simulation, J. Chem. Phys. 116 (2002) 2194–2200.
[91] R. Qiao, N. R. Aluru, Ion concentrations and velocity profiles in nanochannel electroosmotic flows, J. Chem. Phys. 118 (2003) 4692–4701.
[92] A. P. Thompson, Nonequilibrium molecular dynamics simulation of electro-osmotic flow in a charged nanopore, Journal of Chemical Physics 119 (14) (2003) 7503–7511. doi:10.1063/1.1609194.
[93] L. Joly, C. Ybert, E. Trizac, L. Bocquet, Hydrodynamics within the electric double layer on slipping surfaces, Phys. Rev. Lett. 93 (2004) art. no. 257805.
[94] C. D. Lorenz, P. S. Crozier, J. A. Anderson, A. Travesset, Molecular dynamics of ionic transport and electrokinetic effects in realistic silica channels, Journal of Physical Chemistry C 112 (27) (2008) 10222–10232. doi:10.1021/jp711510k.
[95] M. Z. Bazant, K. Thornton, A. Ajdari, Diffuse charge dynamics in electrochemical systems, Phys. Rev. E 70 (2004) 021506.
[96] M. S. Kilic, M. Z. Bazant, A. Ajdari, Steric effects on the dynamics of electrolytes at large applied voltages: II modified nernst-planck equations, Phys. Rev. E 75 (2007) 034702.
[97] K. T. Chu, M. Z. Bazant, Nonlinear electrochemical relaxation around conductors, Physical Review E 74 (2006) 060601.
[98] I. Rubinstein, B. Zaltzman, Electro-osmotic slip of the second kind and instability in concentration polarization at electrodialysis membranes, Math. Models Meth. Appl. Sci. 2 (2001) 263–299.
[99] B. Zaltzman, I. Rubinstein, Electro-osmotic slip and electroconvective instability, Journal of Fluid Mechanics 579 (2007) 173–226.
[100] M. R. Bown, C. D. Meinhart, AC electroosmotic flow in a dna concentrator, J. Microfluidics Nanofluidics 2 (2006) 513–523.
[101] N. Loucaides, A. Ramos, G. E. Georghiou, Novel systems for configurable AC electroosmotic pumping, J. Microfluidics Nanofluidics 3 (2007) 709–714.
[102] D. N. Burch, M. Z. Bazant, Design principle for improved three-dimensional ac electro-osmotic pumps, Phys. Rev. E 77 (2008) art. no. 055303(R).
[103] F. Nadal, F. Argoul, P. Hanusse, B. Pouligny, A. Ajdari, Electrically induced interactions between colloidal particles in the vicinity of a conducting plane, Phys. Rev. E 65.
[104] F. Nadal, F. Argoul, P. Kestener, B. Pouligny, C. Ybert, A. Ajdari, Electrically-induced flows in the vicinity of a dielectric stripe on a conducting plane, Eur. Phys. J. E 9 (2002) 387–399.
[105] W. D. Ristenpart, I. A. Aksay, D. A. Saville, Electrically guided assembly of planar superlattices in binary colloidal

suspensions, Phys. Rev. Lett. 90 (2003) 128303.
[106] W. D. Ristenpart, I. A. Aksay, D. A. Saville, Ehd flow around a colloidal particle near an electrode with an oscillating potential, J. Fluid Mech. 575 (2007) 83–109.
[107] H. Zhao, H. H. Bau, Microfluidic chaotic stirrer utilizing induced-charge electro-osmosis, Phys. Rev. E 75 (2007) 066217.
[108] Z. Wu, D. Li, Mixing and flow regulating by induced-charge electrokinetic flow in a microchannel with a pair of conducting triangle hurdles, Microfluidics and Nanofluidics 5 (1) (2008) 65–76.
[109] Z. Wu, D. Li, Micromixing using induced-charge electrokinetic flow, Electrochimica Acta 53 (19) (2008) 5827–5835.
[110] G. Yossifon, I. Frankel, T. Miloh, Symmetry breaking in induced-charge electro-osmosis over polarizable spheroids, Phys. Fluids 19 (2007) 068105.
[111] E. Yariv, Nonlinear electrophoresis of ideally polarizable particles, Europhysics Letters 82 (5) (2008) 54004.
[112] G. Soni, T. M. Squires, C. D. Meinhart, Nonlinear phenomena in induced-charge electroosmosis: A numerical and experimental investigation, in: J. L. Viovy, P. Tabeling, S. Descroix, L. Malaquin (Eds.), Micro Total Analysis Systems 2007, Vol. 1, Chemical and Biological Microsystems Society, 2007, pp. 291–293.
[113] D. Saintillan, E. S. G. Shaqfeh, E. Darve, Stabilization of a suspension of sedimenting rods by induced-charge electrophoresis, Physics of Fluids 18 (2006) 121701.
[114] D. Saintillan, Nonlinear interactions in electrophoresis of ideally polarizable particles, Physics of Fluids 20 (6) (2008) 067104.
[115] H. Zhao, H. H. Bau, On the effect of induced electro-osmosis on a cylindrical particle next to a surface, Langmuir 23 (2007) 4053–4063.
[116] A. Gonzalez, , A. Ramos, P. García-Sanchez, A. Castellanos, Effect of the difference in ion mobilities on traveling wave electro-osmosis, in: IEEE International Conference on Dielectric Liquids, 2008, pp. 1–4. doi:DOI 10.1109/ICDL.2008.4622452.
[117] E. Yariv, T. Miloh, Electro-convection about conducting particles, Journal of Fluid Mechanics 595 (2008) 163–172.
[118] T. Miloh, Dipolophoresis of nanoparticles, Physics of Fluids 20 (6). doi:10.1063/1.2931080.
[119] J. O. Bockris, A. K. N. Reddy, Modern Electrochemistry, Plenum, New York, 1970.
[120] N. G. Green, A. Ramos, H. Morgan, AC electrokinetics: a survey of submicrometre particle dynamics, J. Appl. Phys. D 33 (2000) 632–641.
[121] J. A. Levitan, Experimental study of induced-charge electro-osmosis, Ph.D. thesis, MIT (2005).
[122] R. Schasfoort, S. Schlautmann, J. Hendrikse, A. van den Berg, Field-effect flow control for microfabricated fluidic networks, Science 286 (1999) 942.
[123] E. van der Wouden, T. Heuser, R. O. D.C. Hermes, J. Gardeniers, A. van den Berg, Field-effect control of electro-osmotic flow in microfluidic networks, Colloids and Surfaces A: Physicochemical and Engineering Aspects 267 (2005) 110–116.
[124] E. J. van der Wouden, D. C. Hermes, J. G. E. Gardeniers, A. van den Berg, Directional flow induced by synchronized longitudinal and zeta-potential controlling ac-electrical fields, Lab on a Chip 6 (2006) 1300 – 1305.
[125] P. J. Sides, Electrohydrodynamic particle aggregation on an electrode driven by an alternating electric field normal to it, Langmuir 17 (2001) 5791–5800.
[126] P. García-Sanchez, A. Ramos, N. G. Green, H. Morgan, Traveling-wave electrokinetic micropumps: Velocity, electrical current, and impedance measurements, Langmuir 24 (2008) 9361–9369.
[127] D. Lastochkin, R. H. Zhou, P. Wang, Y. X. Ben, H. C. Chang, Electrokinetic micropump and micromixer design based on ac faradaic polarization, Journal of Applied Physics 96 (2004) 1730–1733.
[128] A. González, A. Ramos, H. Morgan, N. G. Green, A. Castellanos, Electrothermal flows generated by alternating and rotating electric fields in microsystems, Journal of Fluid Mechanics 564 (2006) 415–433.
[129] J. Wu, M. Lian, K. Yang, Micropumping of biofluids by alternating current electrothermal effects, Applied Physics Letters 90 (2007) 234103.
[130] J. Wu, Y. Ben, H.-C. Chang, Particle detection by electrical impedance spectroscopy with asymmetric-polarization AC electroosmotic trapping, J. Microfluidics and Nanofluidics 1 (2005) 161–167.
[131] J. Wu, Biased AC electro-osmosis for on-chip bioparticle processing, IEEE Transactions on Nanotechnology 5 (2006) 84–88.
[132] M. M. Gregersen, L. H. Olesen, A. Brask, M. F. Hansen, H. Bruus, Flow reversal at low voltage and low frequency in a microfabricated ac electrokinetic pump, Phys. Rev. E 76 (2007) 056305.
[133] D. L. Chapman, A contribution to the theory of electrocapillarity, Philos. Mag. 25 (1913) 475–481.
[134] M. Gouy, Sur la constitution de la charge électrique a la surface d'un électrolyte, J. de Phys. 9 (1910) 457–468.
[135] A. Gonzalez, A. Ramos, A. Castellanos, Pumping of liquids using travelling wave electro-osmosis: a nonlinear analysis, in: IEEE International Conference on Dielectric Liquids, 2005, pp. 221–224.
[136] L. H. Olesen, M. Z. Bazant, H. Bruus, Strongly nonlinear dynamics of electrolytes in large ac voltages, in prepa-

ration.
[137] K. T. Chu, M. Z. Bazant, Surface conservation laws at microscopically diffuse interfaces, J. Colloid Interface Science 315 (2007) 319–329.
[138] D. C. Prieve, J. L. Anderson, J. P. Ebel, M. E. Lowell, Motion of a particle generated by chemical gradients. part 2. electrolytes, J. Fluid Mech. 148 (1984) 247–269.
[139] I. Rubinstein, B. Zaltzman, Electro-osmotically induced convection at a permselective membrane, Phys. Rev. E 62 (2000) 2238–2251.
[140] F. Leinweber, J. Eijkel, J. Bomer, A. vandenBerg, Continuous flow microfluidic demixing of electrolytes by induced charge electrokinetics in structured electrode arrays, Analytical Chemistry 78 (5) (2006) 1425–1434.
[141] R. Mancinelli, A. Botti, F. Bruni, M. A. Ricci, A. K. Soper, Hydration of sodium, potassium, and chloride ions in solution and the concept of structure maker/breaker, J. Phys. Chem. B 111 (2007) 13570–13577.
[142] O. Stern, Zur theorie der electrolytischen doppelschicht, Z. Elektrochem. 30 (1924) 508–516.
[143] H. M. Jones, E. E. Kunhardt, Pulsed dielectric breakdown of pressurized water and salt solutions, Journal of Applied Physics 77 (1995) 795–805.
[144] P. Grochowski, J. Trylska, Continuum molecular electrostatics, salt effects, and counterion binding: A review of the Poisson–Boltzmann theory and its modifications, Biopolymers 89 (2008) 93–113.
[145] V. Vlachy, Ionic effects beyond Poisson-Boltzmann theory, Annu. Rev. Phys. Chem. 50 (1990) 145–65.
[146] P. Attard, Electrolytes and the electrical double layer, Adv. Chem. Phys. 92 (1996) 1–159.
[147] J. Newman, Electrochemical Systems, 2nd Edition, Prentice-Hall, Inc., Englewood Cliffs, NJ, 1991.
[148] M. Z. Bazant, K. T. Chu, B. J. Bayly, Current-voltage relations for electrochemical thin films, SIAM J. Appl. Math. 65 (2005) 1463–1484.
[149] K. T. Chu, M. Z. Bazant, Electrochemical thin films at and above the classical limiting current, SIAM J. Appl. Math. 65 (2005) 1485–1505.
[150] D. di Caprio, Z. Borkowska, J. Stafiej, Simple extension of the Gouy-Chapman theory including hard sphere effects: Diffuse layer contribution to the differential capacitance curves for teh electrode—electrolyte interface, J. Electroanal. Chem. 540 (2003) 17–23.
[151] D. di Caprio, Z. Borkowska, J. Stafiej, Specific ionic interactions within a simple extension of the Gouy-Chapman theory including hard sphere effects, J. Electroanal. Chem. 572 (2004) 51–59.
[152] R. Qiao, N. R. Aluru, Multiscale simulation of electroosmotic transport using embedding techniques, International Journal for Multiscale Computational Engineering 2 (2004) 173–188.
[153] V. Freise, Zur theorie der diffusen doppelschicht (theory of the diffuse double layer), Zeitschrift für Elektrochemie 56 (1952) 822–827.
[154] I. Borukhov, D. Andelman, H. Orland, Steric effects in electrolytes: A modified Poisson-Boltzmann approach, Phys. Rev. Lett. 79 (1997) 435–438.
[155] M. Dutta, S. N. Bagchi, On the distribution of ions in solutions of strong electrolytes, Indian J. Physics 24.
[156] S. N. Bagchi, A new equation for strong electrolytes, part i, J. Indian Chem. Soc. 27.
[157] S. N. Bagchi, A new equation for strong electrolytes, part ii, J. Indian Chem. Soc. 27.
[158] M. Dutta, M. Sengupta, A theory of strong electrolytes in solution based on new statistics, Proceedings of the National Institute of Sciences of India 20 (1954) 1–11.
[159] M. Eigen, E. Wicke, Zur theorie der starken elektrolyte, Naturwissenschaften 38 (1951) 453–454.
[160] E. Wicke, M. Eigen, über den einfluß des raumbedarfs von ionen in wässriger lösung auf ihre verteilung im elektrischen feld und ihre aktivitätskoeffizienten, Z. Elektrochem. 56 (1952) 551–561.
[161] M. Eigen, E. Wicke, The thermodynamics of electrolytes at higher concentration, J. Phys. Chem. 58 (1954) 702–714.
[162] A. Iglic, V. Kralj-Iglic, Influence of finite size of ions on electrostatic properties of electric double layer, Electrotecnical Rev. (Slovenia) 61 (1994) 127–133.
[163] V. Kralj-Iglic, A. Iglic, A simple statistical mechanical approach to the free energy of the electric double layer including the excluded volume effect, J. Phys. II France 6 (1996) 477–491.
[164] K. Bohinc, V. Kralj-Iglic, A. Iglic, Thickness of electrical double layer. effect of ion size, Electrochim. Acta 46 (2001) 3033–3040.
[165] K. Bohinc, A. Iglic, T. Slivnik, V. Kralj-Iglic, Charged cylindrical surfaces: Effect of finite ion size, Bioelectrochemistry 57 (2002) 73–81.
[166] I. Borukhov, D. Andelman, H. Orland, Adsorption of large ions from an electrolyte solution: A modified Poisson Boltzmann equation, Electrochim. Acta 46 (2000) 221–229.
[167] I. Borukhov, Charge renormalization of cylinders and spheres: Ion size effects, J. Pol. Sci. B: Pol. Phys. 42 (2004) 3598–3620.
[168] O. Redlich, A. C. Jones, Solutions of electrolytes, Annu. Rev. Phys. Chem. 6 (1955) 71–98.
[169] P. M. Biesheuvel, Ionizable polyelectrolyte brushes: brush height and electrosteric interaction, Journal of Colloid and Interface Science 275 (2004) 97–106.

[170] R. Israëls, On the theory of grafted weak polyacids, Macromolecules 27 (1994) 3087.
[171] O. Gonzlez-Amezcua, M. Hernndez-Contreras, Phase evolution of lamellar cationic lipid-dna complex: Steric effect of an electrolyte, J. Chem. Phys. 121 (2004) 10742.
[172] M. van Soestbergen, P. M. Biesheuvel, R. T. H. Rongen, L. J. Ernst, G. Q. Zhang, Modified poisson-nernst-planck theory for ion transport in polymeric electrolytes, J. Electrostatics 66 (2008) 567–573.
[173] G. Valette, Double layer on silver single-crystal electrodes in contact with electrolytes having anios which present a slight specific adsorption: Part I. the (110) face, J. Electroanal. Chem. 122 (1981) 285–297.
[174] G. Valette, Double layer on silver single-crystal electrodes in contact with electrolytes having anios which present a slight specific adsorption: Part I. the (100) face, J. Electroanal. Chem. 138 (1982) 37–54.
[175] A. Hamelin, L. Stoicoviciu, Study of gold low index faces in kpf_6 solutions. i: Experimental behaviour and determination of the points of zero charge, J. Electroanal. Chem. 93.
[176] D. C. Grahame, The electrical double layer and the theory of electrocapillarity, Chem. Rev. 41 (1947) 441–501.
[177] L. Blum, Structure of the electric double layer, Adv. Chem. Phys. 78 (1990) 171.
[178] R. J. E. Porkess, The forbidden volume of a gas, Phys. Educ. 12 (1977) 240–243.
[179] M. J. Sparnaay, Trav. Chim. Pays-Bas 77 (1958) 872.
[180] J. Dufrêche, J. Simonin, P. Turq, Sedimentation of charged colloids in the gravitational field: Relaxation toward equilibrium, J. Molecular Liq. 79 (1999) 137–149.
[181] P. M. Biesheuvel, J. Lyklema, Sedimentation–diffusion equilibrium of binary mixtures of charged colloids including volume effects, J. Phys. Condens. Matter 17 (2005) 6337.
[182] P. Biesheuvel, W. de Vos, V. Amoskov, Semi-analytical continuum model for non-dilute neutral and charged brushes including finite stretching, Macromolecules 41 (2008) 6254–6259.
[183] W. M. de Vos, P. M. Biesheuvel, A. de Keizer, J. M. Kleijn, M. A. Cohen-Stuart, Adsorption of the protein bovine serum albumin in a planar poly(acrylic acid) brush layer as measured by optical reflectometry, Langmuir 24 (2008) 6575–6584.
[184] N. F. Carnahan, K. E. Starling, Equation of state for nonattracting rigid spheres, J. Chem. Phys. 51 (1969) 635–636.
[185] L. Bhuiyan, C. Outhwaite, D. Henderson, A modified Poisson-Boltzmann analysis of the capacitance behaviour of the electric double layer at low temperatures, J. Chem. Phys. 123 (2005) 034704.
[186] J. R. Henderson (Ed.), Fundamentals of Inhomogeneous Fluids, Marcel Dekker, New York, 1992.
[187] D. Gillespie, W. Nonner, R. S. Eisenberg, Density functional theory of charged hard-sphere fluids, Phys. Rev. E 68 (2003) 0313503.
[188] J. Reszko-Zygmunt, S. Sokolowski, D. Henderson, D. Boda, Temperature dependence of the double layer capacitance for the restricted primitive model of an electrolyte solution from a density functional approach, J. Chem. Phys. 122 (2005) 084504.
[189] J.-P. Hansen, I. R. McDonald, Theory of Simple Liquids, Academic, London, 1986.
[190] T. Boublik, Hard sphere equation of state, J. Chem. Phys. 53 (1970) 471–472.
[191] G. A. Mansoori, N. F. Carnahan, K. E. Starling, T. W. Leland, Equilibrium thermodynamic properties of the mixture of hard spheres, J. Chem. Phys. 54 (1971) 1523–1525.
[192] R. Stokes, T. Mills, Viscosity of Electrolytes and Related Properties, Pergamon Press Ltd, 1965.
[193] E. R. Nightingale, Phenomenological theory of ion solvation. effective radii of hydrated ions, J. Phys. Chem. 63 (1959) 1381–1387.
[194] K. L. Gering, Prediction of electrolyte viscosity for aqueous and non-aqueous systems: Results from a molecular model based on ion solvation and a chemical physics framework, Electrochimica Acta 51 (2006) 3125–3138.
[195] V. L. Shapovalov, G. Brezesinski, Breakdown of the Gouy-Chapman model for highly charged langmuir monolayers: Counterion size effect, J. Phys. Chem. B 110 (2006) 10032.
[196] V. L. Shapovalov, M. E. Ryskin, O. V. Konovalov, A. Hermelink, G. Brezesinski, Elemental analysis within the electrical double layer using total reflection x-ray fluorescence technique, J. Phys. Chem. B 111 (2007) 3927–3934.
[197] M. S. Kilic, Induced-charge electrokinetics at large voltages, Ph.D. thesis, Massachusetts Institute of Technology (2008).
[198] S. S. Dukhin, B. V. Derjaguin, Surface and Colloid Science, Vol. Vol. 7, Academic Press, New York, 1974, Ch. Ch. 2.
[199] S. S. Dukhin, Non-equilibrium electric surface phenomena, Adv. Colloid Interface Sci. 44 (1993) 1–134.
[200] R. W. O'Brien, L. B. White, Electrophoretic mobility of a spherical colloidal particle, J. Chem. Soc. Faraday Trans. II 74 (1978) 1607–1626.
[201] B. J. Kirby, E. H. Hasselbrink, Zeta potential of microfluidic substrates: 1. theory, experimental techniques, and effects on separations, Electrophoresis 25 (2004) 187–2002.
[202] O. I. Vinogradova, Slippage of water over hydrophobic surfaces, Int. J. Miner. Proc. 56 (1999) 31–60.
[203] L. Bocquet, J. L. Barrat, Flow boundary conditions from nano- to micro- scales, Soft Matter 3 (2007) 685–693.

[204] V. Vand, Viscosity of solutions and suspensions, J. Phys. Chem. 52 (1948) 277–299.
[205] H. A. Stone, A. D. Stroock, A. Ajdari, Engineering Flows in Small Devices, Annual Review of Fluid Mechanics 36 (2004) 381–411.
[206] E. Lauga, M. P. Brenner, H. A. Stone, Handbook of Experimental Fluid Dynamics, Springer, NY, 2007, Ch. 19, pp. 1219–1240.
[207] O. I. Vinogradova, G. E. Yakubov, Dynamic effects on force measurements. 2. lubrication and the atomic force microscope, Langmuir 19 (2003) 1227–1234.
[208] C. Cottin-Bizonne, B. Cross, A. Steinberger, E. Charlaix, Boundary slip on smooth hydrophobic surfaces: Intrinsic effects and possible artifacts, Phys. Rev. Lett. 94 (2005) 056102.
[209] L. Joly, C. Ybert, L. Bocquet, Probing the nanohydrodynamics at liquid-solid interfaces using thermal motion, Phys. Rev. Lett. 96 (2006) 046101.
[210] R. Qiao, N. R. Aluru, Scaling of electrokinetic transport in nanometer channels, Langmuir 21 (2005) 8972–8977.
[211] P. Olsson, S. Teitel, Critical scaling of shear viscosity at the jamming transition, Physical Review Letters 99 (2007) 178001.
[212] A. J. Liu, S. R. Nagel, Jamming is not just cool any more, Nature (London) 396 (1998) 21.
[213] C. S. O'Hern, L. E. Silbert, A. J. Liu, S. R. Nagel, Jamming at zero temperature and zero applied stress: The epitome of disorder, Phys. Rev. E 68 (2003) 011306.
[214] B. I. Shklovskii, Screening of a macroion by multivalent ions: Correlation-induced inversion of charge, Phys. Rev. E 60 (1999) 5802–5811.
[215] T. T. Nguyen, B. I. Shklovskii, Adsorption of charged particles on an oppositely charged surface: Oscillating inversion of charge, Phys. Rev. E 64 (2001) 0410407.
[216] A. Y. Grosberg, T. T. Nguyen, B. I. Shklovskii, The physics of charge inversion in chemical and biological systems, Rev. Mod. Phys. 74 (2002) 329–345.
[217] D. Kim, E. Darve, Molecular dynamics simulations of rough wall microchannels, Phys. Rev. E 73 (2006) 051203.
[218] G. Jones, M. Dole, The viscosity of aqueous solutions of strong electrolytes with special reference to barium chloride, J. Am. Chem. Soc. 51 (1929) 2950–2964.
[219] G. Jones, S. K. Talley, The viscosity of aqueous solutions as a function of concentration, J. Am. Chem. Soc. 55 (1933) 624–642.
[220] H. D. Jenkins, Y. Marcus, Viscosity B-coefficients of ions in solution, Chem. Rev. 95 (1995) 2695–2724.
[221] D. R. Lide, CRC Handbook of chemistry and physics, 89th Edition, CRC Press, 2008.
[222] S. Chakraborty, Generalization of interfacial electrohydrodynamics in the presence of hydrophobic interactions in narrow fluidic confinements, Phys. Rev. Lett. 100 (2008) 09801.
[223] J. J. López-Garcia, C. Grosse, J. Horno, Numerical study of colloidal suspensions of soft spherical particles using the network method 1. dc electrophoretic mobility, J. Colloid Interface Sci. 265 (2003) 327.
[224] J. J. López-Garcia, C. Grosse, J. Horno, Numerical study of colloidal suspensions of soft spherical particles using the network method 2. ac electrokinetic and dielectric properties, J. Colloid Interface Sci. 265 (2003) 341.
[225] C. F. Zukowski, D. A. Saville, The interpretation of electrokinetic measurements using a dynamic model of the stern layer i. the dynamic model, J. Colloid Interface Sci. 114 (1986) 32.
[226] C. F. Zukowski, D. A. Saville, The interpretation of electrokinetic measurements using a dynamic model of the stern layer i. comparisons between theory and experiment, J. Colloid Interface Sci. 114 (1986) 32.
[227] C. S. Mangelsdorf, L. R. White, Effects of stern-layer conductance on electrokinetic transport properties of colloidal particles, J. Chem. Soc. Faraday Trans. 86 (1990) 2859.
[228] C. S. Mangelsdorf, L. R. White, The dynamic double layer part 1: Theory of a mobile stern layer, J. Chem. Soc. Faraday Trans. 94 (1998) 2441–2452.
[229] C. S. Mangelsdorf, L. R. White, The dynamic double layer part 2: Effects of stern-layer conduction on the high-frequency electrokinetic transport properties, J. Chem. Soc. Faraday Trans. 94 (1998) 2583–2593.
[230] J. J. López-Garcia, C. Grosse, J. Horno, A new generalization of the standard electrokinetic model, J. Phys. Chem B 111 (2007) 8985–8992.
[231] C. H. Rycroft, G. S. Grest, J. W. Landry, M. Z. Bazant, Analysis of granular flow in a pebble-bed nuclear reactor, Physical Review E (Statistical, Nonlinear, and Soft Matter Physics) 74 (2).
[232] V. A. Murtsovkin, G. I. Mantrov, Study of the motion of anisometric particles in a uniform variable electric field, Colloid J. USSR 52 (1990) 933–936.
[233] D. Long, A. Ajdari, Electrophoretic mobility of composite objects in free solution: Application to dna separation, Electrophoresis 17 (1996) 1161–1166.
[234] D. Long, A. Ajdari, Symmetry properties of the electrophoretic motion of patterned colloidal particles, Phys. Rev. Lett. 81 (1998) 1529–1532.
[235] J. J. Bikerman, Surface Chemistry for Industrial Research, Academic Press, New York, 1948.
[236] J. J. Bikerman, Physical Surfaces, Academic Press, London, 1970.
[237] C. D. Santangelo, Computing counterion densities at intermediate coupling, Physical Review E 73 (4) (2006)

041512.
[238] G. K. Singh, G. Ceder, M. Z. Bazant, Intercalation dynamics in rechargeable battery materials: General theory and phase-transformation waves in $LiFePO_4$, Electrochimica Acta 53 (26) (2008) 7599–7613. doi:10.1016/j.electacta.2008.03.083.
[239] L. Zhang, L. Scriven, H. T. Davis, A three-component model of the electrical double layer, J. Chem. Phys. 97 (1992) 494–502.
[240] L. Zhang, H. T. Davis, H. White, Simulations of solvent effects on confined electrolytes, J. Chem. Phys. 98 (1993) 5793–5799.
[241] S. Marcelja, Exact description of aqueous electrical double layers, Langmuir 16 (2000) 6081– 6083.
[242] J. Lyklema, J. F. L. Duval, Hetero-interaction between gouystern double layers: Charge and potential regulation, Advances in Colloid and Interface Science 114-115 (2005) 27–45.
[243] J. F. L. Duval, F. A. M. Leermakers, H. P. van Leeuwen, Electrostatic interactions between double layers: influence of surface roughness, regulation, and chemical heterogeneities 20 (2004) 5052–5065.
[244] L. I. Daikhin, A. A. Kornyshev, M. Urbakh, Double-layer capacitance on a rough metal surface, Phys. Rev. E 53 (1995) 6192–6199.
[245] L. I. Daikhin, A. A. Kornyshev, M. Urbakh, Double-layer capacitance on a rough metal surface: surface roughness by 'debye ruler', Electrochimica Acta 42 (1997) 2853–2860.
[246] B. B. Damaskin, V. A. Safonov, Analysis of modern phenomenological approaches toward describing the structure and properties of the electrical double layer dense part on the metal solution interface, Electrochimica Acta 42 (1997) 737–746.
[247] D. Gillespie, W. Nonner, R. S. Eisenberg, Coupling Poisson-Nernst-Planck and density functional theory to calculate ion flux, J. Phys.: Condens. Matter 14 (2002) 12129–12145.
[248] R. Roth, D. Gillespie, Physics of size selectivity, Phys. Rev. Lett. 95 (2005) 247801.
[249] S. R. D. Groot, P. Mazur, Non-equilibrium Thermodynamics, Interscience Publishers, Inc., New York, NY, 1962.
[250] R. Taylor, R. Krishna, Multicomponent Mass Transfer, Wiley - IEEE, 1993.
[251] J. R. Macdonald, Theory of the differential capacitance of the double layer in unadsorbed electrolytes, J. Chem. Phys. 22 (1954) 1857–1866.
[252] A. Abrashkin, D. Andelman, H. Orland, Dipolar poissin-boltzmann equation: Ions and dipoles close to charge interfaces, Physical Review Letters 99 (2007) 077801.
[253] J. D. Jackson, Classical Electrodynamics, 3rd Edition, Wiley, 1999.
[254] A. Frumkin, Wasserstoffüberspannung und struktur der doppelschict, Z. Phys. Chem. 164A (1933) 121–133.
[255] P. M. Biesheuvel, M. van Soestbergen, M. Z. Bazant, Imposed currents in galvanic cells, Electrochimica Acta to appear.
[256] A. Bonnefont, F. Argoul, M. Bazant, Analysis of diffuse-layer effects on time-dependent interfacial kinetics, J. Electroanal. Chem. 500 (2001) 52–61.
[257] P. M. Biesheuvel, A. A. Franco, M. Z. Bazant, Diffuse charge effects in fuel cell membranes, Journal of the Elecrochemical Society 156 (2009) B225–B233.
[258] M. Z. Bazant, D. Lacoste, K. Sekimoto, Transition-rate theory based on chemical potentials with applications in electrochemistry, in preparation.
[259] C. L. M. H. Navier, Mémoire sur les lois du mouvement des fluides, Mémoire de l'Académie Royale des Sciences de lÍnstitut de France 6 (1823) 389–440.
[260] O. I. Vinogradova, N. F. Bunkin, N. V. Churaev, O. A. Kiseleva, A. V. Lobeyev, B. W. Ninham, Submicrocavity structure of water between hydrophobic and hydrophilic walls as revealed by optical cavitation, J. Colloid Interface Sci. 173 (1995) 443–447.
[261] C. Cottin-Bizonne, J. L. Barrat, L. Bocquet, E. Charlaix, Low-friction flows of liquid at nanopatterned interfaces, Nat. Mater. 2 (2003) 237–240.
[262] J. Ou, J. P. Rothstein, Direct velocity measurements of the flow past drag-reducing ultrahydrophobic surfaces, Physics of Fluids 17 (2005) 103606. doi:10.1063/1.2109867.
[263] P. Joseph, C. Cottin-Bizonne, J. M. Benoĭ, C. Ybert, C. Journet, P. Tabeling, L. Bocquet, Slippage of water past superhydrophobic carbon nanotube forests in microchannels, Phys. Rev. Lett. 97 (2006) 156104.
[264] C. H. Choi, U. Ulmanella, J. Kim, C. M. Ho, C. J. Kim, Effective slip and friction reduction in nanograted superhydrophobic microchannels, Phys. Fluids 18 (2006) 087105.
[265] O. A. Kiseleva, V. D. Sobolev, V. M. Starov, N. V. Churaev, Colloid J. USSR 41 (2) (1979) 926 (Russian).
[266] V. M. Muller, I. P. Sergeeva, V. D. Sobolev, N. V. Churaev, Boundary effects in the theory of electrokinetic phenomena, Colloid J. USSR 48 (1986) 606–614 (English), 718–727 (Russian).
[267] A. Ajdari, L. Bocquet, Giant amplification of interfacially driven transport by hydrodynamic slip: Diffusio-osmosis and beyond, Physical Review Letters 96 (18) (2006) 186102.
[268] V. Tandon, B. J. Kirby, Zeta potential and electroosmotic mobility in microfluidic devices fabricated from hydrophobic polymers: 2. slip and interfacial water structure, Electrophoresis 29 (2008) 1102–1114.

[269] M. Z. Bazant, O. I. Vinogradova, Tensorial hydrodynamic slip, Journal of Fluid Mechanics 613 (2008) 125–134.
[270] F. Beunis, F. Strubbe, M. Marescaux, J. Beeckman, K. Neyts, A. R. M. Verschueren, Dynamics of charge transport in planar devices, Phys. Rev. E 78 (2008) 031504.